Spring 2017

Cyclostratigraphic Trends of δ13C in Upper Cambrian Strata, Great Basin, Usa: Implications for Astronomical Forcing

Wesley Donald Weichert
Missouri State University

CYCLOSTRATIGRAPHIC TRENDS OF $\delta^{13}C$ IN UPPER CAMBRIAN STRATA, GREAT BASIN, USA: IMPLICATIONS FOR ASTRONOMICAL FORCING

A Masters Thesis

Presented to

The Graduate College of

Missouri State University

In Partial Fulfillment

Of the Requirements for the Degree

Masters of Science, Geospatial Sciences in Geography and Geology

By

Wesley Donald Weichert

May 2017

CYCLOSTRATIGRAPHIC TRENDS OF $\delta^{13}C$ IN UPPER CAMBRIAN STRATA, GREAT BASIN, USA: IMPLICATIONS FOR ASTRONOMICAL FORCING

Geography, Geology, and Planning

Missouri State University, May 2017

Master of Science

Wesley Donald Weichert

ABSTRACT

Composite geochemical studies of carbonate isotope values ($\delta^{13}C$) by other investigators have established that the Cambrian period is punctuated by a series of significant, globally correlated, positive and negative $\delta^{13}C$ excursions. However, it remains unclear if low-amplitude secular variations in $\delta^{13}C$ values exist superimposed on, or between large-scale perturbations in the Cambrian carbon cycle, especially in cyclic successions. Rocks of Steptoean-Sunwaptan (Paibian-Jiangshanian) stage, exposed in the Great Basin of Utah and Nevada, are excellent candidates for testing the hypothesis that sedimentary cycles record minor variations in Earth's orbit (Milankovitch cycles) through application of high-resolution chemostratigraphic analysis. High-resolution $\delta^{13}C$ data was collected from intervals in two correlative sections in Utah and Nevada. In addition, gamma-ray profiles were measured from a total of eight sections across the Great Basin, providing a sequence stratigraphic framework. Here, secular variations in $\delta^{13}C$ values up to +/- 1.33 ‰ and +/- 0.70 ‰ exist between correlative 5th order cycles in Utah and Nevada respectively. Carbonate cycles can be correlated laterally 115 km based on key marker beds in the dominantly subtidal succession. REDFIT time-series analyses of $\delta^{13}C$ reveals peak frequencies that compare favorably with the precession, obliquity, and eccentricity bands estimated from long-term sedimentation rates. A 1:1, 2:1 and 5:1 bundling of cycles additionally suggests astronomical controls on sedimentation. This investigation of Late Cambrian cyclic carbonates provides evidence of putative Milankovitch-style cyclicity recorded in mid-to outer-shelf carbonate deposits of Laurentia.

KEYWORDS: Cambrian, sequence stratigraphy, carbon isotopes, time-series analysis, Milankovitch cycles.

This abstract is approved as to form and content

_____

Kevin Ray Evans
Chairperson, Advisory Committee
Missouri State University

CYCLOSTRATIGRAPHIC TRENDS OF $\delta^{13}C$ IN UPPER CAMBRIAN STRATA, GREAT BASIN, USA: IMPLICATIONS FOR ASTRONOMICAL FORCING

By

Wesley Donald Weichert

A Masters Thesis
Submitted to the Graduate College
Of Missouri State University
In Partial Fulfillment of the Requirements
For the Degree of Masters of Science, Geospatial Science in Geography and Geology

May 2017

Approved:

_____
Kevin Ray Evans, PhD

_____
Gary Michelfelder, PhD

_____
Melida Gutierrez, PhD

_____
Julie Masterson, PhD: Dean, Graduate College

ACKNOWLEDGEMENTS

Foremost, I would like to give special thanks to Dr. Kevin Evans for introducing me to the Cambrian stratigraphy of the Great Basin. Without Kevin's expertise and experience, I would have never had the opportunity to study the geology of the American West. Additionally, Kevin inspired me to pursue my academic goals and aspirations with confidence, a trait that will never leave me.

I want to extend a special thanks to Brett Kenning, whom joined Kevin and I in the field and facilitated sample collection and measurements of gamma-ray profiles. I am especially appreciative for the help of Damon Basset for teaching the fundamentals of carbon isotope geochemistry, sample preparation, and analysis. In addition, I would like to thank Ken MacLeod and Shannon Haynes at the stable isotope laboratory at the University of Missouri for allowing me access to their facility.

This thesis was made possible through the financial support from the American Association of Petroleum Geologists grants-in-aid of graduate research, the Geologic Society of America grants-in-aid of graduate research, and the Missouri State University Graduate College for funding this thesis research. Without this support, this project would not be possible.

Finally, I want to dedicate this thesis to all my family and friends whom were always there to support me. Especially my wife, Morgan, who always believed in me and my abilities.

TABLE OF CONTENTS

LIST OF TABLES

LIST OF FIGURES

INTRODUCTION

Composite geochemical studies of carbonate isotope values ($\delta^{13}C$) by previous investigators have established that the Cambrian period is punctuated by a series of significant, globally correlated, positive and negative $\delta^{13}C$ excursions (Zhu et al., 2006; Babcock et al., 2015). Isotopic excursions of large magnitude are thought to be the result of major perturbations in earth's biogeochemical cycles and are often associated with biotic crises (e.g. Palmer, 1984; Saltzman et al., 2000), as well as potential global cooling or warming events (Babcock et al., 2015). One of these significant and globally correlated positive $\delta^{13}C$ excursions is known as the Steptoean Positive Isotope Carbon Excursion or SPICE event (Saltzman et al., 2004). The SPICE event is a + 4 – 5 ‰ excursion of $\delta^{13}C$ values and is attributed to enhanced weathering and burial of isotopically light ^{12}C during eustatic fall (Saltzman et al., 2004). The SPICE event coincides with the formation of the Sauk II-III sub-sequence boundary and is believed to be related to this first order regressive-transgressive sea-level cycle (Saltzman et al., 2000; 2004). Although the SPICE event has been interpreted to be a result of a first-order sea-level cycle of Sloss (1963), it remains unknown if small-scale or low-amplitude variations in $\delta^{13}C$ values exist within or between higher-order sea-level cycles, such as fourth, fifth, or sixth order sea-level cycles.

In addition to secular variations in $\delta^{13}C$ values, meter-scale patterns of cyclic sedimentation are expressed in Cambrian rock throughout parts of the eastern Great Basin in Laurentia, the ancestral continent of North America (Osleger, 1991; Osleger & Read, 1993). However, no studies in the Great Basin have attempted to introduce the use of

high-resolution chemostratigraphic analysis on a cycle-to-cycle sampling interval to determine if small-amplitude secular variations of $\delta^{13}C$ values exist within these successions of fifth and sixth order carbonate cycles.

A mechanism for small-amplitude secular variations in $\delta^{13}C$ values could be a result of variations in earth's orbital parameters, known as Milankovitch cycles. Milankovitch cycles are a result of periodic changes in the precession, obliquity, and eccentricity of earth's orbit around the sun. These cycles occur at approximately 19-23 kyr, 41 kyr, and 99-125 kyr and 413 kyr periods respectively (Weedon, 2003). Fluctuations in astronomical conditions on the scale of Milankovitch cycles can influence environmental conditions, such as temperature and solar insolation, and thus affect carbon isotope values (Berger, 1978). Because the residence time of carbon in the carbon cycle is brief (10 kyr), fluctuations can be accurately recorded in the sedimentary record (Sharp, 2007). If these rhythmic sediments are a result of climatic forcing, the signal may be recorded in the isotopic record as low-amplitude, high-frequency secular variations in $\delta^{13}C$ between cycles of rock. Furthermore, if cyclic sedimentation is controlled by variations in earth's orbital parameters such as Milankovitch cycles, individual cycles may in fact represent a predictable period of time.

A key requisite for recording and preserving signals of astronomical forcing is near-complete deposition and high sedimentation rates. Rocks of Steptoean-Sunwaptan (Paibian-Jiangshanian) stage exposed in the Great Basin of Utah and Nevada experienced both rapid subsidence and high sedimentation rates (Miller et al., 2012). This interval also is characterized by family level trilobite extinction events (Palmer, 1965a); a major perturbation in the carbon cycle, the SPICE event of Saltzman et al. (2004); and, at least

in part, by anomalously uniform meter-scale carbonate cycles (Osleger, 1991; Osleger & Read, 1993). These characteristics make the Great Basin an exemplary candidate for exploring the relationship between carbon isotopes and cyclic strata.

The purpose of this study is to examine depositional patterns and carbon isotope ratios in the upper Steptoean and lowermost Sunwaptan stages in the eastern Great Basin. Within these parameters, it's hypothesized that secular variations of $\delta^{13}C$ exist between fifth-order carbonate cycles and that calculated sedimentation rates from correlative cyclostratigraphic records can be used to independently test the idea of Milankovitch-influenced cyclicity affecting oceanographic circulation. Power-spectral-analysis of stratigraphic $\delta^{13}C$ data is used to test for regular sedimentary cyclicity (periodicity) in the stratigraphic thickness domain (not time). Sedimentation rates calculated from published data determine the approximate periods at which spectral peaks would be expected if the succession was influenced by changes in orbital parameters. If peaks generated with spectral analysis compare favorably to Milankovitch forcing, it is a potential indicator that fluctuations in earth's orbital parameters influenced late Cambrian patterns of $\delta^{13}C$ variation and oceanographic circulation. In addition, if spectral peaks compare to peaks estimated from sedimentation rates, cyclostratigraphy allows for the prediction of a cycle periods in time. By coupling sedimentation rates with correlative cyclostratigraphic records the rate of isotopic change between cycles can be estimated (Weedon, 2006). Because sedimentary cycles typically represent a time interval below the resolution of traditional radiometric dating techniques, cyclostratigraphic methods provide a unique opportunity to approximate time intervals. Finally, peak spectral frequencies identified

with time series analysis were used to correlate cyclic strata, to test the practical use of cyclostratigraphic methods to regional correlations.

First, sequence stratigraphy, in combination with carbon isotope chemostratigraphy and gamma-ray profiles, were used for high-resolution correlations of cyclic sections between Utah and Nevada. Stratigraphic cross-sections were hung on the Pterocephaliid-Ptychaspid biomere boundary, allowing for near-synchronous correlation between stratigraphic sections at the crisis interval. A disconformable paleokarst surface was identified at three sections in Utah and is here interpreted as a sequence boundary. Utilizing stratal surfaces, strata stacking patterns, and depositional trends, all the sections have been placed in a systems tract model. This allows for interpretations of base-level change, subsidence, and ultimately accommodation to be made with some confidence. Once the regional depositional environments and sea-level trends are understood, time-series analysis was used to determine if there are periodic components encoded within carbon isotope profiles or gamma-ray profiles. If periodic components were detected, the cycles period (in meters) could compared to predicted periods that would be expected if the cycles were a result of climatic forcing such as Milankovitch cycles. This is done by calculating an approximate gross sedimentation rate for the Great Basin, allowing stratigraphic thickness to be viewed as time. Once a sedimentation rate was determined, an approximate timing is applied to each cycle. If timing assigned to each cycle (or bundles of cycles) matches the timing expected for astronomical forcing, it is a strong argument that these cycles may have been the result of allocyclic processes, such as climatic forcing related to Milankovitch cyclicity (Osleger & Read, 1993).

This investigation of late Cambrian cyclic carbonates indicates that secular variations of $\delta^{13}C$ values exist between carbonate cycles. Meter-scale cycles can be confidently correlated laterally over 60 km between sections in Utah. Cycles cannot be intrabasinally correlated cycle-for-cycle between sections in Utah and Nevada. Time series analysis of $\delta^{13}C$ data in the Northern Schell Creek Range in Nevada reveal four distinctive peaks within an 80% confidence interval that may correspond to astronomical forcing of sedimentation and putative Milankovitch style cyclicity in outer-shelf deposits of Laurentia.

BACKGROUND: A REVIEW OF PREVIOUS WORK AND CONCEPTS

Geology of the Great American Carbonate Bank

Strata exposed in the eastern Great Basin are among the most studied Cambrian rocks in the world (e.g., Palmer, 1965a; Hintze & Palmer, 1976; Hintze, 1988; Osleger & Read, 1993; Saltzman et al., 2000; Miller et al., 2012). Ranging from trilobite biotic crises (Palmer, 1965a) to major, globally correlated carbon excursions (Saltzman et al., 2000), much research has been conducted within this interval. This chapter aims to provide a brief literature review of previous work and a background on relevant concepts that will be built upon in this thesis.

The Great American Carbonate Bank (GACB) exposed in western Utah and eastern Nevada records a thick succession of Cambrian and Ordovician strata deposited on a tropical carbonate platform (Miller et al., 2012). Rapid thermal subsidence following the rifting of a Neoproterozoic continent generated enough accommodation to allow for the deposition of a nearly complete and conformable succession of mixed carbonates and siliciclastics (Miller et al., 2012). Accommodation refers to the amount of space available for sediment to accumulate (Catuneanu, 2006). These strata have been studied intensively because of their thickness, rich fossil content, and excellent repeated exposures in a series of mountain ranges due to Basin and Range extension (Walcott, 1908; Palmer, 1965a; Hintze & Palmer, 1976; Osleger & Read, 1993; Miller et al., 2012). During the Steptoean-Sunwaptan (Paibian lower Jiangshanian) stages, Laurentia was located at equatorial latitudes (Hintze, 1988) with Utah positioned just south of the equator. Nevada

was located to the paleo-North, more basinward and in somewhat deeper water than Utah, although still on the carbonate shelf (Fig. 1).

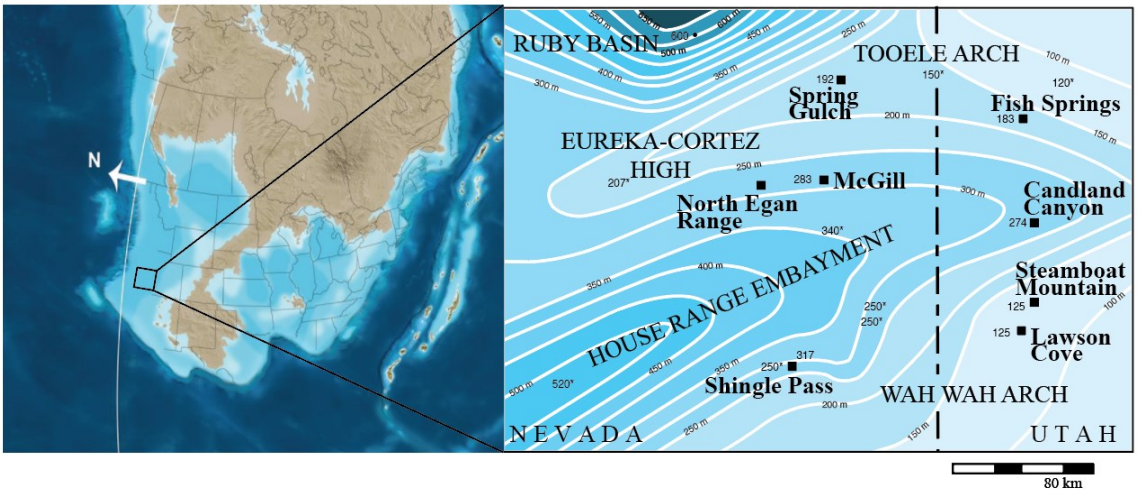

Figure 1 – Paleogeographic reconstruction of Laurentia during the late Cambrian (Blakey, 2013; left) and non-palinspastic isopach map (Evans, 1997; right). Measured thicknesses are shown in meters to the best available resolution.

There are several structural elements that affected sedimentation in the Great Basin during the middle through late Cambrian. Figure 1 depicts a paleogeographic reconstruction of Laurentia during the late Cambrian that highlights some of the most important structural elements. The map on the left is from Blakey (2013) and to the right is an inset non-palinspastic isopach map drafted by Evans (1997). Measured thicknesses of the entire Steptoean Stage are shown on the isopach map in meters to the best available stratigraphic resolution. Levy & Christie-Blick (1989) drafted palinspastic reconstructions in which the sections in Utah would be shifted westward and rotated slightly clockwise. However, the shift of these sections relative to one another does not significantly change the overall pattern observed in figure 1, and are excluded for this

reason (Evans, 1997). The House Range Embayment, a regional trough-like depression, remained at least into the late Cambrian. Strata within this depocenter shows westward thickening, however sections to the north and south thin (Miller et al., 2012). To the north is a topographically positive feature known as the Tooele Arch that extended westward from the ancestral Uinta Uplift (Evans, 1997). South of the House Range Embayment, sections in the Wah-Wah Mountains, Southern House Range, and South Egan Range are all located on a structural high known as the Wah Wah Arch (Evans, 1997; Miller et al., 2012).

The strata deposited during the late Cambrian have subsequently experienced several tectonic events and are now exposed as a series of isolated north-south trending mountain ranges (Hintze, 1988). During the Paleozoic, this region was disrupted along the north-south Antler orogenic belt in central Nevada by series of thrust faults (Palmer, 1971). During the Mesozoic, the Sevier orogenic belt disrupted the eastern margins of the region with parallel overthrust belts with large horizontal displacements (Palmer, 1971). Additionally, Mesozoic igneous intrusions have metamorphosed Cambrian rock in some sections (Palmer, 1971). A series of low-angle, and younger high-angle normal faults created some minor disruptions during the otherwise tectonically quiescent Cenozoic period (Palmer, 1971; Levy & Christie-Blick, 1989).

The Biomere Concept

Palmer (1965a) subdivided part of the upper Cambrian into regional, stage-level biostratigraphic units known as biomeres. Biomeres define geologically significant boundaries constrained by the abrupt extinction of the dominant elements of a single

phylum (Palmer, 1965a). Each biomere contains distinctive trilobite faunas that allow for relatively precise biochronostratigraphic correlation. Individual biomeres can be further subdivided into faunal zones, which are assemblages based on a few common taxa that

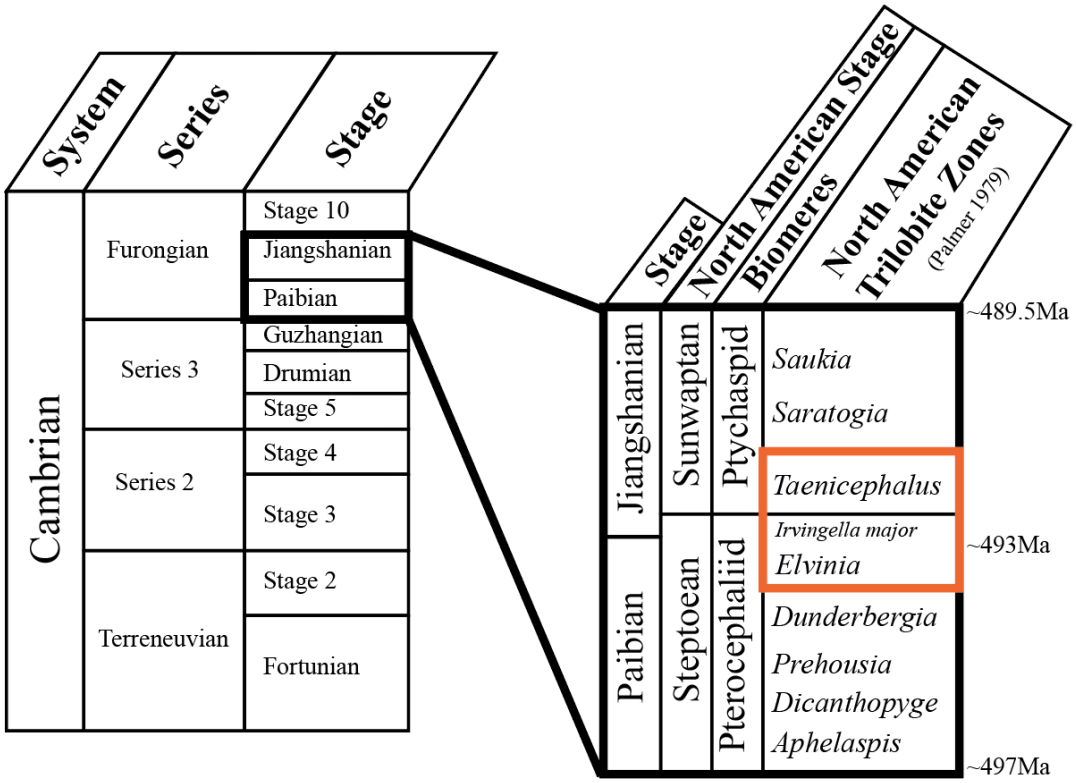

Figure 2 – Upper Cambrian chronostratigraphic and biostratigraphic framework. Trilobite zones and North American stages modified from Palmer (1979). Chronostratigraphy taken from the International Stratigraphic Chart 2016. The interval investigated in this thesis is approximated by the orange box.

are thought to show evolutionary succession (Palmer, 1965b). Each zone comprises a host of common to rare taxa and some species range through more than one zone. Despite the fossiliferous nature of biomeres, faunal zone boundaries within the biomeres cannot be constrained as precisely as the actual biomere boundaries (Palmer, 1984).

Three distinct Cambrian biomeres are recognized in Laurentia, the Marjumiid, the Pterocephaliid, and the Ptychaspid (Fig. 2; Palmer, 1965a; Palmer, 1984; Taylor, 2006). The base of the Pterocephaliid biomere coincides approximately with the base of the Paibian Stage (Steptoean stage in Laurentia) and the Furongian Series aged approximately 497 Ma (Peng et al., 2004). This study will focus on the upper Pterocephaliid and lower most Ptychaspid biomeres. Trilobite zones of interest after Palmer (1979) include in ascending order include the *Elvinia* and *Irvingella major* zones of the Pterocephaliid biomere, and the *Taenicephalus* zone of the lower Ptychaspid biomere (Fig. 2; Palmer, 1965a). Additionally, the inarticulate brachiopod *Linnarssonella girtyi* is found in conjunction with *Elvinia* zone trilobites (Kurtz, 1971; Evans, 1997) and can be used as a proxy index fossil for the base of *Elvinia*. Together, these faunal elements provide a relative timeline and serve as a correlation tool and datum for testing stratigraphic models. Biomere boundaries themselves commonly occur in a single bed and are thought to be nearly isochronous (Palmer, 1984). Therefore, these biostratigraphic horizons have chronostratigraphic significance. The bedset that contains the Pterocephaliid-Ptychaspid biomere crisis interval is distinctive, as the limestone transitions in color from light-medium gray to a dark gray, providing an approximate location to begin sampling trilobites (Evans, 1997). In addition to the biotic crisis, Saltzman et al. (1995) reported a positive shift of +2.0 ‰ in $\delta^{13}C$ values at the Pterocephaliid-Ptychaspid biomere boundary in Wyoming and Utah. This potentially provides an independent means for identifying the Pterocephaliid-Ptychaspid biomere boundary where faunal resolution is poorly constrained.

Although it is not the aim of this study to investigate the cause or causes of biomere extinctions, it is noteworthy to mention that Stitt (1975) published a widely-cited model that proposed the extinction boundaries represent cold, offshore waters rising onto the continental shelf. This model suggests as cool waters rise, shelf taxa are replaced by colder-water-adapted species from beyond the shelf break. This model has been debated (e.g. Westrop, 1988) but, as reviewed by Taylor (2006), evidence for this model is now available and suggests water temperature decline, relative sea-level rise, and potentially anoxic oceanic conditions at the trilobite turnover.

Carbon Isotope Geochemistry

Biotic crises observed in late Cambrian biomeres (Palmer, 1965a) have prompted studies of potential perturbations in the ocean-atmosphere-biosphere system during this critical period in Earth history (e.g. Saltzman et al., 1995; 2000). Stable carbon isotope geochemical methods are commonly applied to carbonates. Samples of carbonate material are analyzed by mass spectrometry to determine the ratio of stable isotopes of carbon, ^{13}C:^{12}C. This measured ratio is then normalized to a standard and is reported in delta notation (δ) with units parts per thousand or per mil (‰; Fig. 3). The standard established for Carbon-13 is the Pee Dee Belemnite (PDB) and is based on a Cretaceous Belemnite fossil from the Pee Dee Formation in South Carolina (Sharp, 2007). The Pee Dee Belemnite has an anomalously high ^{13}C : ^{12}C ratio leading to typically negative values. Much of the Cambrian is marked by secular variations in carbon isotope values (Fig. 3; Zhu et al., 2006). Variations are the result of long-term changes in the carbon flux in the oceans and from isotopic fractionation of carbon into reduced or oxidized

$$\delta^{13}C = \left(\frac{\left(\frac{^{13}C\ sample}{^{12}C\ sample}\right)}{\left(\frac{^{13}C\ standard}{^{12}C\ standard}\right)} - 1 \right) * 1000\ ‰$$

Figure 3 – Equation for delta notation (δ), from Sharp 2007.

reservoirs (Kump & Arthur, 1999). Drivers of these processes are hypothesized to be a result of fluctuations in continental weathering, sedimentation rates, organic carbon burial, primary productivity, or changes in oceanographic circulation (Saltzman et al., 2004). Four positive and six negative carbon isotope excursions punctuate the Cambrian period, five of which concede with major biotic crises (Fig. 4; Zhu et al., 2006). This suggests a relationship between some of the events, however not all carbon isotope excursions are correlated with extinctions. Because most of these events can be globally correlated, $\delta^{13}C$ profiles are an important tool for intercontinental correlation (Babcock & Peng, 2007). Chemostratigraphic studies of stable carbon isotope values from upper Cambrian strata in the Great Basin conducted by Brasier (1993) discovered a significant positive $\delta^{13}C$ excursion. These studies record one of the most prominent positive isotope excursions of the Phanerozoic, referred to as the Steptoean Positive Isotope Carbon Excursion (SPICE) by Saltzman et al., (2000).

The SPICE event is characterized by a globally correlated, positive $\delta^{13}C$ excursion of approximately + 4–6 ‰ (Fig. 3; Saltzman et al., 2000). The event has been measured in coeval sections in North America, China, Kazakhstan, and Australia (Saltzman et al., 2004). The SPICE event has been recorded spanning over 200 m of limestone at Shingle Pass, Nevada (Saltzman et al., 2000; 2004). This positive shift in

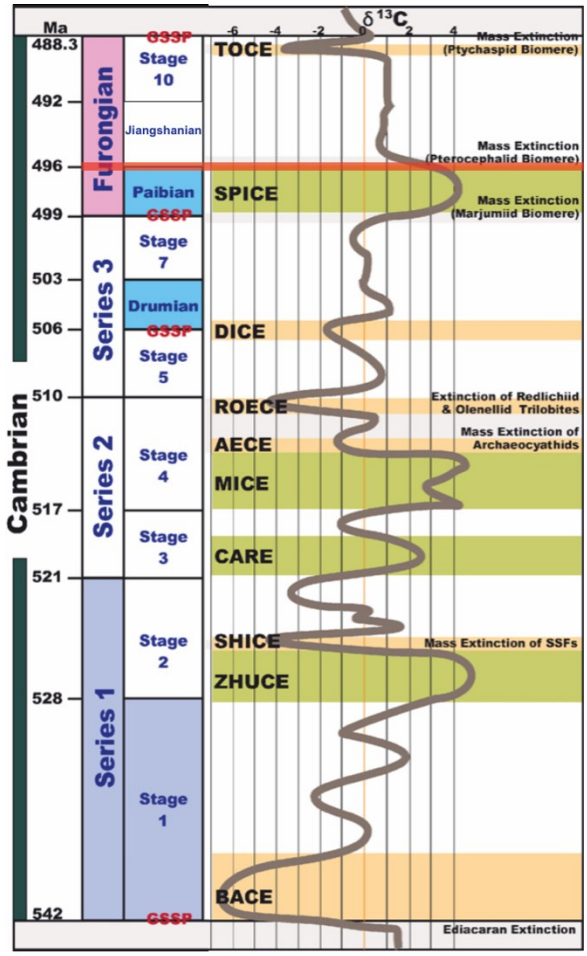

Figure 4 - Secular variation in δ13C throughout the Cambrian. Modified from Zhu et al. (2006).

carbon isotopic values has been interpreted to be the result of enhanced burial of organic carbon and is potentially driven by sea-level change at the Sauk II-III boundary (Saltzman et al., 2000; 2004). The duration of the SPICE event was estimated by Saltzman et al., (2004). Two U-Pb age dates, one at 491+/-1 Myr at the *Peltura scarabaeoides* zone and one at 503+/-4 Myr at the *Lejopyge laevigata* level span fifteen trilobite zones (Saltzman et al., 2004). This estimates that each trilobite zone spanned about 0.8 Myr on average. Therefore, he argued that the SPICE event, which spans the

Aphelaspis through mid-*Elvinia* zones, would have lasted approximately 3.6 Myr (Saltzman et al., 2004). However, accumulation rates likely would not remain constant over this great a period of time and more importantly, it does not account for hiatuses in sedimentation or erosion. Trilobite zones are not all necessary 0.8 Myr in duration nor would one expect trilobite zones to be uniform in duration. Nevertheless, it provides a general temporal range for the timing of the SPICE event and allows for assumptions of approximate timing of the interval examined in this thesis.

Sea-level History of the Pterocephaliid Biomere

Despite intensive study, models of sea-level change during the late Cambrian have had conflicting interpretations, mainly around timing. Here, an interpretation presented by Evans (1997; 2003; 2012) is applied. The Corset Spring Shale through the Hellnmaria members and its correlative units were deposited during a major relative sea-level rise and transgression that began in the *Elvinia* Zone (Evans, 1997; 2003). Unconformable surfaces exist within the succession, although no significant break in sedimentation is recognized between the interpreted sequence boundary in the Corset Spring Shale and the Hellnmaria member. The simplest explanation for a major long-term sea-level rise could be due to recession of large-scale glaciers, however there are no known glacial deposits of Cambrian age. An alternative explanation for sea-level rise could be tectonic. Following the breakup of a Proterozoic supercontinent, the Cambrian was a period of major tectonic reorganization (Miller et al., 2012). Variations in sea-floor spreading rates or mid-ocean ridge lengths and the emplacement of oceanic plateaus have been shown to produce sea-level rise (Miller et al., 2005). Sea-level rise, rapid thermal

subsidence, and a paucity of disruptive events are key requisites for a nearly complete record of sedimentation. Conditions in the Great Basin were more favorable given these requisites, but the actual record may respond to a variety of external perturbations that may in turn have disrupted sedimentation.

Past Studies of Meter-scale Cycles

A well-known and often cited study of upper Cambrian cycles was conducted by Osleger & Read (1993). In this study, late Cambrian carbonate cycles were correlated across the United States, from the Appalachians to Utah and Texas to southern Oklahoma. The section in Utah was measured at Orr Ridge, just several kilometers from the Candland Canyon section measured in this study. The propose was to assess the use of quantitative techniques, such as Fischer plots and subsidence analysis, to determine accommodation history across the North American Craton. Fischer plots allow for the determination of 3rd-order or higher sea-level fluctuations from high-frequency cycles (Osleger & Read, 1993). The plot consists of two axes, one representing relative time (or average cycle thickness) and the other representing the actual stratigraphic thickness of the cycles. The thickness of the cyclic interval divided by the number of cycles is equal to the average cycle duration (Osleger & Read, 1993). The plotted difference between these values is presumed to represent changes in accommodation over time.

Fischer plots are prone to several limitations. For example, they do not consider variability in sedimentation rates, cycle duration, or the compaction of sediment. Also, missing cycles referred to as "missed beats" can lead to erroneous results. Finally, this technique will not work in non-cyclic successions, regular cycles must be present.

Alternative methods for studying cyclic successions have since been developed and will be covered in the following section on cyclostratigraphy.

Cyclostratigraphy and Milankovitch Cycles

Cyclostratigraphy is the study of environmental cycles recorded in the stratigraphic record (Fischer et al., 1990). This methodology was profoundly influenced by the development of two concepts: Milankovitch theory and sequence stratigraphy. Milankovitch theory, calculated and published by Milankovitch (1941), explains changes in climate due to perturbations in the earth's orbit around the sun. Changes in orbit are due to the gravitational interaction between the Sun, the Earth, the Moon, and the planets. As the orbital configuration varies, the amount of solar radiation reaching earth (insolation) will vary, leading to changes in climate (Weedon, 2003). The changes in orbital parameters occur as periodic cycles that operate on a time scale of thousands of years. Changes in precession occur between 19-23 kyr, changes in obliquity occur around 41 kyr, and changes in eccentricity occur at approximately 95-125 kyr and 413 kyr intervals (Weedon, 2003).

Eccentricity is the term used to describe the elliptical shape of the Earth's orbit around the Sun. This elliptical orbit is due to interactions with gravitational forces from Jupiter and Saturn (Weedon, 2003). The eccentricity of the Earth is not constant and varies on a predictable time-scale. The most important period of eccentricity occurs at 413 kyr, with a superimposed 95 and 125 kyr cycle (Algeo & Wilkinson, 1988). The 95 and 125 kyr periods loosely superimpose into an approximately 100 kyr cycle that is often recognized in the cyclostratigraphic record (Weedon, 2003). Additionally, long-

term, small amplitude variations with a modern period of 2.4 Myr have been identified in stratigraphic records (Hilgen et al., 1995). This long-term variation in eccentricity has been shown to modulate, or alter the amplitude or the frequency of the precession signal (Weedon, 2003), however this affect is often limited due to the protracted time-scale and low-amplitude variation in the eccentricity. Here, amplitude refers to the change of a periodic variable (i.e. $\delta^{18}O$, $\delta^{13}C$, $\%CaCO_3$, %TOC, etc.) over one orbital period, and the frequency refers to the number of occurrences of repeating components per unit thickness (cycles per meter). The frequency is equal to the reciprocal of the orbital period.

Obliquity, or the axial tilt of the Earth's orbit varies between 22.1º to 24.5º with a dominant period of approximately 41 kyr (Weedon, 2003). Earth's obliquity stays within this relatively narrow range due to the moon's capacity for stabilizing the planet gravitationally (Algeo & Wilkinson, 1988). The tilt of the Earth is ultimately responsible for the existence of the seasons. If the axial tilt was equal to zero degrees, the sun would take the same path over the equator every day with both the northern and southern hemispheres receiving the same amount of insolation. When obliquity reaches its minimum (22.1º), insolation decreases resulting in more intense winters and mild summers in both hemispheres. Conversely, when obliquity reaches its maximum, insolation increases resulting in warmer summers and milder winters. The annual changes in insolation from obliquity are most evident at higher latitudes where the Earth is more sensitive to changes in insolation (Weedon, 2003).

Axial precession, or wobble, describes the direction of the axis of the Earth at a point in time relative to the stars (Weedon, 2003). Precession has a calculated period of approximately 26 kyr, and is a result of gravitational interactions between the Sun and the

Moon acting on the Earth. Because of axial precessions gyroscopic motion, seasons in each hemisphere do not remain constant over this 26 kyr period. Currently, summer in the southern hemisphere occurs at perihelion (point at which Earth is closest to the Sun). However, in 13 kyr at perihelion, the north pole will be tilted more towards the sun and summer will occur at aphelion in the southern hemisphere (point at which Earth is farthest from the Sun). In addition to axial precession, eccentricity also precesses in space and complicates the concept of precession. As the direction of the tilt of the Earth changes, the eccentricity of Earth is simultaneously rotating in a counter-clockwise ellipse. This phenomenon is known as apsidal precession and results in a in a modified precessional period, so the period is actually closer to 21 kyr. Because variations in eccentricity modulate the amplitude of this cycle, axial precessional durations vary between 19 and 23 kyr (Weedon, 2003).

The *caveat* to the timing of these parameters is that not all Milankovitch orbital periodicities have remained constant throughout the Phanerozoic (Algeo & Wilkinson, 1988). Precession and obliquity periods would have changed due to the evolving Earth-Moon system (Weedon, 2003). It has been calculated that at the beginning of the Phanerozoic the precession would have been approximately 17 kyr and obliquity would have been 28 kyr (Walker & Zahnle, 1986). However, because eccentricity is a result of interplanetary gravitational interaction, the periods of approximately 100 kyr and 400 kyr would have likely remained stable for the at least the Phanerozoic (Algeo & Wilkinson, 1988). Solutions for the orbital history of Earth dating back to the Permian (~250 Myr) have been calculated by Laskar et al. (2011). For rocks of this age or younger, data can be tuned using the orbital solutions as a target (Weedon, 2003). Orbital tuning involves

matching cyclic patterns of sedimentological climate data with cyclic changes in orbital parameters predicted by Laskar et al. (2011). The basis for the astronomical tuning method is grounded by the fact that changes in climate records are directly related to changes in insolation (Weedon, 2003). If tuned data favorably matches the orbital solutions, it is a strong argument for Milankovitch style cyclicity and ultimately serves as a method to accurately date intervals of sediment (Weedon, 2003). However, for Paleozoic rocks older than Permian in age, a different approach must be taken. For pre-Mesozoic successions, sedimentation rates are commonly used to approximate expected Milankovitch periods (Weedon, 2003). A mean sedimentation rate is calculated by measuring the thickness of strata between two dated horizons. This will allow for the approximation of how many centimeters or meters accumulated per thousand years. In the absence of radiometric dates or an orbital-tuning target, an obvious problem is the potential for unknown and unaccounted for gaps in sedimentation. Nevertheless, power-spectral analysis is conducted on the time-series data to detect periodic components. These calculated periods are then compared to the predicted periods expected if the succession was the result of astronomical forcing. Although it cannot be demonstrably shown that pre-Mesozoic successions lacking radiometric dates correlate directly to Milankovitch forcing, these methods can provide invaluable information about the timing of a succession and the possible controls on sedimentation.

In addition to Milankovitch theory, the advent of sequence stratigraphy influenced the development of cyclostratigraphy. Sequence stratigraphy studies sedimentary sequences, which are defined as unconformity bounded packages of genetically related strata (Vail et al., 1977). Sequence stratigraphy explains the expression of sedimentary

stacking patterns and stratal geometries as a result of changing accommodation. One of the major controls on accommodation is changes in relative sea-level. During the early development of sequence stratigraphy, Sloss (1963) devised a classification system of depositional sequences based on the duration of sea-level cycles. These range from first order sequences (lasting more than 50 Myr) to sixth order sequences (10 kyr to 30 kyr; Sloss, 1963; Vail et al., 1977). The duration of these sea-level cycles provides clues to the processes responsible for their generation. Generally, higher-order sequences (fifth and sixth-order) or parasequences are thought to be a result of Milankovitch cycles. A parasequence is a relatively conformable, genetically related succession of beds or bedsets bounded by marine-flooding surfaces or their correlative surfaces (Van Wagoner et al., 1988). In addition to the development of cyclostratigraphy, sequence stratigraphy coupled with biostratigraphy is a powerful tool for regional and interregional correlations (Weedon, 2003). Tuned astronomical records can often be correlated based on periodic components that are present in the record. However, pre-Mesozoic successions lacking a tuned orbital history or accurate radiometric dates requires traditional methods, such as sequence stratigraphy for reliable correlations.

The earliest cyclostratigraphic studies built upon the Milankovitch Theory and the concept of Sloss sequences. Schwarzacher (1975) developed the concept that the thickness of successive beds provides information of fundamental importance in the understanding of sedimentary cyclicity. Thickness of a depositional unit may be directly related to the timing of deposition. This is one of the first studies to recognize that stratigraphic data can be collected and analyzed as a time-series. Shortly after the work of Schwarzacher (1975), studies of remnant magnetization in deep-sea drill core, coupled

with radiometric dates, demonstrated that Milankovitch cyclicity is a reasonable explanation for Pleistocene climate change (Hays et al., 1976). Hays et al. (1976) discovered within cyclic ocean sediments, bounded by radiometric age dates, discrete spectral peaks occurring at periods of 23 kyr, 41 kyr, and 100 kyr. These periods correlate well the periods of precession, obliquity, and eccentricity, respectively.

Fischer et al. (1990) defined cyclostratigraphy as the description and study of cyclic sedimentary successions. Shackleton et al. (1999) confirmed the validity of independently derived orbital cycle chronologies based on tuning sedimentary cycles and oxygen isotope curves to calculated Milankovitch cycles and cross-checking with radiometric ages. This has resulted in the development of an astronomical time-scale of part of the Cenozoic (Shackleton et al., 1999). Serro et al. (2000) conducted a similar study on Cretaceous rocks and established an astronomical time-scale for part of the Mesozoic. Current research has shifted focus to establishing an astronomical time-scale for pre-Mesozoic cycles (Weedon, 2003). Wu et al. (2013) suggested an astronomical time-scale for Permian rocks, the first ever for the Paleozoic. In the Wu et al. (2013) study, radiometric dates of the Permian strata aligned remarkably close to the astronomical time-scale that was calibrated for these rocks. Although, studies of astronomical forcing on Cambrian rocks is limited, stratigraphic sections in the Great Basin may provide an excellent location for applying cyclostratigraphic methods. As deposition took place during a major relative rise of sea-level in a region that experienced both rapid subsidence and high sedimentation rates with few obvious hiatuses in the successions (Evans, 1997; 2012; Miller et al., 2012).

METHODS

Stratigraphic Sections and Sampling

Stratigraphic sections were measured and described on a centimeter-scale at four locations in Utah and four locations in Nevada. The sections measured in Utah include: The Fish Springs Range, Candland Canyon, Steamboat Mountain, and Lawson Cove.

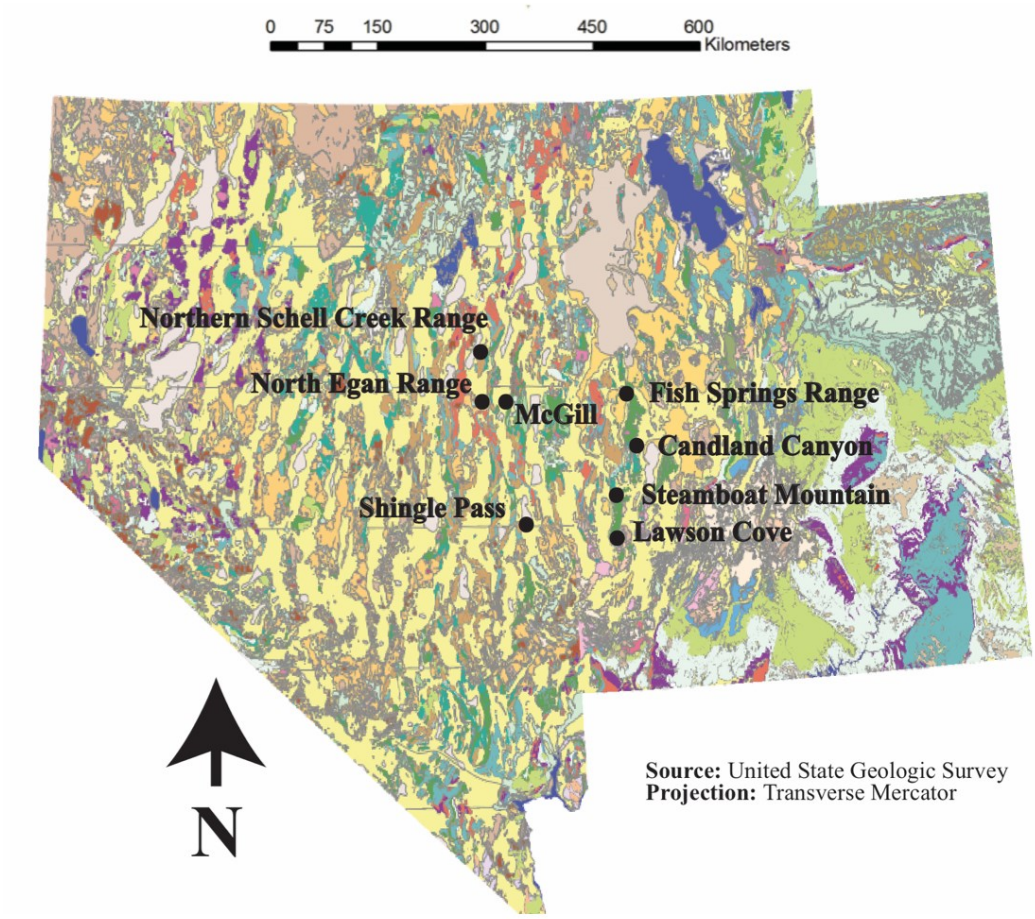

Figure 5 - Georeferenced geologic map of Utah and Nevada depicting the eight stratigraphic sections measured in this study.

Section measured in Nevada include: Spring Gulch, the North Egan Range, McGill, and Shingle Pass (Fig. 5).

Detailed descriptions of each section can be found in the results section. Accompanying drafted stratigraphic sections are in Appendix A, along with GPS coordinates of each section. All the sections were drafted in MATLAB using the MatStrat package (Lewis et al., 2011). The exact thickness and lithologies of each cycle along with gamma-ray values and carbon isotope ratios were recorded in Microsoft Excel and uploaded into MATLAB for precise drafting. This allows for the exact measured thickness of each bed to be drafted and for precise placement of gamma-ray measurement points and carbon isotope values.

Each section was carefully selected based on the quality of exposure of the Sneakover limestone or its equivalents or for the potential for repeatability of previous studies (e.g., Shingle Pass). Each section was measured and discretely painted using a Jacob Staff. Detailed descriptions of lithofacies, sedimentary structures, and contacts were made along with accompanying digital photographs. A focus was put on surfaces of significance, such as unconformities and lithologic transitions, as these contacts determine the placement of systems tracts and allow for interpretations about relative sea-level.

Carbonate samples were collected for stable isotope ratio analysis from sections at Candland Canyon, Utah and Spring Gulch, Nevada. All samples were collected at an equally spaced interval of 25 cm where possible. This is done for two reasons: first to provide high-resolution data for correlations of $\delta^{13}C$ profiles across the Great Basin and as a necessary requirement for most power-spectral/time-series analysis. Mathematically,

a time-series is a continuous function and is commonly decomposed into its components waveforms with a Fourier transform (Weedon, 2003). However, continuous sampling of the outcrop is not possible, so discrete and arbitrarily close points were selected. Utilizing summations as opposed to integrals in the Fourier transform allows for the decomposition of a time-series that is represented by a series of discrete sample points. Since observational time-series are discrete points, it is impossible to detect instantaneous changes in $\delta^{13}C$, instead there is a limit to the highest frequency information that can be obtained from real data known as the Nyquist frequency (Weedon, 2003). The Nyquist frequency is defined as 1/(2 x sample interval). This definition assumes that samples are taken at a constant depth interval (Weedon, 2003). With a 25 cm sampling interval, the Nyquist frequency is 2 cycles per meter, meaning that up to 2 cycles per meter can be detected, allowing for cycles with a minimum wavelength or period of 0.5 m to be measured. Periodicities smaller than the spacing of two data points cannot be reliably detected (Hammer et al., 2001). This sampling should be sufficient because most of the cycles are on the scale of one-meter or thicker. Although measures have been taken to avoid problems arising from improper sampling, it remains uncertain that these sedimentary successions actually reflect deposition at invariable rates or that bioturbation and other process have not affected them. Assumption of uniform time is inherent in the analysis and the source for potential error.

Additional samples for isotope analysis were collected from the disrupted surface in a limestone bed at Lawson Cove and at Steamboat Mountain. Although geochemical studies have shown the robust nature of carbon isotope records (O'Neil, 1987), secondary alteration and diagenesis are still of concern. Samples were recovered from outcrop using

rock hammers while taking special care to avoid weathered, fractured, and diagenetically altered zones. Poor exposures were avoided by laterally tracing beds to better exposures.

Gamma-ray Profiles

In addition to stratigraphic measurements and lithostratigraphic descriptions, gamma-ray profiles were measured using a Urtec Miniscint UG130 solid-state crystal spectral scintillometer. Gamma-ray logs are commonly used in the oil industry to aid in precise correlation from near-shore to offshore facies. The source of gamma-rays is from the natural decay of radiogenic nuclides such as uranium, thorium, and potassium. These elements are typically found in higher concentrations clay-rich rocks. Fine-grained mudrocks such as shale and siltstone produce higher values, whereas mature quartz sandstone and limestone will produce lower values. The basic concept is that when a gamma-ray strikes a NaI crystal within the scintillometer, there is some probability that the gamma-ray will be captured. If it is captured, photons will be emitted and a photomultiplier mounted to the opposite side of the crystal will convert the light into an electronic pulse which is counted and displayed as a value in Counts Per Second (CPS). Values here were recorded as a 10 second average in CPS. This is a relative measure, so absolute values are not comparable between different sections, however, unique or distinctive shifts in the gamma-log response can be identified and correlated over long distances. The persistence of geological attributes over a significant area is key to differentiating regionally controlled stratal units from local depositional effects.

Isotope Sample Preparation and Analysis

Upon return to the Laboratory, samples were cut with a rock saw, washed in an ultra-sonic bath, and rinsed with deionized water. Homogenous micrite was targeted and microdrilled from surfaces without any obvious secondary diagenetic features. Carbonate carbon ($\delta^{13}C$) preserved in micrite has been shown to be rock-buffered over a wide range of diagenetic settings commonly encountered in ancient carbonate successions (Kump and Arthur, 1999; Saltzman et al., 2004). Whereas, $\delta^{18}O$, which is commonly used for calculating paleo-temperatures, is easily reset during diagenesis (Saltzman et al., 2004). Despite $\delta^{13}C$ resistance to diagenesis and potential for primary recovery, diagenetic alteration is still a concern and measures were taken to avoid any obvious signs of alteration (i.e. calcite veins, weathered surfaces, etc.).

Carbonate Carbon ($\delta^{13}C$) and Oxygen ($\delta^{18}O$) Isotope Analysis

Measurements of carbon ($\delta^{13}C$) and oxygen ($\delta^{18}O$) isotopic values on bulk carbonates were made at the University of Missouri biogeochemistry stable isotope laboratory. Approximately 50 μg of powered carbonate was reacted with 103% phosphoric acid for 4 minutes at 70°C using a Kiel III automated carbonate device. Evolved CO_2 gas was cryogenically cleaned and analyzed on a Thermo Finnigan DeltaPlus mass spectrometer operated in dual inlet mode. Results for each run were normalized to the National Bureau of Standards (NBS)-19 standard with nominal values of -2.20‰ and +1.95‰ for $\delta^{18}O$ and $\delta^{13}C$ respectively. Results for uncorrected measurements of NBS-19 run during the course of the study indicate an external

analytical precision of 0.02‰ (±1σ) for $\delta^{13}C$ and 0.06‰ (±1σ) for $\delta^{18}O$ values. All results are reported in delta (δ) notation relative to the Pee Dee Belemnite (PDB) scale.

Sequence Stratigraphy

Before any paleoclimatological interpretations can be made the sedimentation patterns and depositional environments must be understood. For example, variations in sediment influx and accumulation rates may affect the preservation of climatic signals in rhythmically bedded strata (Weedon, 2003). Here, a sequence stratigraphic systems tract model was developed to better understand variables controlling sedimentation such as the interplay between sediment influx, base-level changes, subsidence rates, and accommodation (Catuneanu, 2006). The framework is interpreted to have been formed during changes in relative or eustatic base level (Van Wagoner, 1995). This leads to the formation of surfaces of sedimentary significance, such as unconformities and flooding surfaces, that are then used to interpret the depositional setting.

Sequence stratigraphic models of mixed clastic and carbonate sequences differs from that of a purely siliciclastic system (Fig. 6). The systems tract model was developed to subdivide packages based on stratal stacking patterns. Here, the ideal model will be presented. In nature, factors such as sedimentation rates or the rate of sea-level change may be extremely variable and the predicted behaviors of the systems tracts may not always manifest. When describing the basic systems tract model, it is simplest to begin following a highstand of relative sea-level. As relative sea-level falls, a sub-aerial surface of erosion will form in the underlying highstand systems tract (HST). This unconformable surface is termed a sequence boundary (SB). Basinward, where subaerial

erosion did not occur, this surface is called a correlative conformity (CC). When relative sea-level reaches a minimum, the package of sediment deposited is referred to as the low stand systems tract (LST). The LST typically is characterized by shallower water conditions and is dominated by clastic sediments which inhibit the precipitation of carbonates (Kendall & Schlager, 1981). As relative sea-level rises during transgression, basinward regions are starved of siliciclastic input and progradation of carbonates may initiate. The resulting surface of onlap between these two sedimentary packages is referred to as the transgressive surface (TS).

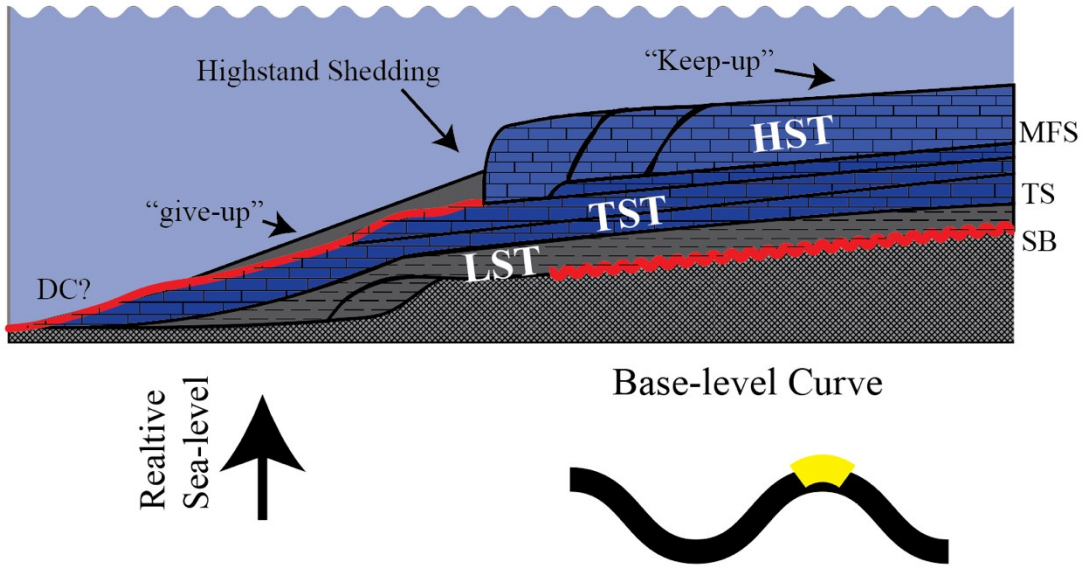

Figure 6 - Sequence stratigraphic model of mixed carbonate and siliciclastic succession, after Catuneanu (2006).

With continued transgression, carbonates are able to "keep-up" with sea-level rise as clastic input is starved. The package of rock that is deposited is called the transgressive systems tract (TST) Successions may exhibit fining-upward, retrogradational, or

backstepping parasequences (Van Wagoner et al., 1988). However, if sedimentation rates are high the parasequences may aggrade. As relative sea-level reaches near maxima, carbonates in offshore or shelf margin deposits may become stressed due to the deeper water depths and low light conditions. Additionally, the carbonate composition depth (CCD) may be exceeded and carbonate precipitation may become chemically impossible (Sharp, 2007). This forces the carbonates to "give-up" and a drowning unconformity may be formed, and preserved as a carbonate hardground (Catuneanu, 2006). However, in more near shore deposits, carbonates will be able to "keep-up" with the rising sea-level. The TST terminates when sea-level reaches a near maximum depth. The surface that forms is referred to as the maximum flooding surface (MFS). As sea-level rise begins to slow, highstand normal regression will begin the fill the basin with HST carbonates. However, if the volume of carbonate sediment is to exceed the available accommodation, the over budget in sediment will be shed to the deep-water environment and a significant accumulation of clastic carbonates may occur on the slope or the basin floor (Catuneanu, 2006). Late in the HST as relative sea-level begins to fall, offshore regions may "catch-up" and carbonate deposition may resume on the shelf margin (Kendall & Schlager, 1981). Following the HST, as relative sea-level falls and forced regression ensues, subaerial erosion and the formation of a sequence boundary will occur, and the depositional cycle will hypothetically repeat.

The workflow used to subdivide rock packages into a systems tract model is as follows. First stratigraphic sections were drafted and interpretations about the vertical stratal succession, such as bed-set stacking patterns were identified. Next, candidates for flooding surfaces and sequence boundaries were interpreted using changes in bed-set

stacking patterns and parasequence stacking patterns. When these surfaces were interpreted, all the section were hung on the Pterocephaliid-Ptychaspid biomere boundary. Once the sections were datumed, correlations of flooding surfaces and sequence boundaries were made. Cycles were correlated next, working from the bottom of the section up until correlation became problematic. Then working downwards from the datum until correlation became problematic. As a final step, the parasequence stacking patterns and inferred stratal geometries were used to interpret systems tracts and make inferences about relative sea-level.

Time Series Analysis

Spectral time-series analysis was conducted on both gamma-ray profiles and carbon isotope profiles to determine if any periodicities exist within the data. This was achieved by applying a Fourier Transform. Per Fourier's theorem, any time-series can be recreated by adding together a series of sine and cosine waves of the correct wavelength and amplitude (Weedon, 2003). This holds true for all time-series, no matter the complexity or shape, assuming there is some oscillation in the series and no infinite values. All time-series can be thought of as an orthogonal function, simply the sum of a series of sine and cosine waves (Weedon, 2003). Therefore, the time series can be decomposed into these components.

One of the most common techniques for decomposing a time series into its component waveforms is using power-spectral analysis. When plotted, the power spectrum depicts the squared amplitudes and wavelength (or period) of any regular components in the data (Fig. 7). Frequency is plotted on the horizontal axis by convention

with the lowest frequencies plotting farther to the left. The period of a cycle is defined as the time elapsed between two values of approximately the same magnitude. The frequency is the number indicating how many repetitions of a cycle occur per time interval. Frequency is equal to the reciprocal of the period (1/period), and from this relationship, the period, with units in cycles per meter can be determined. An example of this procedure is depicted in Figure 7. Here, two waveforms with wavelengths of 10.0 m and 2.78 m are added together to form the time-series on the left side of the figure. Although this time-series is just the sum of two waveforms, the expression of the summed waves is significantly more complicated than a simple sine or cosine wave.

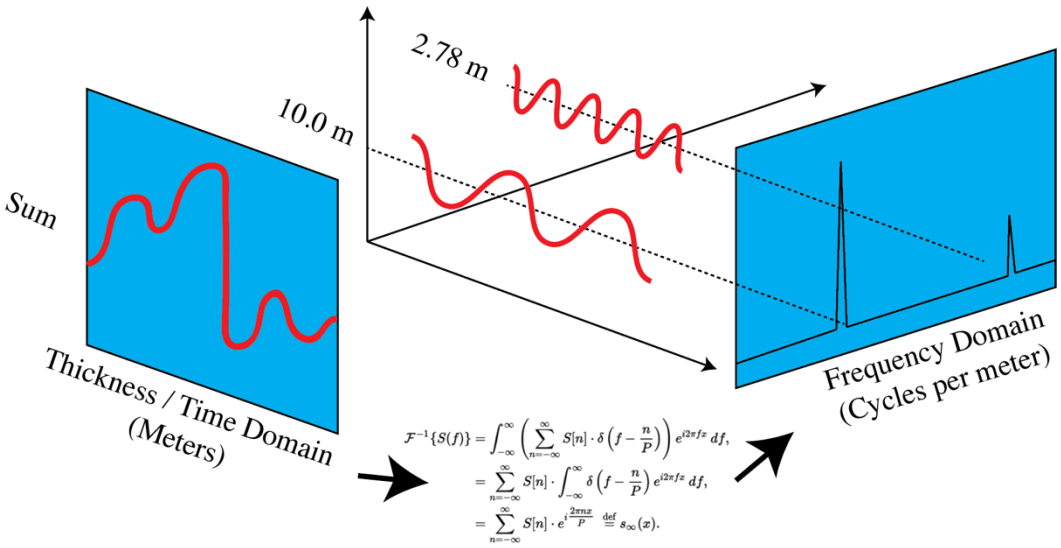

Figure 7 - Example of a Fourier Transform. The time series on the left is composed of two wave lengths at 10.0 m and 2.78 m. A Fourier Transform can decompose this sinusoid into its component wave forms which are then plotted to the right as power spectral peaks. Two peaks occur and correlate to the two wave forms that made up the original time series. Example after Weedon (2003).

In addition to the time series, the resulting power-spectrum is plotted to the right. Two peaks of equal height are depicted. The first peak corresponds to the lower frequency 10 m wave and the other peak to the right corresponds to the 2.78 m wave. The height of both spectral peaks is the same because the amplitude of both the 10 m and 2.78 m waves is the same.

A variety of computer programs exist for time series analysis. For the purposes of this study, a program called PAleontological STastistics (PAST) was used. PAST is an open source software package that contains numerous functions for plotting, data manipulation, univariate and multivariate statistics, spatial analysis, and time series analysis (Hammer et al., 2001). Two modules were used extensively used in this project: (1) the REDFIT spectral analysis and (2) sinusoidal regression. The REDFIT spectral analysis module is based on the REDFIT method developed by Schulz & Mudelsee (2002). This Fourier-based method fits the time-series to a first-order autoregressive (AR1) process, also called a red noise model (Schulz & Mudelsee, 2002). Fitting time-series data to a simple noise process is a common method used to assess the statistical significance of spectral peaks (Weedon, 2003). Red noise is a concept based on the random motion of particles in a fluid known as Brownian motion (Hammer et al., 2001). Red noise is a seemingly random, stochastic process with constant variance and zero mean. The REDFIT module uses a time series composed of purely red noise and fits it to the time series under investigation (Schulz & Mudelsee, 2002). This technique tests the null hypothesis that the power spectrum was generated purely by red noise. Any periodicity present in the data will not fit the REDFIT model and will show up as spectral peaks when plotted.

The REDFIT method in PAST allows the user to determine several mathematical parameters to be used in the Fourier transform. These parameters include the window function, oversampling, and time series segmentation. Choosing a proper window function is important to avoid periodogram or spectral leakage, which can lead to underestimated or false spectral peaks (Weedon, 2003). Spectral leakage is also referred to as side-lobe rejection (Hammer et al., 2001). Although the specifics of windowing functions are outside of the scope of this thesis, the basic idea is that data in a geological time series ends abruptly where sampling is discontinued; the time series is not closed form. That is, the value at the start of the time series does not match the final value. This discontinuity allows some of the "power" of the real peaks to escape laterally, or "leak" because the periods do not converge on a common point. This phenomenon is known as periodogram or spectral leakage and appears in a power-spectrum as low-amplitude components from every frequency (Weedon, 2003). By applying a window function, the oscillations of a time series are tapered near the ends, making the time series closed form, effectively reducing the effect of spectra leakage. The default setting in PAST uses the simplest window function, known as a rectangular window. A rectangular window will provide high spectral resolution although it is prone to periodogram leakage. Other window functions, such a triangular window, allow for the shape of the window or taper to be controlled. For example, a triangular window is less prone to periodogram leakage and has little effect on spectral resolution. The tradeoff between periodogram leakage and spectral resolution seems to be best managed with the triangular window and is the window function used for $\delta^{13}C$ analyses. A Blackman-Harris window gives the lowest spectral resolution, but is the least prone to spectral leakage. This window is used for

time series that contain a significant amount of noise and need to be smoothed. Due to the low spectral resolution, this window is prone to missing high-frequency, low-amplitude periods and should be used in conjunction with other window functions.

Oversampling specifies the number of points to be sampled along the frequency axis beyond the Nyquist frequency. Individual values in the time series are sampled multiple times and each time the value is sampled, random noise is added. Averaging the multiple samples together produces a new value in which the noise is reduced by the oversample factor. This is done namely to improve resolution and reduce noise in the time series. In addition to oversampling, the time series may be segmented into discrete packages. By increasing segments, noise in the time series can be reduced, however this also can drastically decrease the spectral resolution in the time series.

The other PAST module that was used extensively is sinusoidal regression. Also known as sinusoidal curve fitting, this method uses a matching pursuit algorithm to sum up to eight sinusoids with specified periods, allowing for the reconstruction of nearly any time series (Weedon, 2003). It provides a robust means for checking how well calculated periods from a time series actually fit the data. This procedure is essentially the antithesis of power-spectral analysis and can be carried out in PAST one of two ways. Either the user can enter periods, typically calculated from power-spectral analysis of time series data or from cycle thickness and bundling, or periods can be calculated using the "fit periods" option, which will sequentially optimize the period of the component sinusoids up to the Nyquist frequency (Hammer et al., 2001). This is achieved by fitting a sinusoid form to a period and then subtracting area this sinusoid before fitting the next period. After sinusoidal regression is run, the resulting period-optimized time series is plotted on

the original data set to visually check the fit. In addition, a X^2 (chi-square) value, a coefficient of determination or Pearson's product (r^2), and a p-value based on an F-test are also calculated (Hammer et al., 2001). A small X^2 value or an r^2 value close to 1.0 represents a good fit. The p-value gives the significance of fit between the two models by testing the null hypothesis that the model fitted provides a statistically poorer fit than original time series. The null hypothesis is rejected if is $p \leq 0.05$. PAST allows for sinusoidal regression using either sine or cosine waves or a combination of the two waveforms, known as free phase. In this analysis, the free phase option was used to optimize the fit of the sinusoidal regression.

In addition to spectral analysis of $\delta^{13}C$ values, gamma-ray profiles from each section were also analyzed to determine if periodic components can be identified in the logs. However, using gamma-ray counts for spectral analysis is potentially problematic. Measured gamma-ray values are the result of the natural decay of radiogenic nuclides within a rock. Higher values are produced from clays and shales which are often rich in potassium. This a lithology dependent effect which reflects the environment of deposition, however may not record climatic conditions at the time of deposition. Nevertheless, frequencies identified are compared to expected frequencies estimated from long-term sedimentation rates. Spectral analysis of gamma-rays also provides a means for testing the use of time-series analysis for correlation purposes. The concept is that if cyclic successions are correlative bed for bed, the spectral signature from both sections should show parallel behavior. However, differences in subsidence, sediment flux, accommodation or more importantly, differences in clay mineral fractions among lithologic types may distort these values leading to erroneous spectral peaks.

Estimated Sedimentation Rates

Limitations of the astronomical solutions of Laskar (2011) prevent the tuning of stratigraphic time-series to calculated orbital periods beyond 250 Myr. To determine if periodicities potentially relate to climatological or astronomical forcing in successions from the early Paleozoic, long-term sedimentation rates are used. First an approximation of the mean accumulation rate in centimeters-per-one-thousand (cm/kyr) years is derived from calculated sedimentation rates of others. This value is then multiplied by the number of years corresponding to precession (19-23 kyr), obliquity (41 kyr), and eccentricity (99-123 & 413 kyr), approximating the periodicities that would be expected if the cycles were directly influenced by astronomical forcing. If the periods approximated with accumulation rates match the periods in the time series data, it is a strong argument that these cycles may have been influenced by astronomical forcing. Moreover, this associates sedimentary thickness with the time-domain and allows for the approximation of the rate of cycle development and isotopic variation. Estimated accumulation rates in the Great Basin will be determined in the results section.

RESULTS

Stratigraphy of Measured Sections

Rocks exposed in stratigraphic sections are central to the interpretation of marine successions. Aside from allowing the construction of regional correlations and interpretation of ancient depositional environments, drafted sections provide a means to better understand some of the variables controlling sedimentation. These variables include sediment influx, subsidence, and accommodation, which in turn provide both objective and subjective criteria for evaluating paleobathymetry, paleogeography, eustasy, and climate change. Although it is impossible to separate out these individual variables based on measured sections alone, when placed into a stratigraphic framework, the most dominant variables controlling sedimentation may become evident. Understanding depositional patterns and controls on sedimentation is paramount to coupling astronomical forcing of climate with sedimentary successions. Differing water depths, paleogeography, sediment flux, or differential subsidence will produce sections with different thicknesses and different characteristics. Identifying these differences in correlative sections is an extra measure to ensure that the interpretations about controls on cyclic sediments are geologically sound.

This section provides detailed descriptions of lithologies and stacking patterns present at each of the eight measured sections. These descriptions are meant to complement the drafted stratigraphic sections that can be found in Appendix A. In addition to descriptions, brief accounts of previous work, lithofacies associations, and faunal control will be discussed here. Note that drafted stratigraphic sections and cross-

sections are somewhat interpretative illustrations representing the rock bodies exposed in outcrop and some of the fauna present. They convey a general sense of the geology present at each location, however some of specifics and details of each individual section may not be apparent from the drawings alone. All stratigraphic sections along with gamma-ray and isotope profiles were plotted in MATLAB using the MatStrat package for stratigraphic analysis (Lewis et al., 2011).

Fish Springs Section - Fish Springs Range – Juab County, Utah

The succession exposed in the Fish Springs Range is the northernmost section in Utah, located in Juab County. The section appears fairly complete and is similar in certain respects to other sections in Utah (Fig. 8). The base of the section in this study begins in the poorly exposed, non-resistant, slope forming Corset Spring Shale Member of the Orr formation. The Corset Spring Shale is approximately 25 m thick at this section and is interbedded by only a few beds of limestone (Fig. 8). This is the only section in Utah where a disrupted limestone horizon and interpreted sequence boundary could not be identified within the Corset Springs Shale, likely due to poor exposure and extensive cover on the outcrop.

The Sneakover Member is expressed as a series of 14 remarkably uniform meter-scale carbonate cycles which form a series of "step ledges". These cycles can easily be identified on gamma-ray profiles. The section measures approximately 17 m thick and aside from the top bed, all the cycles are nearly 1 m in thickness. The base of the section is a light to medium gray skeletal grainstone to packstone with extensive calcite veins. This grainstone fines upward to a fairly homogenous trilobite wackestone and lime

mudstone with some eocrinoid fragments. Wavy laminations are present in some of the beds along with calcisiltite filled burrows. Between cycles is a thin, argillaceous, recessive nodular lime mudstone. Near the top of the section there is a significant lithologic transition between a light to medium gray skeletal wackestone and a significantly thicker and darker-gray bed. This single 2.5 m bed is composed of fine wavy-laminated ribbon limestone, capped by a flat-pebble conglomerate. This lithology is unique for the top of the Sneakover Member and is very similar in respects to the Whipple Cave Formation at the Shingle Pass section. The fining-upward succession likely records a relative deepening during the late *Elvinia* zone in the Sneakover limestone. However, because the uppermost and thickest bed of ribbon limestone is capped by a flat-pebble conglomerate and may reflect a return to storm-influenced inner-ramp facies (Evans, 1997).

Hintze and Palmer (1976) have provided correlations of the Orr formation members throughout the Great Basin, however the Pterocephaliid-Ptychaspid biomere boundary is poorly constrained in the Fish Springs Range. The biomere boundary was not identified in this study, however at the base of cycle 14 there is a transition from light gray trilobite wackestone to dark gray-black lime mudstone. Although color is generally considered a poor physical property for identifying lithologies, the bed which contains the Pterocephaliid-Ptychaspid biomere in other locations is marked by a distinctive transition to a darker lithology at the crisis interval. This is observed in other sections in Utah such as Candland Canyon, Steamboat Mountain, and Lawson Cove. In these sections, faunal control is much better and the boundary is apparent by the darker nature of the limestone. Here the biomere boundary will be assigned to the base of bed 14 where

Figure 8 – Outcrop photograph of the section measured at the Fish Springs Range. Note uniform meter-scale cycles and thick bed at the top of the section.

the lithology becomes distinctively darker and a small excursion in the gamma-ray profile occurs. The overlying Hellnmaria is poorly exposed at this location and no isotope data was collected from this section.

Candland Canyon Section – Central House Range – Millard County, Utah

The House Range area is in Millard County, Utah the where virtually the entire Cambrian System is exposed (Miller et al., 2012). Excellent sections of the Orr Formation outcrop within this region and are among the most studied Cambrian rocks in the world (Miller et al., 2012). The faunal control on the Orr Formation in the House Range is excellent compared to other sections and the Pterocephaliid-Ptychaspid boundary is known within a few centimeters (Palmer & Taylor, 1984). Typically, the

Sneakover Limestone Member is expressed as a series of step ledges, however a well-exposed cliff of the Sneakover Member was identified, allowing for a near-perfect sampling at a uniform interval. Because of these characteristics, the Candland Canyon section was picked for isotope analysis and samples were collected through the Sneakover Limestone at a 0.25 m interval.

At Candland Canyon a disconformable disrupted limestone surface can be located in the slope-forming Corset Spring Shale, approximately 20.5 m below the first outcrops of the Sneakover Limestone (Fig. 9). This disrupted surface is the only clear evidence of sub-areal exposure within Corset Springs Shale and it can be correlated laterally approximately 60 km to Steamboat Mountain and Lawson cove (Fig. 9). The lower surface is a truncated flat-pebble conglomerate that is in sharp contact with a skeletal grainstone. The grainstone fills in areas of erosional relief or paleokarst and contains mudstone intraclasts suspended in the matrix. Possible vadose silt can be found in conjunction with the grainstone in areas of paleo-karst. This disconformable surface is interpreted as a sequence boundary and marks the base of interval in this study.

Samples were collected for isotope analysis from above and below the sequence boundary. Relatively high $\delta^{13}C$ values are observed at the sequence boundary where three samples were collected. Below the surface in a flat-pebble conglomerate produced $\delta^{13}C$ values of 1.69‰. A sample from a grainstone overlying the surface was 1.0‰ and 0.82‰. Higher values are observed below the surface at Candland Canyon. A similar trend in isotopic values at the sequence boundary at both Steamboat Mountain and at Lawson Cove. However, because this surface is disconformable there is a higher

probability of secondary alteration of isotopic values through interactions with soil-gas CO_2 and meteoric fluids (Burns et al., 2005).

Figure 9 - Disrupted limestone horizon at Candland Canyon. Note the truncation of flat-pebble conglomerate and paleokarst features indicating erosion.

Above the disrupted the surface the Corset Spring Shale Member is mostly covered apart from several meter-thick or less beds of skeletal grainstone to packstone and thromboltic bioherms (Fig. 10). Where exposed, the Corset Springs Shale is dominated by fine-grained carbonate mud and olive green shales. Up-section, limestone becomes more common in the Corset Springs Shale until reaching the Sneakover Limestone. No gamma-ray profiles were measured because of extensive cover.

The base of the Sneakover Limestone is made up of an interval of thinly cross-bedded and planar laminated grainstones that formed overhanging limestone shelves and nodular lime mudstone that formed the subjacent recesses (Fig. 10). The grainstone contains a significant number of peloids and ooids indicating shallow water depths. Beds of flat-pebble conglomerate are also present in this lower section indicating possible storm influence. Above these thinly bedded grainstones, the entire succession has a cyclic appearance that is characteristic of the Sneakover Limestone.

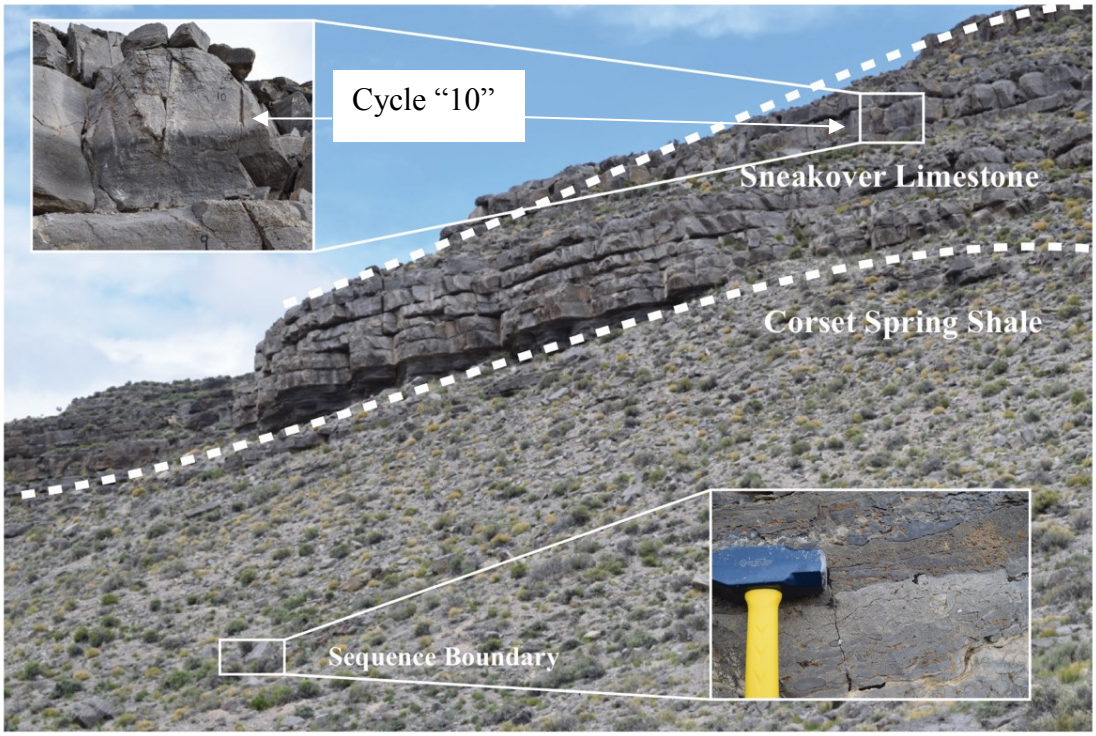

Figure 10 - Outcrop photograph of the section at Candland Canyon. Note the relative position of the sequence boundary and distinctive cycle "10”.

Like the Fish Spring Range, the section fines upward from a skeletal grainstone to homogenous lime mudstone and trilobite wackestone by cycle 6. Bed number 10 from

the base of the Sneakover Member, which is positioned exactly 10 m above the base has a distinctive coloration (Fig. 11). This bed will be referred to as “cycle 10.” The bottom is dark to medium gray mudstone to wackestone and the top is light gray mudstone/wackestone. A darker gray band of skeletal packstone runs through the center of this bed that splits the dark portion from the light portion. Note that at 10 m from the base of the Sneakover at Steamboat Mountain this distinctively colored bed is also observed. Above 10 m the cliffy exposures taper out and the uniform sampling interval was interrupted, although tracing laterally allowed for nearly continuous sampling. Lithologies remained light to medium gray mudstone with recessive argillaceous nodular lime mudstone between beds.

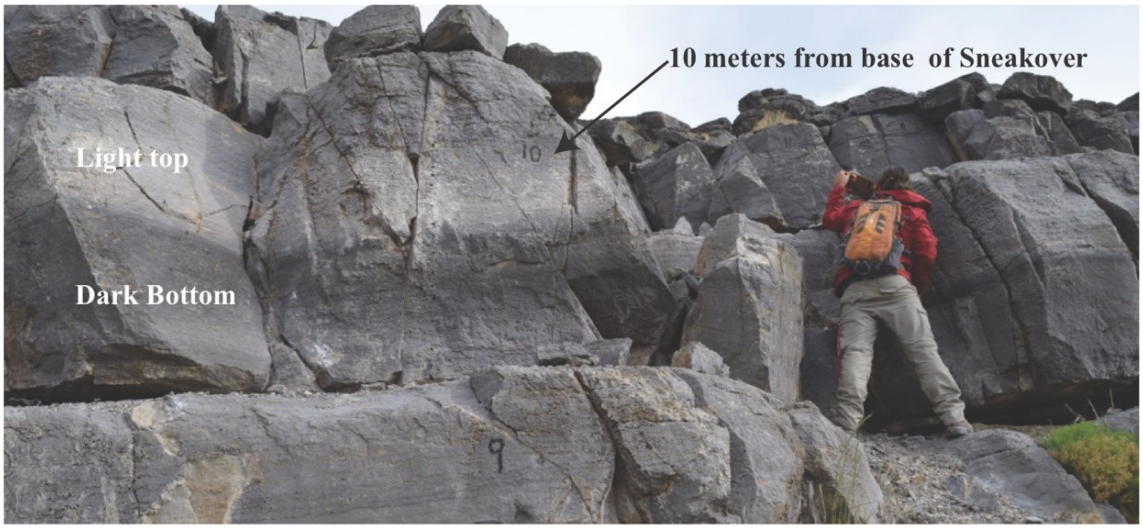

Figure 11 - Photograph of dark and light colored cycle “10” at Candland Canyon. This bed occurs at 10 m from the base of the Sneakover and can be correlated 60 km to the Southern House Range and the Wah Wah Mountains.

At approximately 20 m from the base of the Sneakover Member, a change in the expression of the cycles is observed. Cycle 12 is markedly thicker and medium to dark gray mudstone with numerous stylolites. Black chert also becomes common in the outcrop. Several specimens of *Irvingella major* were also collected just below the crisis interval at approximately 25 m. At 29.5 m a possible *Taenicephalus* was collected indicating the lower part of the Ptychaspid biomere was reached. In addition to the presence of Ptychaspid trilobites, a + 2.6 ‰ positive excursion of $\delta^{13}C$ values is observed at the biomere boundary. This follows the findings of Saltzman et al. (1995) and provides an additional indicator of the biomere boundary. Unfortunately, only one sample was recovered from this bed, although the sample was run twice, with both measured values falling within 0.04 ‰ of each other. Measurements were discontinued above the biomere boundary because of extensive cover, although at the summit of the section the Hellnmaria Member of the Notch Peak Formation is exposed as a short cliff.

Cycles are easily identifiable on gamma-ray profiles, with higher values produced by the argillaceous components in between cycles. The gamma-ray profiles provide an additional check for the lumping and splitting of cycles. Little variation in $\delta^{13}C$ values is observed throughout much of the Sneakover Member, although from the profiles it appears that generally the higher values are also produced from the argillaceous components in between cycles. Before the crisis interval a decrease in $\delta^{13}C$ values from +1.0‰ to +0.1‰ is observed, followed by a positive excursion of +2.6‰ at the crisis interval. Time series analysis of both gamma-ray profiles and carbon isotope data will be covered extensively in the discussion section.

Steamboat Mountain Section – Southern House Range – Millard County, Utah

On Steamboat Mountain in the southern House Range, excellent outcrops of the upper Orr Formation are exposed (Fig. 12). The upper part of the Steamboat Pass Shale Member and lower Sneakover Limestone Member at Steamboat Pass and Lawson Cove is similar in thickness to the Corset Spring Shale and the lower Sneakover on Orr Ridge. Nearly the entire Sneakover is exposed in a series of short cliffs and step ledges with the Hellnmaria Member forming a prominent cliff overlying the entire section. The base of this section begins at the disrupted limestone horizon that is interpreted as a sequence boundary. Four samples were collected for $\delta^{13}C$ analysis at the disrupted limestone. Two samples collected below the surface from a flat-pebble conglomerate yield $\delta^{13}C$ values of -0.05‰ and +0.16‰. Above the surface is a skeletal grainstone that yields higher $\delta^{13}C$ values of +0.74‰ and +1.28‰. Because this surface likely represents subaerial exposure and possible erosion, the isotope ratios in this rock are susceptible to diagenetic alteration, however the $\delta^{13}C$ values at Steamboat Mountain are generally within the accepted range for marine carbonates (Burns et al., 2005). Overlying the disrupted limestone is the Steamboat Pass Shale, which is expressed as a slope forming shale unit with some limestone beds that fine-upward. The Steamboat Pass Shale is mostly covered thus preventing the measurement of gamma-ray profiles.

The base of the Sneakover Limestone is a bioclastic grainstone with some thin recessive beds. A bed of flat-pebble conglomerate forms a prominent shelf, overlain by more thinly bedded and nodular grainstones, similar in respects to the lowest portion of the Sneakover at Candland Canyon. Above the thinly bedded material is a thicker bed that marks the beginning of the cycles. As with the other sections in Utah, carbonate

lithofacies in the cycles fine-upward, from a skeletal packstone and grainstone to homogeneous lime mudstone. Approximately 6 m above the base of the Sneakover Limestone is a 1 m thick bed that has a dark bottom gray bottom, a 4-6 cm dark band of skeletal packstone in the center of the bed, and a light to medium gray mudstone to wackestone top. A distinctive bed like this is also found at Candland Canyon at approximately 10 m and at Lawson Cove at a similar stratigraphic height. Although it is not always the best practice to make correlations based on coloration of beds, the fact that the lithofacies match and the approximate stratigraphic position also match, providing strong evidence for of the correlation of these distinctive beds.

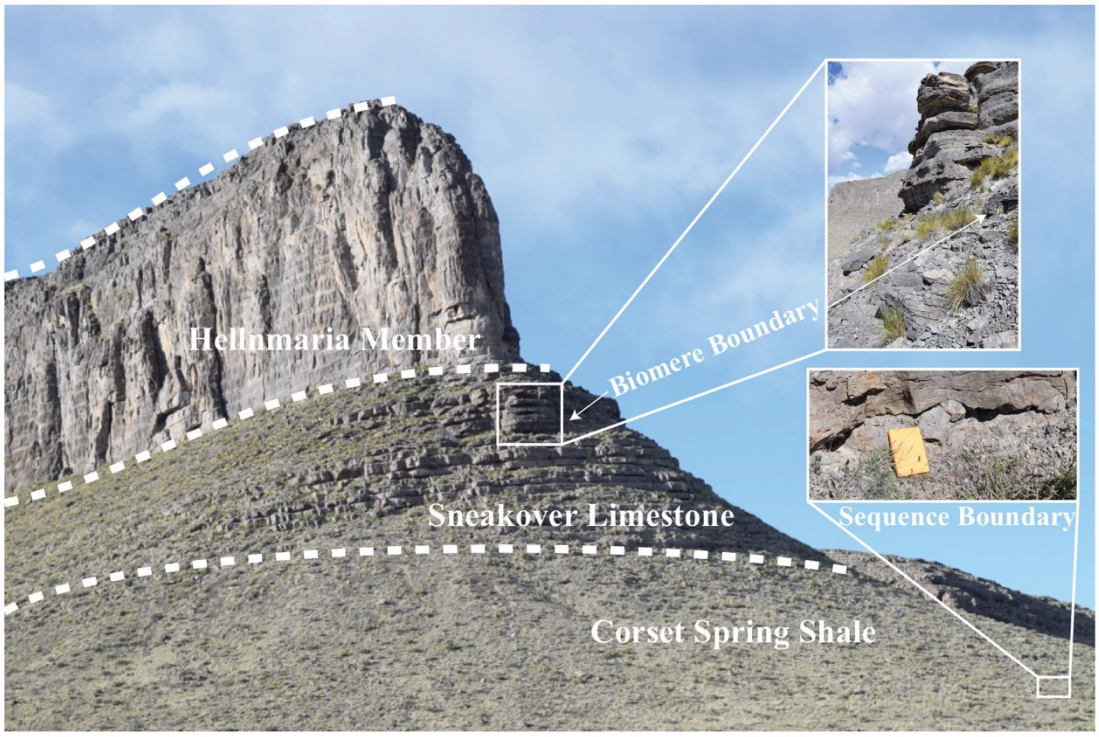

Figure 12 - Outcrop photograph of the section at Steamboat Pass. Note position of the sequence boundary in the lower left corner of the photo and the thick cycles higher in the outcrop.

Moving up section the cycles continue to follow the trend of fining upward into homogeneous mudstone indicating potentially deeper water conditions and rising relative base-level. Additional beds up-section also display the trend of a dark bottom and dark top. Between beds is generally a recessed nodular lime mudstone that yields a higher gamma ray value and allows for identification of cycles on gamma ray profiles. An influx of siliciclastic material may represent shallowing upward of the parasequences (Osleger & Read, 1993) and account for the influx of argillaceous material that is producing higher gamma-ray values.

At approximately 23 m black chert nodules become more common and just above this a darker bed is exposed which may represent the biomere crisis zone. Overlying the potential crisis interval cycles become more recessive, composed of nodular mudstone interbedded with silt. The lithofacies are different than the other sections, possibly due to weathering phenomenon. The appearance of these beds is similar to the so called "black and tan" beds described by Evans (1997). Abundant brachiopod shells and trilobite fragments were recovered from this interval and might represent faunas of the *Taenicephalus* zone. Overlying the recessive cycles, the expression of the Sneakover returns to meter-scale step ledges up to the base of the cliff forming Hellnmaria Member. cycles are distinctively represented by the gamma-ray profiles.

Lawson Cove Section – Wah Wah Mountains – Millard County, Utah

The section exposed at Lawson Cove is approximately 15 km from Steamboat Mountain and contains similar facies with comparable stratigraphic thicknesses. When comparing the gamma-ray profiles of Steamboat Mountain and Lawson Cove, the ability

to make high-resolution correlations based off gamma-ray logs alone becomes apparent. Both profiles are nearly identical, with each individual cycle clearly identifiable on the logs. Hintze & Palmer (1976) published a reference section for the Orr Formation exposed at Lawson Cove. In this paper, the Pterocephaliid-Ptychaspid biomere boundary is known within a few meters. Here, a new section was painted and measured in conjunction with the faunal control of Hintze & Palmer (1976).

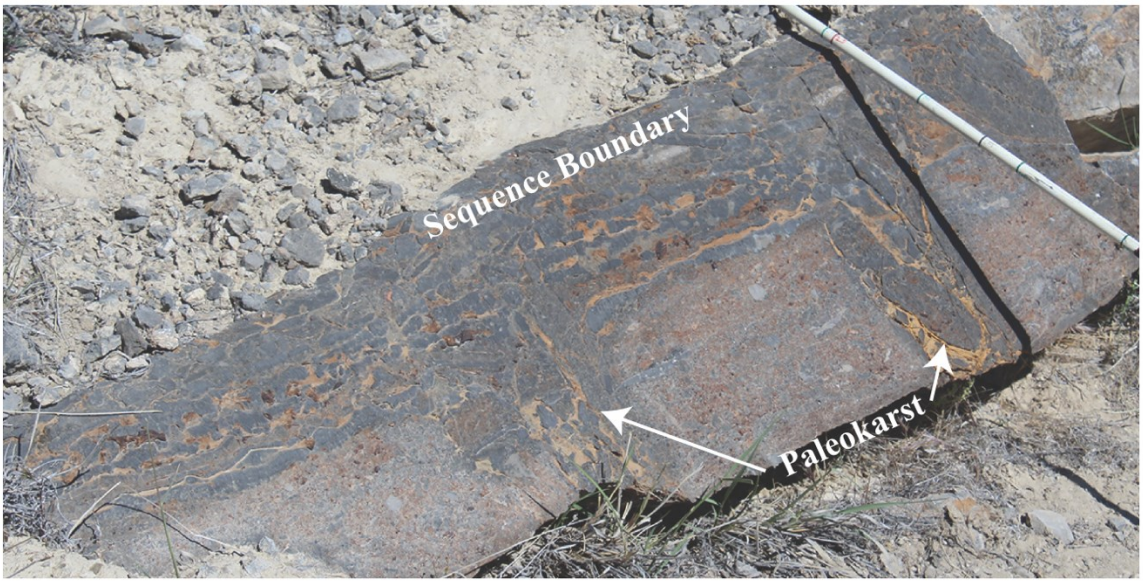

Figure 13 - Disrupted limestone surface exposed at Lawson Cove. Notice paleokarst fill and vadose silt. Truncated grainstone further indicate erosion along this horizon.

The section at Lawson Cove begins at the same disrupted limestone and paleokarst surface that is interpreted as a sequence boundary in other sections in Utah (Fig. 13). This surface displays the similar characteristics as the disrupted horizon present at Steamboat Mountain and Candland Canyon. Dissolution of intraclasts along the surface at Lawson Cove indicates that the lower layer must have been exposed sub-

aerially and is thus why this surface has been identified as a sequence boundary here. Additionally, a shift in gamma-ray values of 50.6 to 68.9 CPS and higher positive $\delta^{13}C$ values between +1.89 to 2.17 ‰ are observed at this boundary, allowing easy identification on a gamma-ray log or isotope profile.

Overlying the disrupted horizon at Lawson Cove is mostly covered apart from several beds of skeletal wackestone and packstone and rare exposures of shale. The grainstone and packstone is medium gray with wavy laminations and minor black chert. The thin carbonate beds fine upward to wackestone up-section. Most of the slope forming Steamboat Pass Shale at Lawson Cove is covered, preventing the measurement of gamma-ray profiles in this Member (Fig. 14).

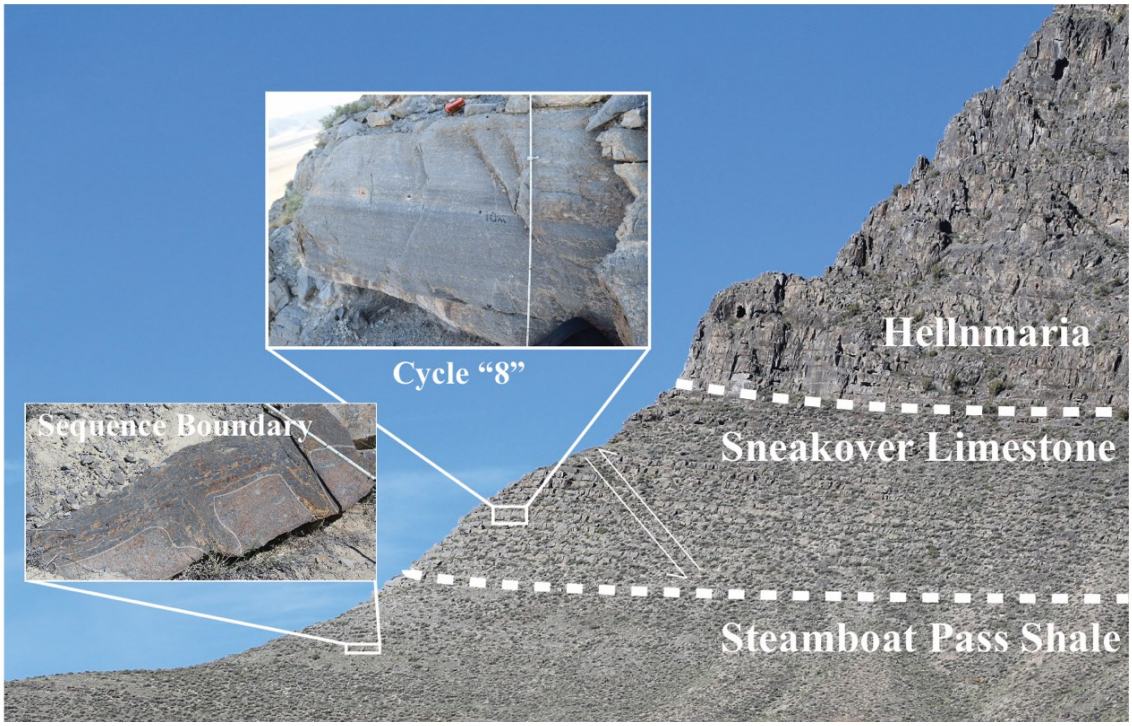

Figure 14 - Outcrop photograph of the section at Lawson Cove. Note the position of the sequence boundary and the distinctive cycle also recognized at Candland Canyon. Although the exact cycle number is different, the stratigraphic position is the same. The difference may be a result of incorrectly splitting cycles. A thrust fault is indicated higher in the section.

The base of the Sneakover Member is a recessive and thinly bedded wackestone to packstone with interbeds of skeletal grainstone and flat-pebble conglomerate, similar in respects to the base of the Candland Canyon section (Fig. 14). Overlying this recessive unit is the beginning of the near-meter-scale carbonate cycles. The first 2.5 m of the section is massive packstone and grainstone. The individual cycles are difficult to see in outcrop aside from subtle partings of nodular lime mudstone. The cycles are easily observed on gamma-ray profiles and begin just below an excursion of 70.3 CPS. Above the short cliff formed by cycles one and two, the rest of the cycles quickly fine-upward, forming a series of step ledges composed of homogeneous mudstone with interbeds of recessive nodular lime mudstone between the cycles. Cover on the step ledges at Lawson cove required that several beds be traced laterally to better exposures.

At “cycle 8”, 10 m exactly from the base of the Sneakover Member, a distinctive dark bottom and light top cycle was identified (Fig. 15). This is at the same stratigraphic height of the distinctive light and dark colored “cycle 10” bed at Candland Canyon. This bed potentially correlates with the lowest distinctly light and dark colored bed at Steamboat Mountain. Color is generally regarded as a poor means of correlation. However, the fact that the subtidal lithofacies, stratigraphic position, coloration, and thickness of this cycle is the same at the other sections demonstrates that individual cycles can be laterally correlated over distances of nearly 60 km. The cycle number may be different from Candland Canyon because of errors in lumping and splitting of the lower cycles.

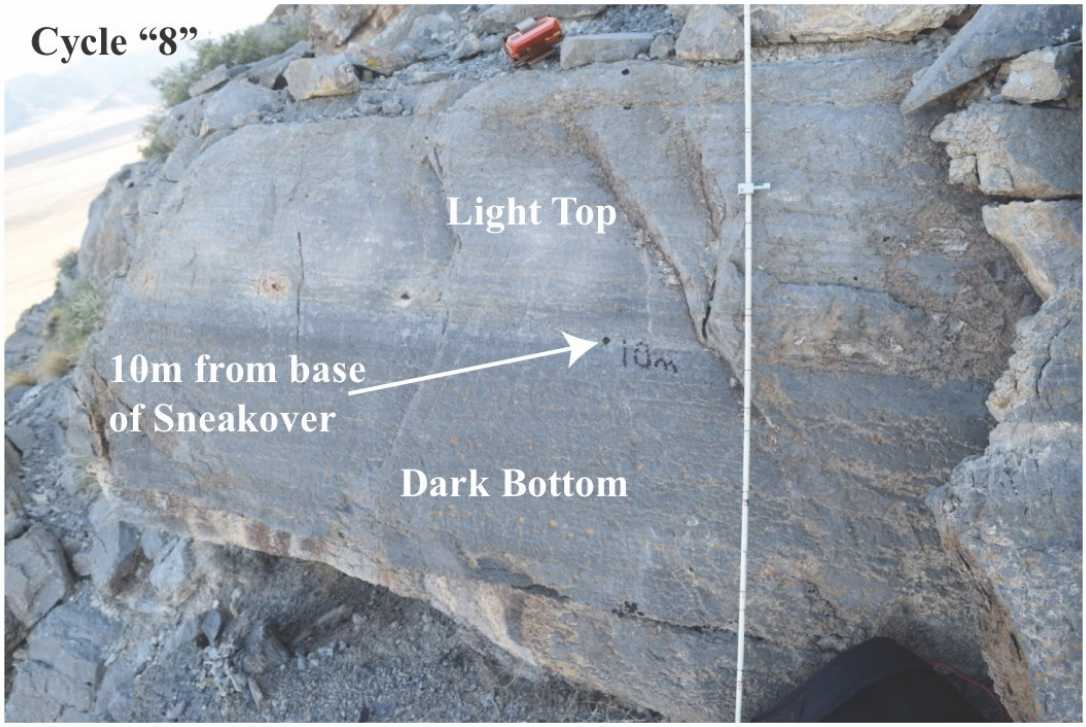

Figure 15 - Photograph of the dark and light colored cycle 8 at Lawson Cove. This is presumably the same cycle identified at Candland Canyon and Steamboat Mountain based on stratigraphic position, coloration, and lithofacies.

Up-section, the cycles continue as homogeneous lime mudstone with recesses of nodular lime mudstone between beds. Some minor black chert and burrows also are observed. At approximately 25 m a fragment of a possible *Irvingella major* was recovered, marking the top of the Pterocephaliid biomere (Taylor, 2006). The actual biomere boundary was identified as a darker bed 28 m from the base of the Sneakover Member. Above the biomere boundary the strata are faulted and repeated. Near the fault, beds become discontinuous, and a small covered bench is formed. The fault can be easily identified in outcrop from a distance and accounts for the thicker Sneakover relative to Steamboat Mountain. Measurements continued above the fault which is noted on the

drafted stratigraphic section. Like Steamboat Mountain, the Hellnmaria Member of the Notch Peak Formation overlies the Sneakover as a prominent cliff, preventing further measurements. From the sequence boundary to the base of the Hellnmaria Member the measured stratigraphic thickness at Lawson Cove was 76 m.

Spring Gulch Section – Northern Schell Creek Range – White Pine County, Nevada

Magnificent exposures of the Barton Canyon Member of the Windfall Formation can be seen miles away from the remote mountain located north of Lovell Peak, near Spring Gulch (Fig. 16). By far the most remote section measured in this study, Spring Gulch can only be accessed by an approximately 1.5 hour bushwhack-hike with a vertical gain of nearly 2000 ft. Below the cliffs of the Barton Canyon is the Dunderberg Shale, the equivalent to the combined Corset Springs Shale, John's Wash Limestone, and Steamboat Pass Shale Members of the Orr Formation in Utah. As with the other sections, the exposure of the slope forming Dunderberg Shale is poor, with intermittent exposures of carbonates interbedded with the shale. A good exposure of lime mudstone and shale within the Dunderberg occurs approximately 20 m below the Barton Canyon Member. This rock was measured and drafted on the stratigraphic column that can be found in Appendix A. As with other sections in Nevada, no disrupted or unconformable surface was identified at Spring Gulch. This may be due to cover in the Dunderberg, though it is possible that this surface is represented as a correlative conformity, as sub-aerial exposure may not have extended this far basinward.

The Barton Canyon Member is well exposed near the summit of the unnamed mountain as a nearly continuous cliff line (Fig. 16). Because of the continuous cliff, this

Figure 16 - Outcrop photograph of the section at Spring Gulch. Note the near perfect cycles of the Barton Canyon Member of the Windfall Formation.

section was selected for isotopic analysis. The modest 14 m tall cliff is comprised of near uniform carbonate cycles with an average thickness of approximately 0.8 m. The Barton Canyon Member is the Nevada equivalent of the Sneakover Limestone Member located in Utah. This correlation is based on lithofacies association (Osleger & Read, 1993) and biostratigraphy (Palmer, 1971), though precise, cycle for cycle correlation is uncertain. It is conceivable that groups of beds in the Barton Canyon may be correlative with discrete step-ledges in the Sneakover Member. The expression of the Sneakover Limestone in the Fish Springs Range is similar to the Barton Canyon. The stratigraphic thicknesses are comparable and the lithofacies are nearly identical. However, in the House Range and the Wah Wah mountains the Sneakover is significantly thicker. For example, the Sneakover

Limestone at Steamboat Mountain is 45 m thick. Whereas the Barton Canyon at Spring Gulch is only 14.5 m thick. Also, the cycles of the Barton Canyon tend to be thinner than the Sneakover, ranging from 0.5 m to 1.3 m with an average of 0.8 m.

The section of cliff measured was nearly vertical and entirely exposed allowing for sampling at an equal interval, although some technical rock climbing was required. Like other sections, the base of the Barton Canyon at Spring Gulch is predominately grainstone, with interbeds of rubbly lime mudstone. The rock is a light gray to brown, recrystallized, and contains eocrinoid fragments. Around 3 m, thrombolite bioherms can be recognized within a grainstone matrix. By 8 m from the base of the Barton Canyon, the grainstone fines upward first to wackestone, then to mostly mudstone with some thin interbeds of trilobite wackestone. Mudstone and bioclastic wackestone make up the rest of the cyclic section. At 10 m there is a thicker bed that potentially correlates with the North Egan Range or the McGill section, based on thickness and lithofacies association. The upper most beds at the Spring Gulch section and the North Egan Range are dark gray lime mudstones that contain *Irvingella major* zone trilobites (Evans, 1997). The Pterocephaliid biomere was not identified at this location, although it is believed to exist just above the cliffs of the Barton Canyon in a covered interval.

The Catlin Member of the Windfall Formation crops out above the Barton Canyon outcrops (Fig. 17). Within this formation, the cyclicity expressed in the Barton Canyon and correlative Sneakover Limestone and Hellnmaria Member is anomalously absent. The expression of the carbonate lithofacies is different, and outcrops as dark gray to black, thinly-bedded, platy mudstone with an argillaceous component. Between beds are silty and weather to a medium tan. Many of these beds are homogenous ranging from

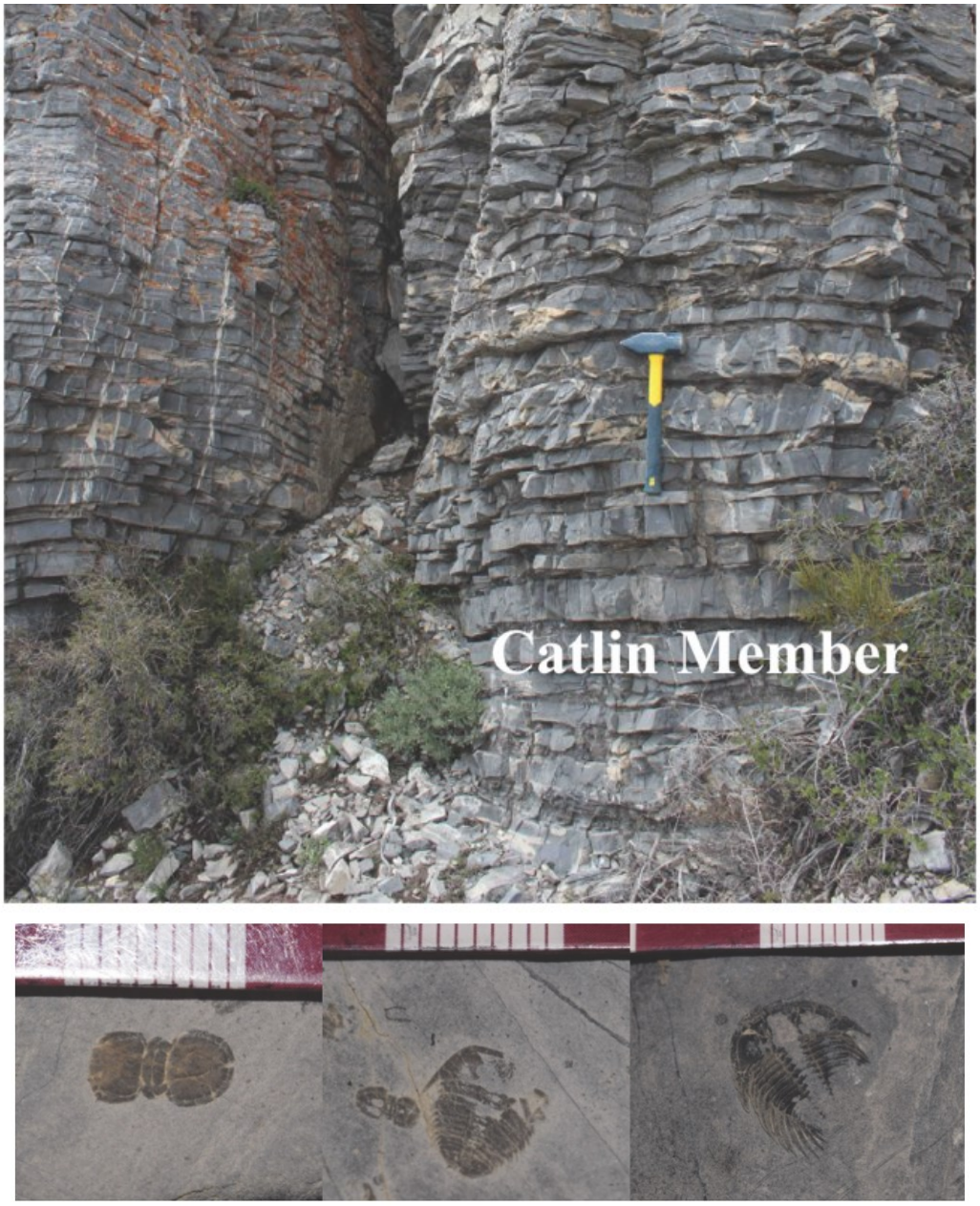

Figure 17 - Photograph of the turbidite deposits of the Catlin Member and some of the example trilobite faunas present, including a *Tatonapsis sp.* along with possible *Parabolinoides* and *Naustia.*

2 – 10 cm thick comprised of parallel-laminated silty lime mudstone to calcisiltite. Some of the beds fine upward and exhibit ripple laminations overlain by finely laminated argillaceous mudstone. Near the summit, approximately 40 m above the Barton Canyon, a series of fine-grained carbonate sediment-gravity flows are interbedded with penecontemporaneously folded 20-cm thick lenticular beds of bioclastic grainstone in the Catlin Member.

In addition to the unique deep marine facies of the Catlin, abundant trilobite fragments, along with numerous whole specimens were recovered from this member at Spring Gulch. Both polymerid and agnostid trilobites were found together in this section. Most of the trilobites recovered remain unidentified, however a *Tatonapsis sp.* along with possible *Parabolinoides* and *Naustia* were recovered. These species are consistent with the "Cherry Creek Fauna" described by Adrain & Westrop (2004). However, Adrain & Westrop (2004) only described a few trilobites in their study. The Catlin Member exposed at Spring Gulch contains abundant trilobites and numerous genera. This discovery is significant and almost certainly contains new, undescribed species. Little work has been done on the trilobites of the Windfall Formation, perhaps due to the inaccessibility of the sections. Abundant faunas this close to the Pterocephaliid-Ptychaspid biomere boundary is also important. Trilobites of the Catlin Member may reveal new information regarding biotic recovery following the extinction events recorded at biomere boundaries. This rich fauna at Spring Gulch is anomalous, in that no fossils were recovered from the correlative Catlin Member at either McGill or the North Egan Range sections.

North Egan Range Section – North Egan Range - White Pine County, Nevada

The Dunderberg Shale is the lowest unit of interest exposed in the North Egan Range. This thick shale is correlative to the Corset Spring Shale and the Steamboat Pass Shale of Utah. As with the other sections, this unit was not measured due to poor exposure and cover of the shale. Overlying the Dunderberg is the Barton Canyon and Catlin Members of the Windfall formation. Also, exposed at the North Egan Section is the cliff-forming upper member of the Windfall Formation, the Bullwacker Limestone. Although the Bullwacker is outside of the interval of interest here, it is noteworthy to

Figure 18 - Photograph of the turbidite deposits of the Catlin Member at the North Egan Range.

mention that the expression of the Bullwacker is remarkably similar to the Hellnmaria Member of the Notch Peak Formation in Utah.

The Barton Canyon is approximately 11 m thick at the North Egan Range with cycles expressed as a series of approximately 1 m thick step ledges that thin upward. The base of the Barton Canyon in the North Egan range is a mudstone to wackestone containing occasional trilobite and echinoderm fossils. This section is one of the only sections that does not follow a distinctive fining upward from grainstone to mudstone, a possible result of cover or deeper water settings. The rock is light to medium gray in color and is darker than other sections. Nearly the whole section is homogeneous mudstone with few accessories aside from extensive calcite veins. Between cycles argillaceous nodular lime mudstone forms recesses, which produce higher gamma-ray values. Towards the top of the 11 m exposure of the Barton Canyon, there is a grainstone bed overlain by a darker mudstone that produced higher gamma ray values of approximately 67.8 cps. Above this, the section forms a slope of cover approximately 30 m thick below exposures of the Catlin Member outcrop. Because of extensive cover, measurements and descriptions ceased until better exposures of the Catlin Member were reached. The Pterocephaliid biomere boundary was not confidently identified at this section. It is presumed to be located near the top of the Barton Canyon Member, possibly within the darker mudstone near the top of the section.

Approximately 30m above the Barton Canyon, good exposures of the Catlin Member were measured and gamma ray profiles were logged (Fig. 18). Like the Spring

Gulch Section, the cyclic expression of the Barton Canyon abruptly ends in the Catlin. Sedimentation continues above as thin bedded lime mudstone and calcisiltite. Most of the beds are made up of fine planar laminations and range in thickness from 2 to 10 cm, but beds up to 50 cm thick exist. Like the Spring Gulch section, some of these beds fine upwards and display ripple marks. Although most beds can be traced laterally across exposures, there are also thin, 1-5 cm thick lenses of structureless carbonate that pinch out laterally within 0.5 m.

Although nearly 15 m of the Catlin Member were measured, described, and logged, no trilobites were recovered. This is in contrast with the Catlin Member exposed to the North in the Spring Gulch section where diverse and abundant trilobite faunas were recovered. The expression of the Catlin Member is very similar throughout Nevada in number of respects. Lithology, color, bedforms, and stratigraphic expression are all remarkably similar.

McGill Section – Duck Creek Range – White Pine County, Nevada

The section exposed at McGill was proposed as the stratotype section for the Steptoean Stage in North America by Ludvigsen & Westrop (1985). The section measured in this study is located approximately 300 m north, near the summit of a small spur-like ridge on the western side of the Duck Creek Range (Fig. 19). The section transverses a dip-slope where the Barton Canyon crops out. As with other sections, the Dunderberg Shale is poorly exposed near the base of Barton Canyon and was not measured. No disrupted surface or unconformable surface was located at the McGill section. Evans (1997) recognized a thick carbonate succession in the lower part of the

Elvinia zone that he considered to be consistent with an interpretation of lowstand wedge sedimentation correlative with the disrupted horizon.

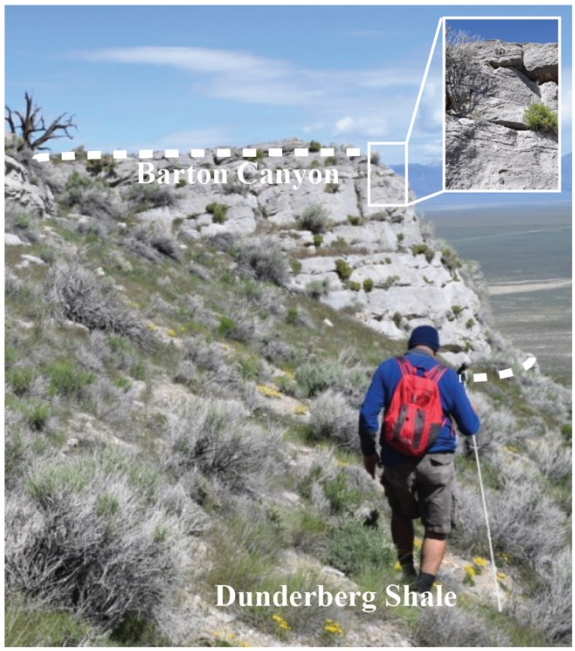

Figure 19 - Outcrop photograph of the section at McGill.

The Barton Canyon Limestone is exposed as a short, less-than-vertical 13 m tall outcrop. The base of the limestone is a light tan to buff white peloid grainstone that is lighter in color than other exposures of the Barton Canyon. Peloid grainstone quickly fines-upward to light gray to buff packstone and wackestone containing thin interbeds of grainstone. By 4 m from the base of the Barton Canyon, the lithology fines to mudstone with interbeds of grainstone within the beds. The color of the rock is homogeneous light gray throughout the entire outcrop. Mudstone is coarse crystalline indicating extensive recrystallization. Calcite veins and trace amounts of pyrite are present. Between cycles of carbonate, recesses of argillaceous nodular lime mudstone are dark gray and rubbly.

Wavy laminations are present in some of the mudstone cycles along with interbedded lenses of packstone. At approximately 10 m, spar-filled burrows are present along with peloid packstone. Above 10 m the cycles thin and recessed intervals between cycles become covered. The mudstone also transitions in color from light to dark gray. Near the top of the section, beds of black chert up to 10 cm thick were observed along with a significant gamma-ray excursion of 116.8 CPS. This bed was relogged and consistantly produced values greater that 110 CPS.

The Pterocephallid-Ptychaspid biomere boundary was projected from Palmer (1965b) and roughly coincides with the color change from light to dark gray at the top of the section. The overlying Catlin Member is poorly exposed and mostly eroded at the top the hill. As a result, the Catlin Member was not measured at the McGill section and no trilobites were recovered.

Shingle Pass Section – South Egan Range – Lincoln County, Nevada

Strata present at Shingle Pass is notably different from the other sections to the North and East. Shingle Pass is made up of thick successions of interbedded carbonate shoals, lagoonal, and tidal flat deposits (Evans, 1997). The Dunderberg Shale, which in this stratigraphic section is equivalent to the Corset Spring Shale, crops out as a slope forming bench above. Planar carbonates and irregular truncation surfaces are found in the lower part of this interval, however much of shale is covered, preventing detailed measurements and descriptions of the unit. Above the Corset Spring Shale equivalent, the Whipple Cave Formation forms a massive cliff of cherty lime mudstone.

The Whipple Cave Formation is correlative to the Barton Canyon and lower Sneakover Limestone, although the lithology is significantly different. The base of the section is medium gray mudstone and forms three step ledges, similar in respects to all the other locations. At 3 m the lithology transitions to medium to dark gray, coarse crystalline mudstone to wackestone with a significant amount of nodular black chert. No cycles are visually present and the rest of the section is massive cherty mudstone. Some trilobite fragments and brachiopods are present in the lower section along with wavy like laminations filled with chert. At 8 m from the base of the section, the mudstone becomes dominated by orange weathering black chert, up to 60% by volume in places. Most of the chert appears to be filling in wavy laminations or bedding planes and forming nodules. At 14 m the black chert content begins to decrease and bedding planes become impossible to distinguish. The top of the Pterocephaliid biomere could not be identified confidently, although the section continues above as homogeneous cherty lime mudstone.

This is the only section where no cycles are observed in the Sneakover and Barton Canyon equivalent. The entire outcrop expression of the Whipple Cave Formation is massive cherty mudstone. However, the gamma-ray logs depict variation on approximately a meter-scale. Although the rock is massive in appearance, there is arguably a cyclic pulse of argillaceous material that is producing minor variation in the logs.

Patterson Pass is located on the opposite side of South Egan Range, in the southern Schell Creek Range, approximately 20 km to the east of Shingle Pass. Here, the Whipple Cave Formation is exposed as a greater than 50 m thick package of carbonate (Evans, 1997). The lowermost lithology of the Whipple Cave Limestone resembles the

Shingle Pass section, but upward, the succession appears similar to the Sneakover Limestone in that step-ledge cycles are expressed (Evans, 1997). Due to time constraints and the scope of this project, Patterson Pass was only photographed from afar and was not measured. However, the fact that step ledges are observed at Patterson Pass and meter-scale variations in gamma-ray profiles demonstrates that Shingle Pass may be a cyclic succession that is expressed as a massive unit due to weathering phenomena.

Gamma-ray Profiles and Time Series Analysis

Carbonate cycles of the Sneakover Limestone and correlative Barton Canyon Member are easily identifiable on most of the gamma-ray profiles. Clean limestones produce characteristically low values and the argillaceous nodular lime mudstone between cycles produce higher values. Figures 20 and 21 depict gamma-ray profiles from all the sections measured along with power-spectra generated with REDFIT analysis.

Gamma-ray profiles can be found in conjunction with described stratigraphic sections in Appendix A. Appendix C contains the raw gamma-ray data in CPS, along with the stratigraphic position of each measurement.

The sections from Utah, which are located more landward relative to the sections in Nevada, have greater variation in the gamma-ray logs. This is likely a result of the paleogeographic location of Utah during the Cambrian, which was located more landward and received a greater siliciclastic input at flooding surfaces between cycles. Nevada was farther basinward, and received less siliciclastic input and therefore has less variation between cycles in the gamma-ray profiles. Nevertheless, when the CPS scale is

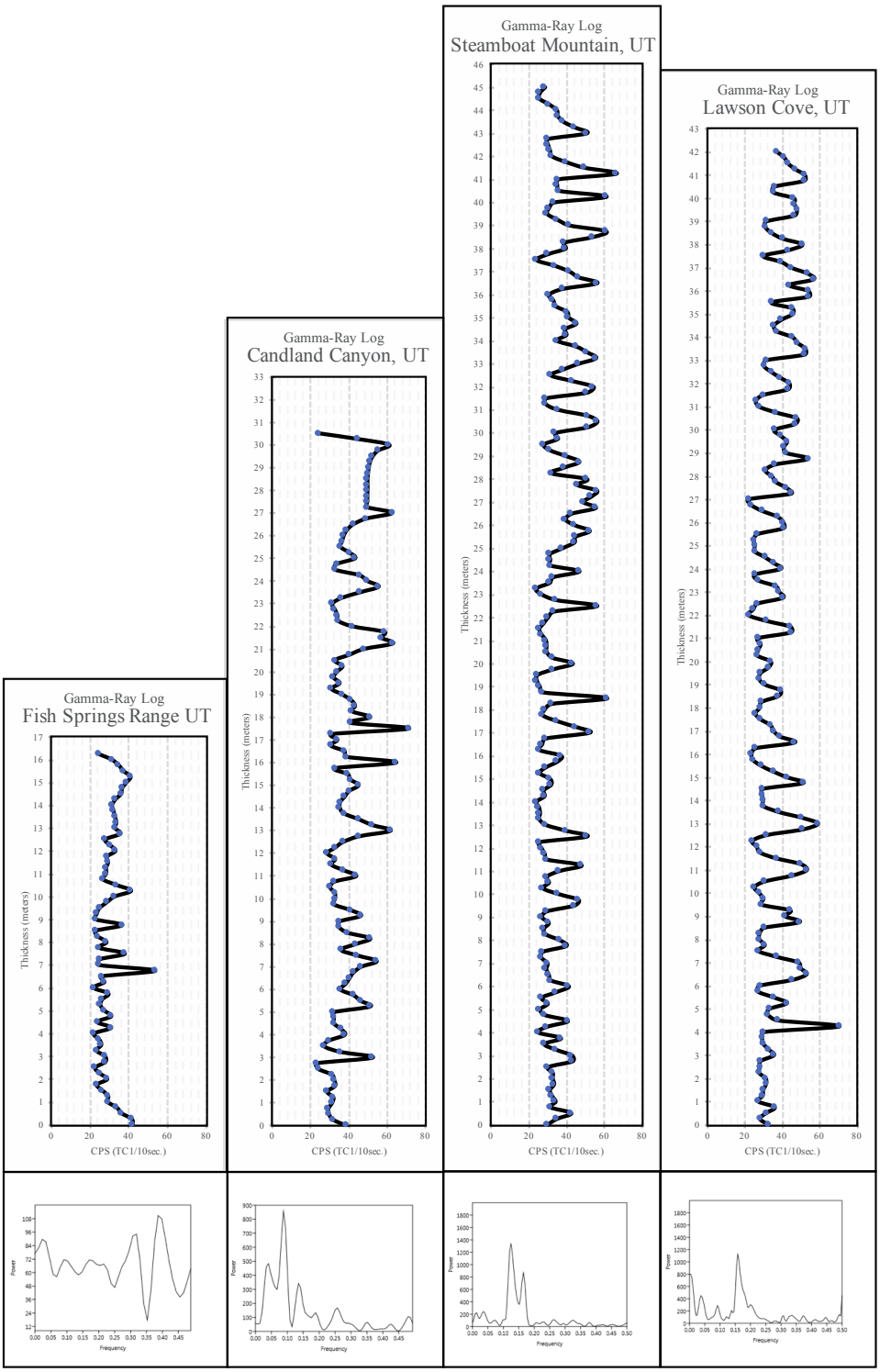

Figure 20 – Gamma-ray profiles and power spectra from Utah.

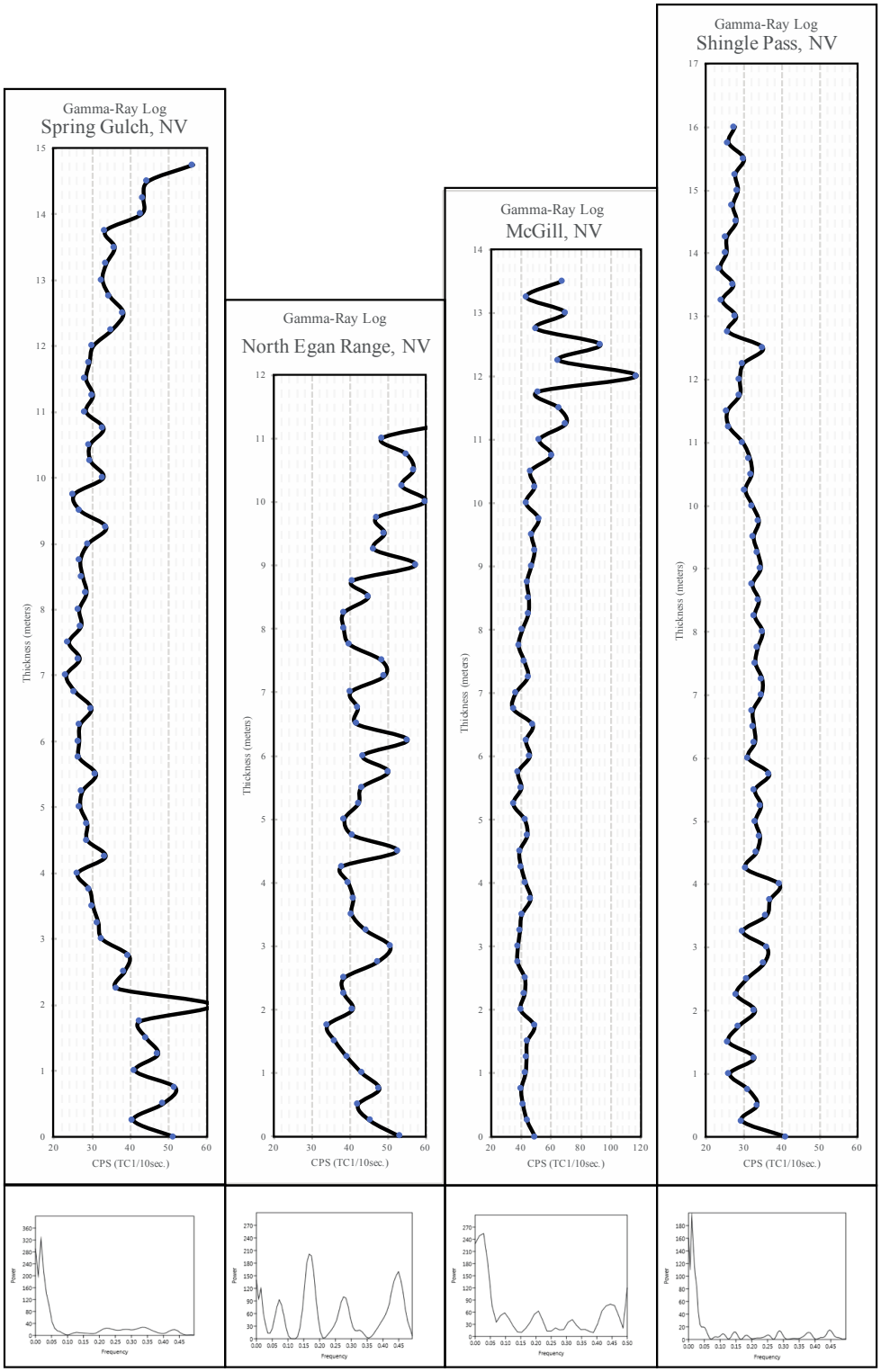

Figure 21 – Gamma-ray profiles and power spectra from Nevada.

adjusted, cycles in Nevada become evident on the logs, with peaks and troughs closely aligning with the cycles on the drafted sections.

Spectral analysis was conducted on all eight gamma-ray profiles for two reasons. First, to check if there are any periodicities recorded in the gamma-ray signal that could be related to environmental or astronomical forcing, and second, to determine if time series analysis of cyclic sections can be used for regional correlations. Power-spectral plots of gamma ray profiles can be found in Figures 20 and 21. Descriptions of gamma-ray profiles from each section along with results of the time series analysis will be described below in the same order that the stratigraphic sections were described. The REDFIT method was used for time series analyses on all the sections. A Blackman-Harris window was used with two oversamples and two segments. Sinusoidal regression was used to cross-check the periods determined from the REDFIT analysis by fitting the original time series to a reconstructed sinusoid using the calculated periods.

In the Fish Springs Range gamma-ray profiles closely track lithology, varying between 21.8-53.5 CPS between cycles with an average value of 30.2 CPS. Between cycle 9 and 10 is an excursion of 53.5 CPS. The thick bed at the top of the section shows increasing values from approximately 26 CPS to 42 CPS at the base of the bed, and rapid cleaning at the top of the bed to 25 CPS. The REDFIT model determined several ambiguous spectral-peaks. Three peaks fell above 80% confidence interval. Sinusoidal regression determined four periods, at 16.79 m, 7.32 m, 1.11 m, and 0.77 m, with a favorable fit excluding the outlying value of 53.5 CPS.

Candland Canyon shows significant variation between cycles, with the highest values falling between cycles in beds of argillaceous nodular lime mudstone. Values vary

between 23.1 CPS to 64.5 CPS with a mean of 39.5 CPS. There are no significant outliers that deviate from the mean. REDFIT analysis shows three peaks above 90% confidence. Similarly, sinusoidal regression determined 3 periods, at 7.54 m, 2.93 m, and 1.82 m, that optimize the fit of the time series.

Lawson Cove shows even greater variation than Candland Canyon, with values ranging between 21.8 CPS to 70.3 CPS with a mean of 36.4 CPS. A minor excursion of 70.3 CPS is observed near the base of the section. Small excursions near the base of the sections are also observed at Steamboat mountain, the North Egan Range, and Shingle Pass. Again, argillaceous nodular lime mudstone between cycles produce the highest values. REDFIT analysis determines two peaks, both falling above a 95% confidence interval. Sinusoidal regression provides a reasonable fit with three periods at 26.65 m, 2.09 m, and 1.52 m.

Gamma ray profiles measured at Steamboat Mountain appear similar to Lawson Cove, in that both sections are similar thickness and show similar variation in the profiles. Values range between 23.6 CPS and 66.2 CPS with a mean of 36.1 CPS. No values deviate far from the mean apart from two values, one near the base of the section and one near the top of the section. REDFIT analysis shows a single distinctive peak above the 90% confidence interval, with three, lower frequency peaks proceeding the dominant frequency. Sinusoidal regression provides a reasonable fit with three periods at 42.51 m, 7.52 m, and 1.36 m. Interestingly, these values do not match the periods at Lawson Cove.

The Spring Gulch section, located in the northern Schell Creek Range, was the first section in Nevada in which time series analysis was conducted. As previously

mentioned, gamma-ray profiles and stratigraphic sections in Nevada are not only thinner in stratigraphic thickness, but also show less variation between the beds. Values range between 23.1 CPS to 61.6 CPS with a mean of 33.4 CPS. A significant outlier (61.6 CPS) exists near the bottom of the section. When values are plotted, the log displays a bow-like shape, with high values near the bottom, gradually moving to lower values in the middle and gradually returning to higher values near the top of the section. REDFIT analysis shows a single peak above the 95% confidence interval, likely corresponding to the bow like shape of the gamma-ray profiles. Sinusoidal regression determined three periods at 14.93 m, 8.39 m, and 0.71 m. These periods provide a good fit of the time series.

The section at the North Egan Range is the thinnest expression of the Barton Canyon measured in this study, at just over 11.25 m. The profile displays a bow like shape similar to Spring Gulch, although the shape is not as pronounced. Values range between 33.9 CPS to 67.8 CPS with a higher mean value of 45.4 CPS. A hot value of 67.8 CPS was measured at the top of the section. REDFIT analysis calculates an ambiguous power-spectra, with five peaks occurring up to the Nyquist frequency. The ambiguous values could be due to the small sample number of n = 46, which could prevent the determination lower frequency periods. Sinusoidal regression also produces equally as ambiguous results, confirming either a lack of sufficient data points for confident time series analysis or simply that regular periodicity is not present in this section. The REDFIT method determined five periods in the time series at 11.25 m, 5.63 m, 3.75 m, 2.25 m, and 1.61 m. However, these periods provide a poor fit with the original time series and therefore cannot be used to confidently identify periods present.

It is assumed that the lack of statistically significant periods is a result of an insufficient number of gamma ray measurements.

McGill shows little variation between cycles and is punctuated by a significant hot bed near the top of the section with a measured value of 116.8 CPS. McGill is also a thinner stratigraphic section, measuring less than 14 m. Gamma-ray values vary between 34.6 CPS all the way to 116.8 CPS with a higher mean value of 48.09 CPS. High gamma-ray values are produced by argillaceous components in the lime mudstone. Thin beds of black chert also occur between these high values. REDFIT analysis of McGill produces up to five peaks, however only one peak occurs above the 90% confidence interval. Sinusoidal regression determines three periods at 13.87 m, 8.20 m, and 0.54 m, however because the variation in gamma-ray values between cycles is very small, fitted time series provides a poor fit. The hot values near the top of the section additionally reduce the statistical significance of the overall fit between the two series.

At Shingle Pass, the step ledges are not present. The correlative Whipple Cave Formation is expressed as a thick succession of massive lime mudstone containing varying amounts of black chert. Although the lithology is homogeneous, small amounts of variation are observed in the gamma-ray profiles on approximately a one meter-scale. Values range between 23.6 CPS to 41.1 CPS, with a mean value of 31.12 CPS. REDFIT analysis produces a one low frequency, low confidence spectral peak. Sinusoidal regression also produces ambiguous results, determining three periods at 16.53 m, 3.05 m, and 0.65 m. The of 16.53 m and 3.05 m provide a reasonable fit, however the high frequency period at 0.65 m does not favorably fit the original time series.

Results of $\delta^{13}C$ and $\delta^{18}O$ Isotopic Values and Time Series Analysis

Raw data from isotopic analysis can be found in Appendix B. Values for $\delta^{13}C$ ranged from + 0.02 to + 2.60 ‰ V-PDB at Candland Canyon and ranged from + 0.72 to + 1.43 ‰ V-PDB at Spring Gulch (Fig. 22 & 23). Aside from the anomalously high value of + 2.6 ‰ obtained from the Pterocephaliid biomere crisis interval, these values fall within the range for typical Paleozoic carbonates (Sharp, 2007). Values for $\delta^{18}O$ ranged from - 11.07 to - 8.96 ‰ V-PDB at Candland Canyon and ranged from - 12.56 to - 9.71 ‰ V-PDB at Spring Gulch. Low $\delta^{18}O$ values suggest alteration of oxygen by meteoric fluids (Bristow & Kennedy, 2008) or from tectonism and burial (O'Neil, 1987). Oxygen isotopic values fall within the typical range for altered lower Paleozoic carbonates (Jaffres et al., 2007). Isotopic values for carbon and oxygen were cross-plotted for both Candland Canyon and Spring Gulch, yielding a poor correlation, $r^2 = 0.05784$ and $r^2 = 0.00283$ respectively (Fig. 22).

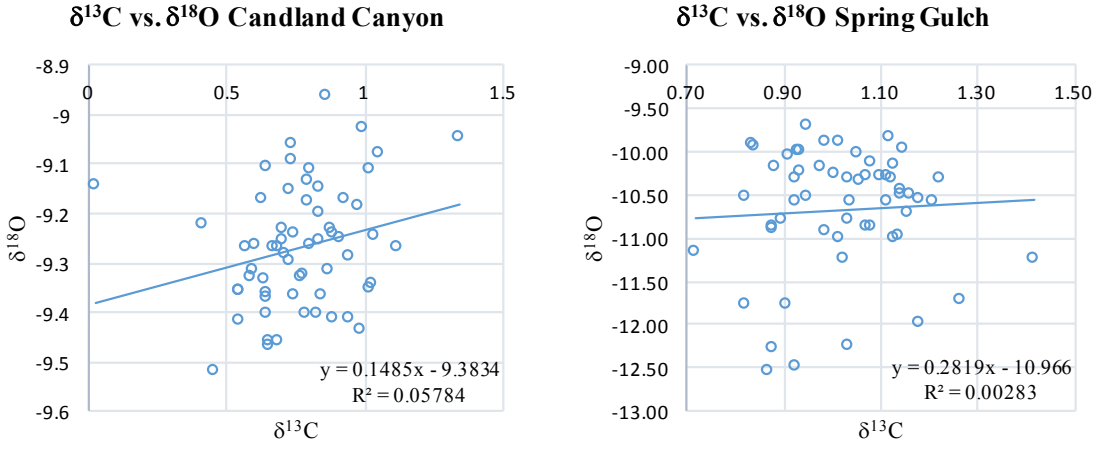

Figure 22 - Cross-plots of $\delta^{13}C$ and $\delta^{18}O$ values from Candland Canyon and Spring Gulch.

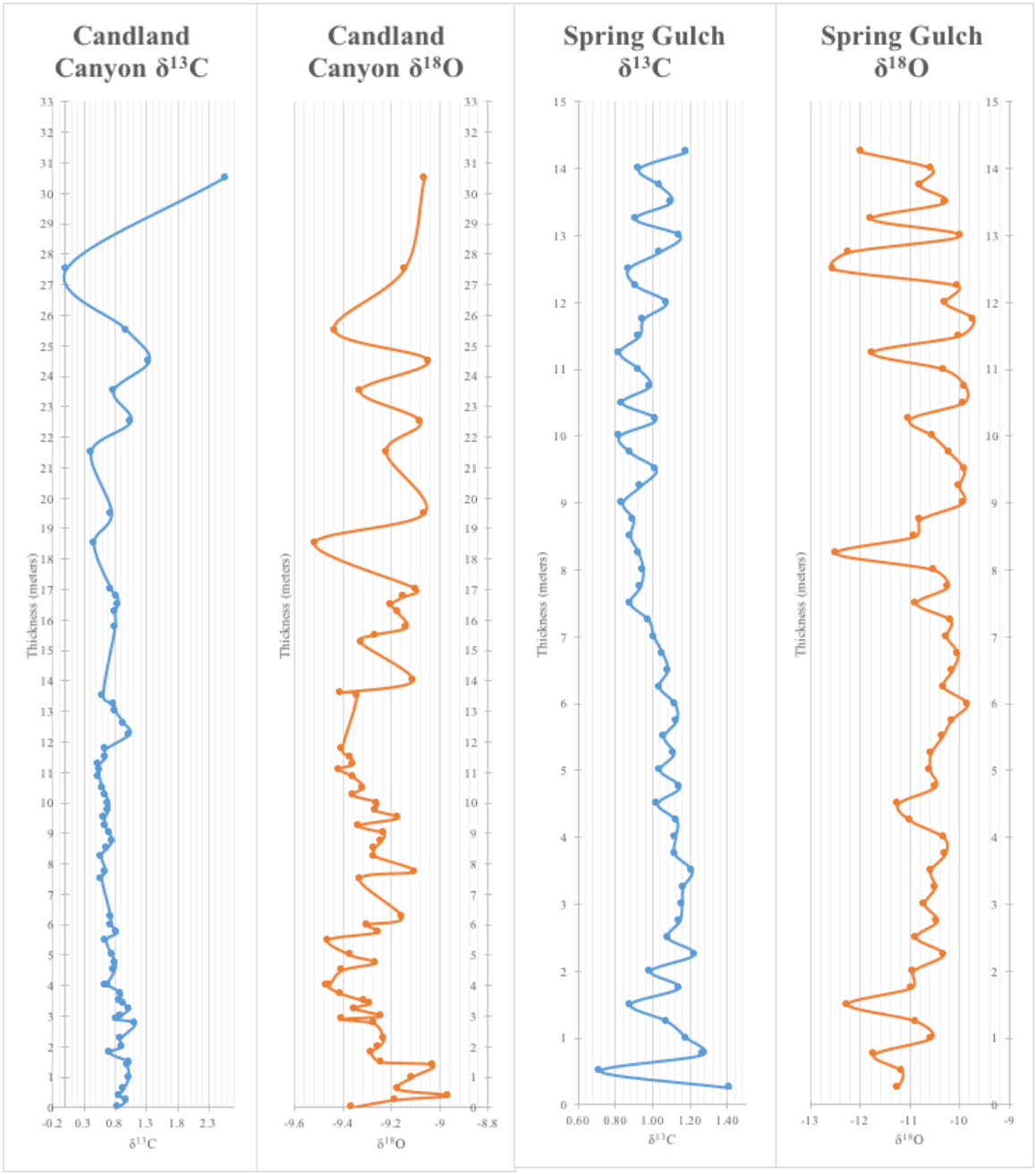

Figure 23 – Profiles of $\delta^{13}C$ and $\delta^{18}O$ values from Candland Canyon and Spring Gulch.

No covariation in cross-plots of $\delta^{13}C$ and $\delta^{18}O$ values indicates that the carbon record most likely remains robust. If both isotopic systems were altered and reset, a strong correlation in cross-plots would be expected.

Several models were used for time series analysis including periodograms, the Multi Taper Method, and the REDFIT method. However, the REDFIT method produced the most robust results and is the only power-spectral analysis described and used here. Sinusoidal regression is used to check the calculated periods by constructing a time series with periods determined from the REDFIT method.

The entire $\delta^{13}C$ data set from Candland Canyon was analyzed using the REDFIT method under default settings of a rectangular window, one oversample, and one segment. The resulting power-spectrum did not produce any distinctive peaks or reveal any periodicity in the time series. Similarly, removing the outlier value of + 2.6 ‰ that occurs at the biomere boundary did not significantly change the resulting power-spectrum. No distinctive periods were detected in the full data set. However, at Candland Canyon, only the base of the Sneakover Limestone crops out as a 10 m tall cliff. Above this cliff, the rest of the Sneakover Member is expressed as a series of step ledges that are partially covered at the base of each cycle. As a result, an equal-spaced sampling interval above 12 m was abandoned. Some of the cover above the cliff exceeded 1.2 m, which equates to five missed samples in a row and could lead to missed periods. Interpolation by averaging values between missing data points is possible, however there is no way of determining if a high-frequency, low-amplitude period exists within a missing interval.

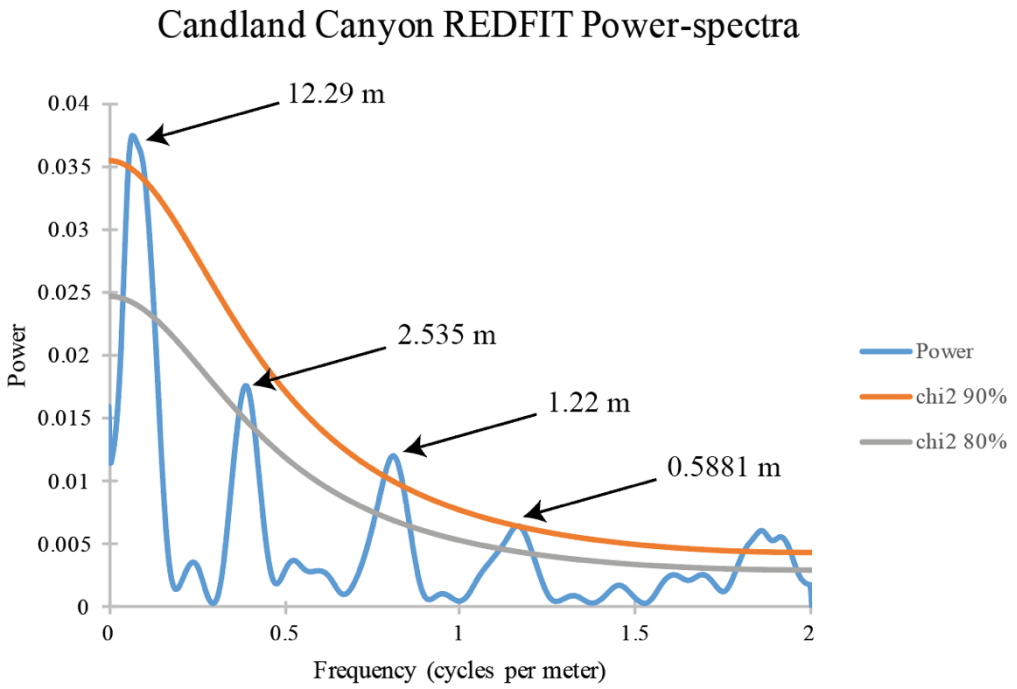

Figure 24 - Candland Canyon REDFIT power-spectra. Five spectral-peaks correlating to period of 12.29 m, 2.535 m, 1.22 m, and 0.5881 m, were determined using a triangular window, 16 oversamples, and 1 segment.

An equally-spaced sampling interval of 0.25 m was maintained in the lower cliff forming portion of the Sneakover Limestone. This 12 m section is dominated by grainstone fining-upward to mudstone and contains 48 isotope samples. Although grainstone is known to produce scatter in isotopic data, the $\delta^{13}C$ values from this 12 m section were isolated from the full data set for power-spectral analysis. The REDFIT method was used with a triangular window, an oversample of 16, and one segment. A triangular window provides good spectral resolution and limits spectral leakage in this time series. An oversample of 16 provides the best spectral resolution. Additional

oversample points beyond 16 had little effect on the resolution of this time series. Using more than one segment significantly decreased spectral resolution.

The resulting power-spectrum displays five spectral peaks (Fig. 24). The highest frequency peak (far right on Fig. 24) exceeds the Nyquist frequency and is likely a result of spectral leakage. If this peak is discarded, the remaining four peaks occur above an 80% confidence interval, and three of the peaks occur above a 90% confidence interval based off a Chi^2 distribution. The lowest frequency peak (far left on Fig. 24) corresponds to periodicity of 12.29 m. The next peak, which occurs above an 80% confidence, corresponds to a periodicity of 2.535 m. The final two peaks fall above a 90% confidence, and correspond to a periodicity of 1.22 m and 0.5881 m respectively.

Periods detected with the REDFIT model are confirmed using sinusoidal regression. Periods of 12.29 m, 2.535 m, 1.22 m, and 0.5881 m are used to construct a sinusoid that is then fitted to the original time series (Fig. 25). The blue line represents the original time series and the orange line represents the fitted time series using the periods determined with the REDFIT method. The fitted time series provides a statistically reasonable fit, with an $r^2 = 0.77825$, $chi^2 = 0.24541$, and a p-value of $p < 0.001$ based on an f-test. Therefore, the null hypothesis that the fitted times series provides a statistically poor fit is rejected. Using these periods, the fitted model provides a statistically good fit of the original time series. Visually, the fitted model overall follows the trend of the original time series, with peaks and troughs aligning favorably. However, there is inversion of some of the amplitudes and there is some diversion in the frequency. Further, the relative amplitudes of each time series do not match well in this model.

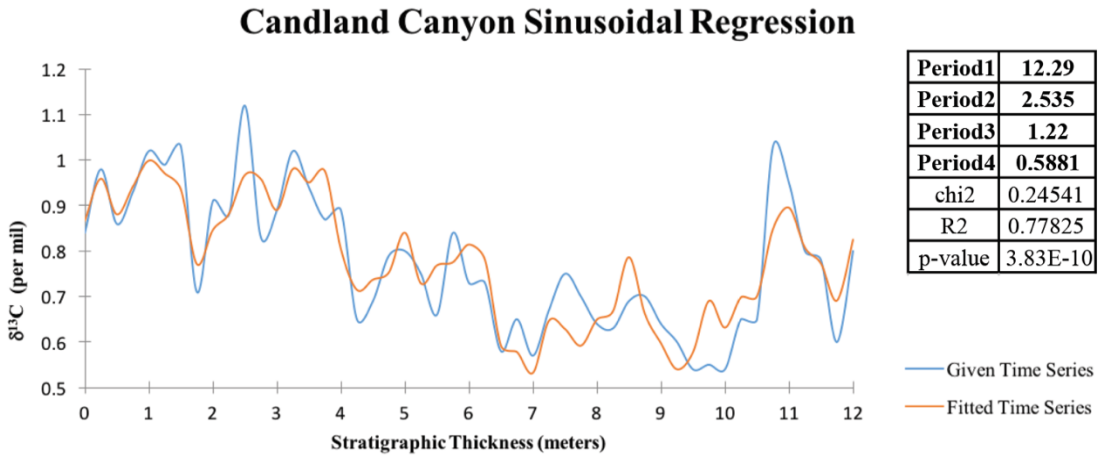

Period1	**12.29**
Period2	**2.535**
Period3	**1.22**
Period4	**0.5881**
chi2	0.24541
R2	0.77825
p-value	3.83E-10

Figure 25 - Candland Canyon sinusoidal regression. Peaks determined with the REDFIT method provide a statistically good fit.

Methods of time series analysis at the Spring Gulch section followed the same workflow as the Candland Canyon section. First, the entire $\delta^{13}C$ data set was analyzed with the REDFIT method using default settings. At Spring Gulch, the Barton Canyon Member outcrops as a vertical cliff, allowing for sampling at an equal 0.25 m interval for the entire 14.5 m section. However, the first REDFIT analysis produced several ambiguous and low confidence peaks. Grainstone to packstone beds make up the bottom 2.5 m of the section and produce significant variation in $\delta^{13}C$ values relative to the rest of the mudstone dominated succession. For this reason, the bottom 2.5 m of data were omitted and the remaining 12 m of section were reanalyzed using the REDFIT method with a triangular window, 16 oversamples and 2 segments. Again, like Candland Canyon, a triangular window provides a good tradeoff between spectral resolution and spectral leakage. More than 16 oversample points had little effect on spectral resolution. Splitting the time series into 2 segments reduced noise and did not affect spectral resolution. This

analysis produced four peaks above an 80% confidence interval, with three of the peaks falling above the 90% confidence interval based on a Chi^2 distribution (Fig. 26).

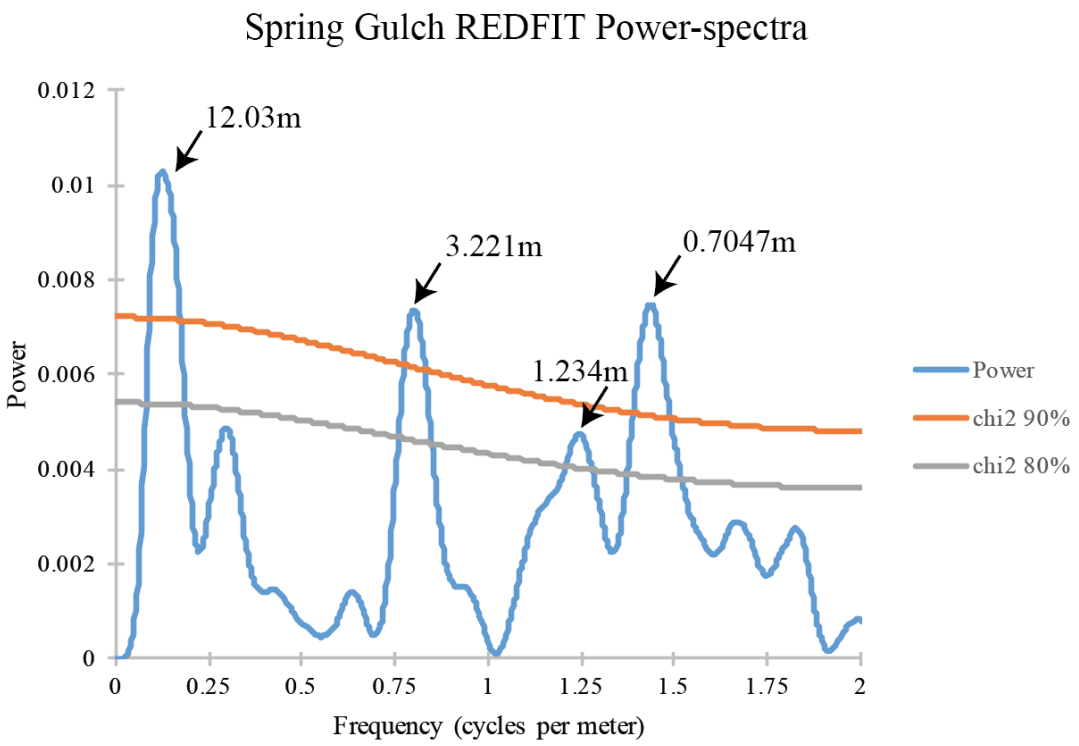

Figure 26 - Spring Gulch REDFIT power-spectra. Five spectral peaks were determined with periods of 12.03 m, 3.221 m, 1.234 m, 0.7047 m using a triangular window, 16 oversamples, and 2 segments.

From the frequencies determined by the REDFIT model, sinusoidal regression is used to produce a fitted times series. Periods of 12.03 m, 3.221 m, 1. 234 m, and 0.7047 m were entered into the model and produce a statistically significant fit (Fig. 27). The periods at Spring Gulch provide a better fit of the data than the sinusoidal regression from Candland Canyon. An $r^2 = 0.75183$, a $Chi^2 = 0.13722$, and a p-value < 0.001 statically

demonstrate the goodness of fit. Visual inspect of figure 27 also highlights the robust fit. Nearly all the frequencies are in phase and relative amplitudes fit agreeably. These four specific periods achieve an impressive fit of the original data.

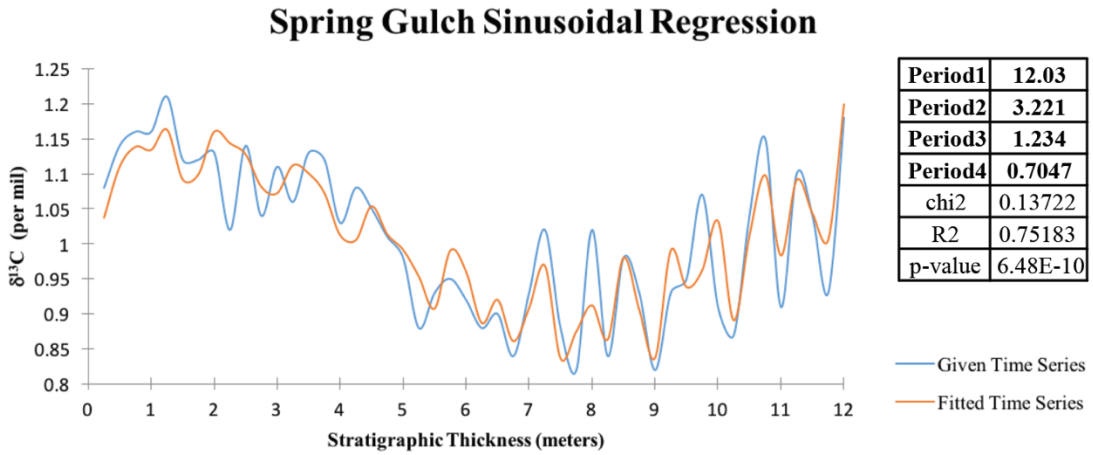

Period1	**12.03**
Period2	**3.221**
Period3	**1.234**
Period4	**0.7047**
chi2	0.13722
R2	0.75183
p-value	6.48E-10

Figure 27 - Spring Gulch sinusoidal regression. Periods determined with the REDFIT method produce a statistically significant fit of the original time series.

Estimated Accumulation Rates in the Great Basin

Estimated accumulation rates are used to predict periods expected if the succession is a result of Milankovitch forcing. These predicted periods are then compared to periods detected within the time series. The base of the Jiangshanian Stage is defined by the first appearance datum (FAD) of the Agnostid trilobite *Agnostina orientalis* in western Zhejiang, China and is estimated to be 494 Myr (Peng et al., 2011). The Ptychopariid trilobite, *Irvingella angustilimbata,* is an auxiliary index species correlative with the base of the Jiangshanian Stage in North America. Westrop & Adrain (2016) recognize the FAD of *Irvingella angustilimbata* approximately 14.8 – 15.0 m above the

base of the Corset Spring Shale. This is about the same stratigraphic position as the paleo-karst surface interpreted as a sequence boundary at three locations in Utah. At Notch Peak in Utah, the Cambrian-Ordovician boundary occurs within the Barn Canyon Member of the House Limestone (Miller et al., 2012). The base of the Ordovician is marked by the FAD of the conodont genius, *Iapetognathus sp.* and is dated at 485.4 Ma. Approximately 650 - 670 m of strata were deposited in the Central House Range during this 8.6 Myr period (Miller et al., 2012). Averaging these stratigraphic thicknesses together predicts a mean sedimentation rate for western Utah of approximately 7.6 cm/kyr. These calculations assume a linear short-term sedimentation rate that approximates long-term sedimentation rates. The sedimentation rate may have been greater than 7.6 cm/kyr, as this estimation does not correct for compaction or bioturbation. Sedimentation rates certainly fluctuate invariably, however this estimation provides a reasonable value to predict periods controlled by Milankovitch cycles (Table 1).

Table 1 - Expected periods related to Milankovitch cycles determined from estimated sedimentation rates. Sedimentation rates were determined from measured stratigraphic sections published by Miller et al. (2012).

Astronomical Parameter	**Utah**	**Nevada**
Precession (19-23 kyr)	1.4 – 1.6 m	0.6 – 0.7 m
Obliquity (41 kyr)	3.1 m	1.4 m
Eccentricity (99-123 kyr)	7.5 – 9.5 m	3.4 – 4.3 m
Eccentricity (413 kyr)	30.4 m	13.7 m

If sedimentation rates were approximately 7.6 cm/kyr and the cycles of the Sneakover and Barton Canyon are a result of Milankovitch forcing, the following periods would be expected in the time series: the precessional period would be between 1.4 to 1.6 m, the obliquity period would be approximately 3.1 m, the 100 kyr eccentricity period would fall between 7.5 to 9.5 m, and the 400 kyr eccentricity period would be approximately 30.4 m (Table. 1).

These values estimate the accumulation rates in Utah, within the House Range Embayment. This depocenter reflects the thickest packages of Cambrian rock in the Great Basin and likely represents maximum sedimentation rates. For example, the stratigraphic thickness of the Barton Canyon in Nevada is significantly thinner than that of most exposures of the Sneakover in Utah. Not only are outcrops thinner, but the cycles are also thinner on average indicating a lower sedimentation rate. At Candland Canyon, 30.5 m of strata were measured from the base of the Sneakover Limestone to the Pterocephaliid-Ptychaspid biomere boundary, compared to the 14.25 m of strata measured from the base of the Barton Canyon to the biomere boundary at Spring Gulch. Graphic correlation indicates that the Spring Gulch section is only 45% as thick as the Candland Canyon section (Fig. 28), the expected periods for Milankovitch forcing would also be less. If sedimentation rates in Nevada are assumed to be 45% of that in Utah, a precessional period would be between 0.6 to 0.7 m, obliquity would be approximately 1.4 m, the 100 kyr eccentricity would be 3.4 to 4.3 m, and the 400 kyr eccentricity would be approximately 13.7 m (Table 1; Figure 28). .

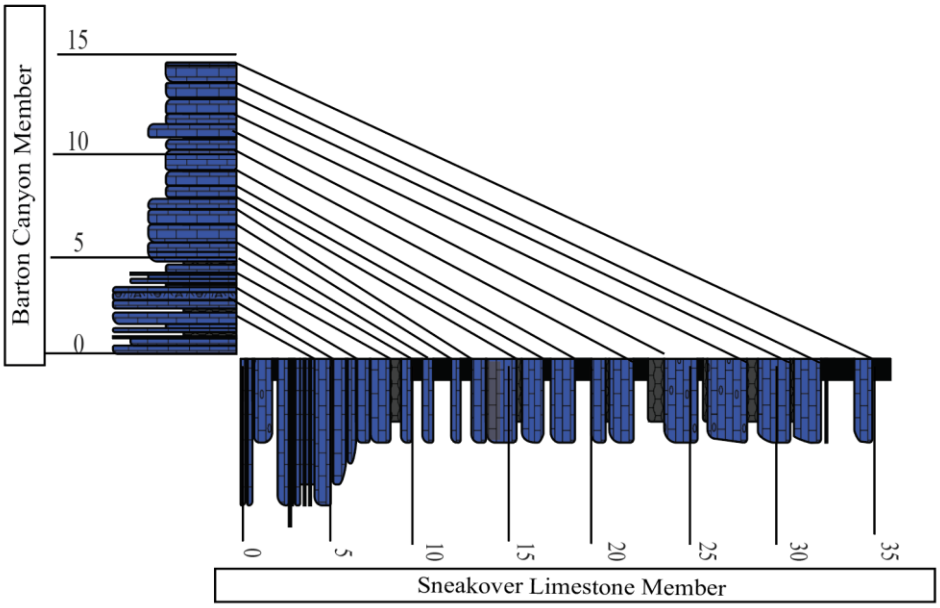

Figure 28 – Graphic correlation of Sneakover Limestone Member at Candland Canyon (x-axis) and the Barton Canyon Member at Spring Gulch (y-axis). The section at Spring Gulch is approximately 45% as thick as the section at Candland Canyon.

DISCUSSION

Sequence Stratigraphy and Platform Evolution

Sequence stratigraphy and platform evolution of the interval investigated here will be discussed first. The evolution of the carbonate platform was split into three stages. Discussion of time series analysis of both gamma-ray profiles and $\delta^{13}C$ values will follow.

Stage 1: Relative Shallowing of Sea-level and Subaerial Exposure of the Platform. The base of three sections in Utah are marked by a subaerial disconformity observed within the Corset Spring Shale and correlative Steamboat Pass Shale and Dunderberg Shale. This disrupted horizon is the only surface in all the measured sections that provides evidence of subaerial exposure and erosion. Truncation of flat-pebble conglomerate clasts and paleo-karst features suggest exposure of this surface. Vertical, *Skolithos*-like burrows are found in the surface at Candland Canyon. These burrows are truncated and filled with overlying sediment, indicating erosion and subsequent reburial. Ripped up and rotated blocks in the overlying grainstone suggests some disruptive event at the time of deposition. Lateral identification of this horizon over a near 60 km distance from the Central House Range to the Wah Wah Mountains provides further evidence suggesting this disrupted surface records some significant event. At Lawson cove, the brecciation and fracturing of the lower portion of the bed and the erosional truncation along part of the surface demonstrates that this horizon must have been cemented prior to disruption. Rounding of in-filling clasts at Lawson Cove and Steamboat mountain along with dissolution of grainstone and paleo-karst features within this surface indicates that

the lower layer must have been exposed. The unique characteristics and lateral continuity of this feature indicate the importance of this surface.

A shift in both gamma-ray values and $\delta^{13}C$ is observed at this surface, allowing for the identification of this surface on gamma-ray logs or isotope profiles. A shift of nearly 20 CPS is observed in gamma-ray profiles from Lawson Cove and decreasing trend in $\delta^{13}C$ values is observed from all sections in Utah. Values of $\delta^{13}C$ vary between + 1.69 ‰ to + 0.82 ‰ at Candland Canyon and between + 1.89 ‰ to 2.17 ‰ at Lawson Cove. These $\delta^{13}C$ values are high for typical Paleozoic carbonates and may be a result of diagenetic alteration from subaerial exposure or interactions with meteoric water. This alteration could also occur from the addition of carbon during cementation or from the dissolution and reprecipitation of carbonate (Sharp, 2007). The $\delta^{13}C$ profiles presented by Saltzman et al. (2000) from Orr Ridge, a location proximal to Candland Canyon, show a similar positive trend at nearly the same stratigraphic position in the Corset Springs Shale. Although this surface consistently produced higher positive values at all the locations sampled in this study and may be a result of alteration, it provides a means for identification from isotope values alone.

This surface also has a chronostratigraphic significance. The FAD of the trilobite *Irvingella angustilimbata,* occurs near the same interval, approximately 14.8 – 15.0 m above the base of the Corset Spring Shale (Westrop & Adrain, 2016). *Irvingella angustilimbata* is an auxiliary index species correlative with the base of the Jiangshanian Stage, estimated at 494 Ma. Because of this, this surface was used in the estimation of sedimentation rates. Because of the erosive nature, lateral continuity, chronostratigraphic significance, and $\delta^{13}C$ excursion, this disconformity is interpreted as a sequence

boundary here. Figure 29 is a cartoon image demonstrating the formation of a sequence boundary.

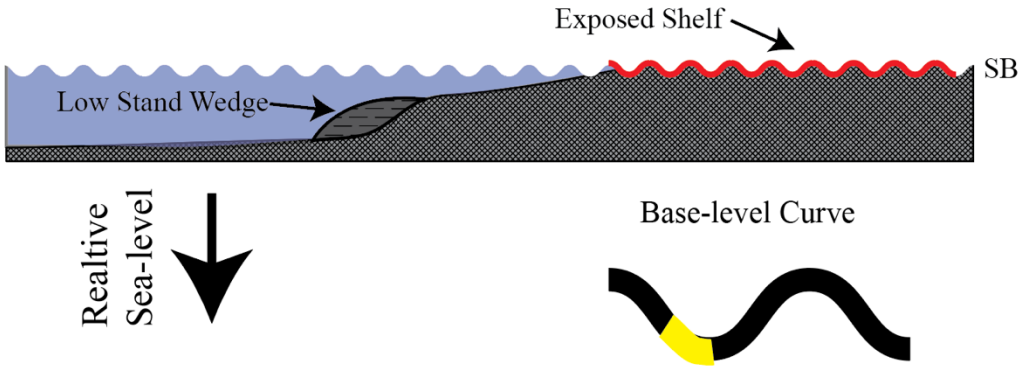

Fig. 29 - Figure depicting the formation of a sequence boundary and LST.

The Sauk II-III hiatus is thought to have formed a type I sequence boundary, supported by evidence of exposure and erosion on the North American craton (Osleger & Read, 1993). This surface may correlate to the Sauk II-III hiatus and represent another possible candidate for the Sauk II-III unconformity. Saltzman et al. (2004) proposed that the SPICE carbon isotope excursion was a possible result of this regressive event. The SPICE event occurs in the middle of the John's Wash Limestone Member in the Central House Range. This limestone Member underlies the Corset Spring Shale Member and is located approximately 15 m below the disrupted horizon at Candland Canyon. The contact between the John's Wash and the Corset Springs Member is paraconformable. However, the overlying disconformable paleokarst surface likely represents the actual

regressive minimum of the Sauk II-III sub-sequence boundary due to the evidence of subaerial exposure and significant disruption.

Following the Sauk II-III hiatus (Palmer, 1981) an influx of siliciclastics and shales were deposited regionally as part of the of the Corset Spring Shale and Steamboat Pass Shale, and the correlative upper part of the Dunderberg Shale. Discrete carbonate beds interbedded in the shale overlying the disrupted horizon at both Lawson Cove and Steamboat Mountain are grainstones and flat pebble conglomerates, indicating higher energy deposition and possible storm influence. This contrasts with Candland Canyon where lime mudstone and wackestone overlie the surface, suggesting that strata deposited at the same horizon in the Wah Wah Mountains was higher energy and likely shallower than the central House Range. The difference in water depth and lithology may be a possible indication of the influence of the House Range Embayment. These rocks that make up this regional shale package are as an interpreted lowstand systems tract (LST; Fig. 30). Typically, LST deposits will onlap the sequence boundary, however this is unsubstantiated by a lack of stratal geometries.

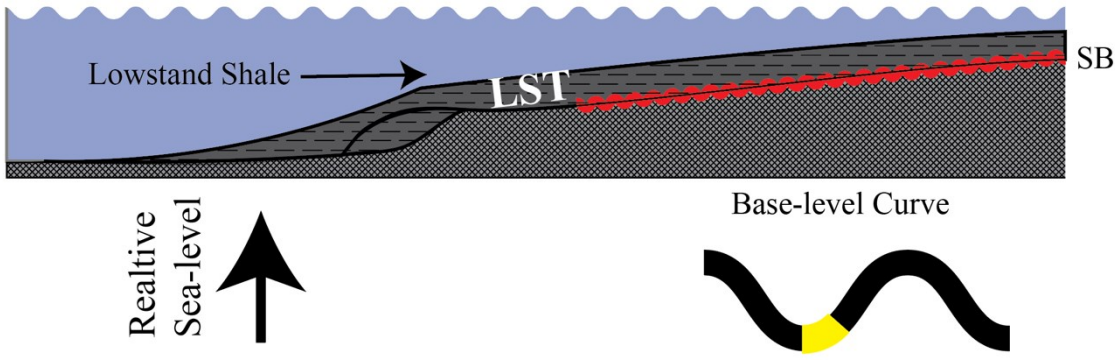

Figure 30 – Cartoon depicting deposition of siliciclastics representing the LST.

Stage 2: Relative Base-level Rise, Carbonate Production and Cyclic Aggradation. As base-level rose following the Sauk II-III lowstand, input from siliciclastic sources decreased and carbonate production became established ("start-up") in the mid-to late *Elvinia* zone. Where carbonate production becomes firmly established marks the transgressive surface (TS; Fig. 31). This coincides with the contact between the Corset Spring Shale or Steamboat Pass Shale and Sneakover Limestone Member in Utah. In Nevada, this the contact between the Dunderberg Shale and the Barton Canyon Member. Carbonate accumulation in the cyclic limestones of the Sneakover Member and correlative Barton Canyon Member likely reflect the early to mid-stages of transgression, and are interpreted as a transgressive systems tract (TST; Fig. 31). The expression of increasing base level is observed in the fining-upward, cyclic succession.

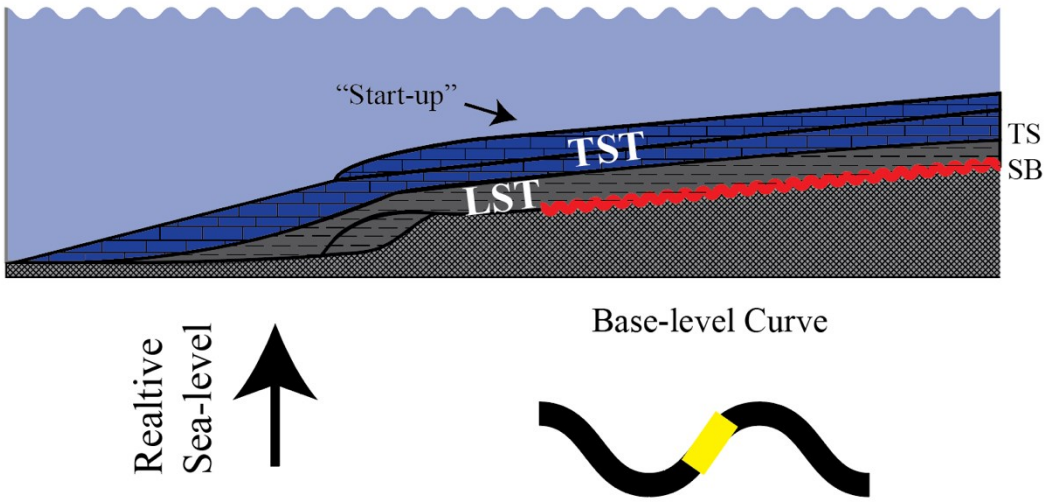

Figure 31 - Cartoon depicting startup of carbonates with sea level rise.

The basal cycles of the Sneakover and Barton Canyon are trilobite and echinoderm grainstones with occasional ooids, peloids, and cryptomicrobial bioherms. Thrombolites were identified in this lower section at Spring Gulch, indicating shallow water conditions initially.

As base-level continued to rise, the rocks fine upward to burrowed trilobite wackestone and mudstone as carbonate production was able to "keep-up" and cycles aggraded upward. These carbonate cycle facies are though to reflect shallowing upward, parasequence sets that accumulated during base-level rise (Osleger & Read, 1991). In Utah, cycles generally thicken upward reflecting increasing accommodation with sea-level rise. However, in Nevada, these cycles are not only thinner, they tend to thin upwards as well. Also, there are fewer cycles in Nevada, as transgression may have caused the basinward carbonates to "give-up". While cycle production ceased in Nevada, carbonate cycles are observed throughout the entire Sneakover Limestone and overlying Hellnmaria Member in Utah. This likely reflects differing accumulation rates, differential subsidence, and the give-up of carbonate production in outer shelf settings. The position at which cycles shut off is represented by a carbonate hardground at Steptoe Ranch (Evans, 1997). This surface represents sea-level maxima and is interpreted as a drowning unconformity and maximum flooding surface (MFS; Fig. 32). In Nevada, the MFS is marked by the transition from the cyclic carbonates of the Barton Canyon Member to thinly bedded Catlin Member. Cyclic accumulation continued upward in Utah, and the MFS is represented by the contact between the Sneakover and the overlying Hellnmaria Member. The MFS is produced by sediment starvation attributed to sea-level maxima. It

results in condensed sections and is often represented as a sharp, increase in gamma-ray values on a log, which is observed at McGill and the Fish Springs Range.

Although stratal geometries are unknown, the fact that there are fewer cycles in Nevada and that all the sections fine-upward and thin-upward, the cycles of the Barton Canyon may reflect backstepping of retrogradational parasequences. Retrogradational trajectories could be a give-up response to transgressive sea-level that may be observed in more basinward settings. Nevertheless, thinning-upward, fining-upward, and fewer cycles present in the Barton Canyon is the only line of evidence supporting this notion of retrogradation. Only 14 cycles are observed at Spring Gulch compared to the 30 cycles exposed at Steamboat Mountain. However, because of the lack of stratal geometries, this hypothesis is unsupported and only is speculation. This hypothesis cannot be confirmed from outcrop data alone.

The Pterocephaliid-Ptychaspid biomere boundary also occurs within this interval. Stitt (1975) proposed a widely-cited hypothesis that attributed the extinction event to the rise of cool offshore waters that flooded the shelf, killing warm-water adopted species and replacing them with deep water faunas. This is also supported by a positive shift in of + 2.6 ‰ shift in $\delta^{13}C$ values over the biomere boundary at Candland Canyon. This may reflect a significant oceanographic event across Laurentia and was perhaps influence by sea-level rise (Saltzman et al., 2004). Cool, anoxic waters may have rose onto the shelf and enhanced the preservation and burial of organic C^{12}, leading to a relative increase in $\delta^{13}C$ values (Saltzman et al., 1998). Anoxic conditions would inhibit the decomposition of organic carbon and would provide a potential kill mechanism at the biomere boundary as proposed by Stitt (1975).

Stage 3: Highstand and Progradation of Carbonates in Utah, and Drowning of the Carbonate Factory in Nevada. Cyclic aggradation continued in Utah, depositing the massive cliffs of the Hellnmaria Member of the Notch Peak Formation. These cliffs were deposited following maximum flooding, during the onset and development of a highstand systems tract (HST; Fig. 32). The Hellnmaria likely reflects progradation and aggradation of an established and healthy carbonate platform that was filling the newly created accommodation space. Conversely, coeval sections in Nevada show deposition of finely laminated carbonate turbidites and grainflows. The parting between the mudstone beds in the Catlin Member may exhibit an alternation between pelagic sediments and sediments deposited as density flows such as turbidites. Based on the graded bedding and textures displayed by this unit, the Catlin Member is interpreted as Bouma type turbidite deposits. This material would have been shed off the landward carbonate platform, either when accommodation was filled or there was instability on the shelf.

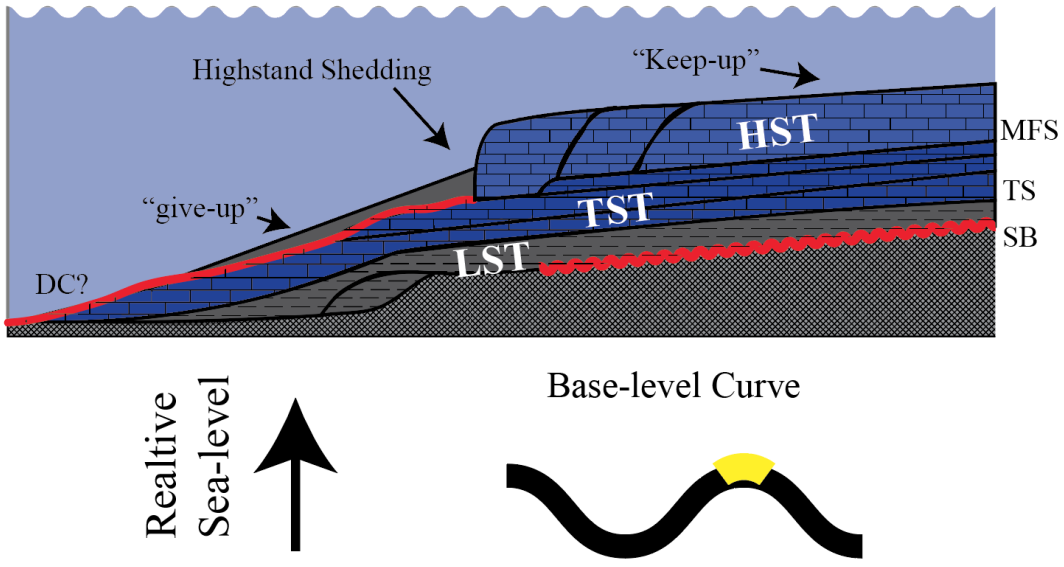

Figure 32 – Cartoon depicting give up and keep up of carbonates during the HST.

Transgression was rapid enough to shut-off carbonate production in the upper Barton Canyon, forming a drowning unconformity that is interpreted as a MFS. The cement encrusted horizon described by Evans (1997) provides support for the existence of a drowning unconformity separating the Catlin Member from the Barton Canyon Member. Once sea-level rise began to slow, the carbonate platform began to prograde, filling the available accommodation with the deposition of the Hellnmaria. In Nevada, turbidites of the Catlin Member of the Windfall Formation are interpreted to have been deposited as a result of highstand shedding of argillaceous carbonate mud off the prograding carbonate platform (Fig. 32). A correlation of all sections in this study can be found in figure 33.

Stratigraphic Trends of Gamma-Ray Values

Due to differences in stratigraphic thickness and siliciclastic input at each section, the resulting plotted power-spectra are unique to each section and do not provide any reliable climatological information, nor do they provide an independent means for correlating stratigraphic sections. A gamma-ray scintillometer measures the decay of naturally occurring radiogenic nuclides in sediment. Gamma-ray values are directly influenced by the lithological composition of the rock. Changing environments certainly influence lithology, however lithology can also be influenced by changes in tectonic regime, subsidence rates, and sediment influx. Additionally, the scintillometer takes a ten-second average of the number of gamma-rays striking the NaI crystal and reports this value in CPS. Because this value is an average, the same bed may not produce the exact

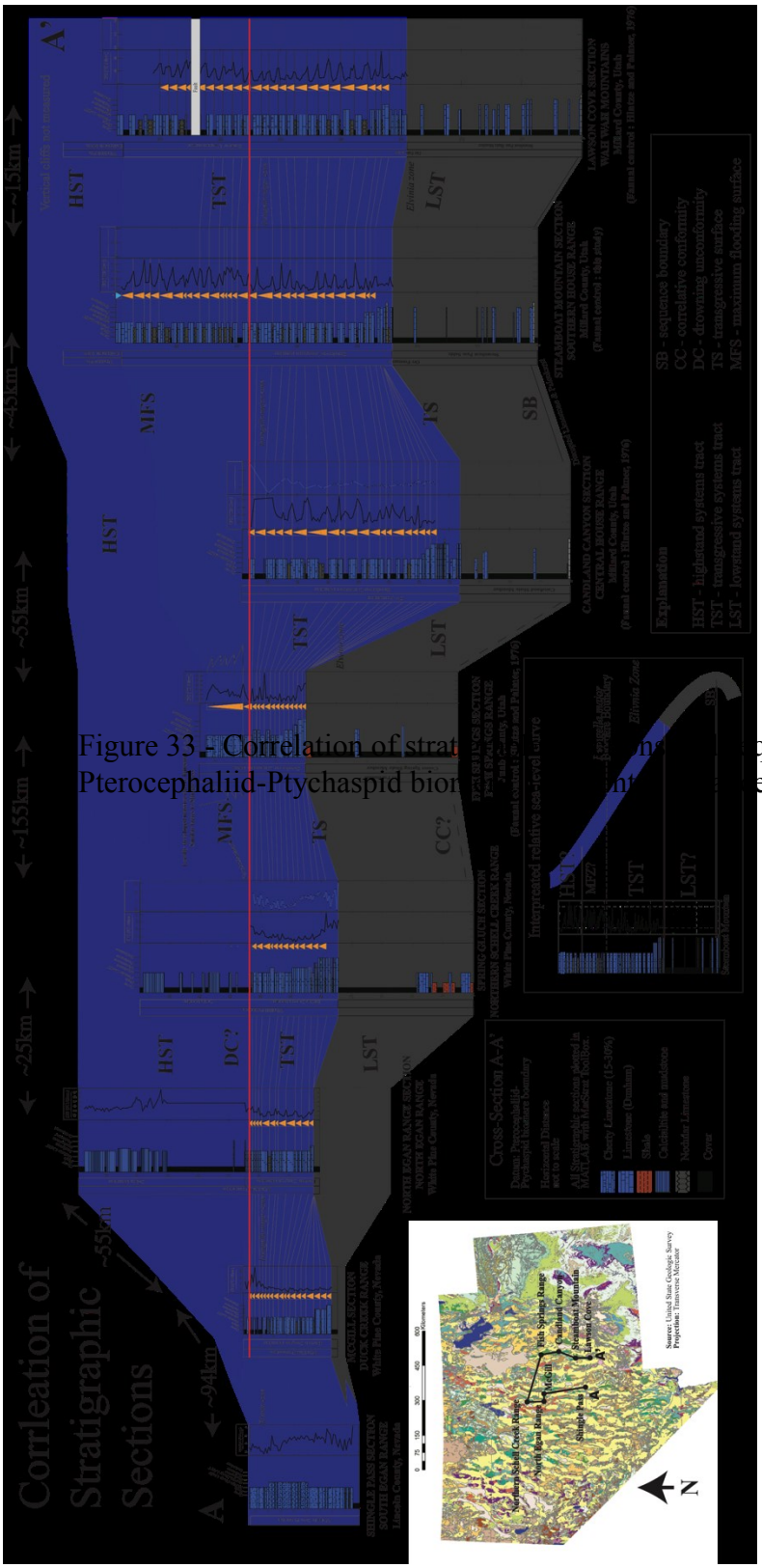

Figure 33 - Correlation of strat nf quence stratigraphic framework. All sections Pterocephaliid-Ptychaspid bion nf es not to scale.

same value every time it is measured. The trends between lithologic contacts in the gamma-ray profile will be the same (i.e. shale produces higher CPS and limestone produces lower CPS). However, there will be some variation in the precise value, limiting the application of time series analysis on this variable.

Although gamma-ray profiles may not provide any reliable climatological information, they allow for identification of cycles in seemly clean (essentially non-radioactive) carbonates. Especially where the contacts between beds are unclear or in a massive succession such as Shingle Pass. In Utah, more variation in gamma-ray values is observed relative to Nevada. This is likely due to a larger siliciclastic input in the more near shore settings. Profiles from Candland Canyon, Lawson Cove and Steamboat Mountain are remarkably similar in their expression, with similar variation in gamma-ray values between cycles. The profile from the Fish Springs Range is similar to profiles in Nevada due to the thinner stratigraphic succession and lower variation in gamma-ray values between cycles. Sections from Nevada show little variation in the clean carbonates of the Barton Canyon Member. These sections are harder to correlate from gamma-ray profiles alone and show little similarity between sections. It is noteworthy to mention that the gamma-ray profile and the $\delta^{13}C$ profile from Spring Gulch follows a similar trend, with higher values lower in the section that decrease up-section before increasing at the top of the section. Higher gamma-ray values indicate a higher proportion of clay rich, argillaceous material. This material is potentially enriched in organic material, leading to the higher $\delta^{13}C$ values observed lower in the section at Spring Gulch. Up-section, gamma-ray values decrease as transgression continued. Concomitantly, $\delta^{13}C$ values decreases up-section, presumably as less argillaceous and organic rich material was

deposited. This concept could be further tested by investigating TOC % throughout the section.

Stratigraphic Trends of $\delta^{13}C$ Values at Spring Gulch, Nevada

Initial power-spectral analysis of $\delta^{13}C$ values from both sections at Candland Canyon and Spring Gulch yielded low confidence peaks with spurious periods. Data were cleaned at Spring Gulch by removing the lower 2.5 m of section. The lithology of the base of the section at Spring Gulch is grainstone to packstone with little micrite matrix. Micrite has been shown to be rock buffered over a large range of diagenetic environments (Saltzman et al., 2004) and thus often retains a robust record. The absence of a fine-grained micritic matrix in grainstone makes these rocks more susceptible to diagenetic alteration and produces scatter in the data. For this reason, the lower 2.5 m were excluded from analysis. The remaining 12 m of section produced four distinctive periods at 12.03 m, 3.221 m, 1.234 m, and 0.7047 m when analyzed with the REDFIT method. What these spectral peaks correspond to becomes visually apparent when the $\delta^{13}C$ profiles are overlain on a properly scaled photograph of the outcrop (Fig. 34). These periods that were encoded in the carbon isotope record closely track the lithology of the succession. The highest frequency period determined roughly estimates the cycle thickness. At Spring Gulch, there are 15 cycles exposed in the 12 m of section analyzed. Cycle thickness varies between 0.5 m to 1.3 m, with an average thickness of 0.8 m. This cycle thickness closely lines with the highest frequency $\delta^{13}C$ period at 0.7047 m. Higher $\delta^{13}C$ values typically fall between the cycles in the argillaceous nodular lime mudstone and lower $\delta^{13}C$ values are produced from the clean lime mudstone.

The next period at 1.6 m appears to correlate to a 2:1 bundling of the cycles, although the third $\delta^{13}C$ period at 1.234 m is less than the average thickness of two cycles bundled. The second period at 3.221 m could arguably correlate to a 5:1 bundling of the cycles, as the average thickness of five cycles is 4.0 m, a difference of 0.779 m. The first, lowest frequency peak at 12.03 m correlates to the section thickness which is 12.0 m. Higher $\delta^{13}C$ values occur lower in the section, with an inflection point near mid-way up, above which lower $\delta^{13}C$ values are observed until just below the top of the section. This sine wave-like trend in the $\delta^{13}C$ profiles explains the highest frequency peak in the power spectrum.

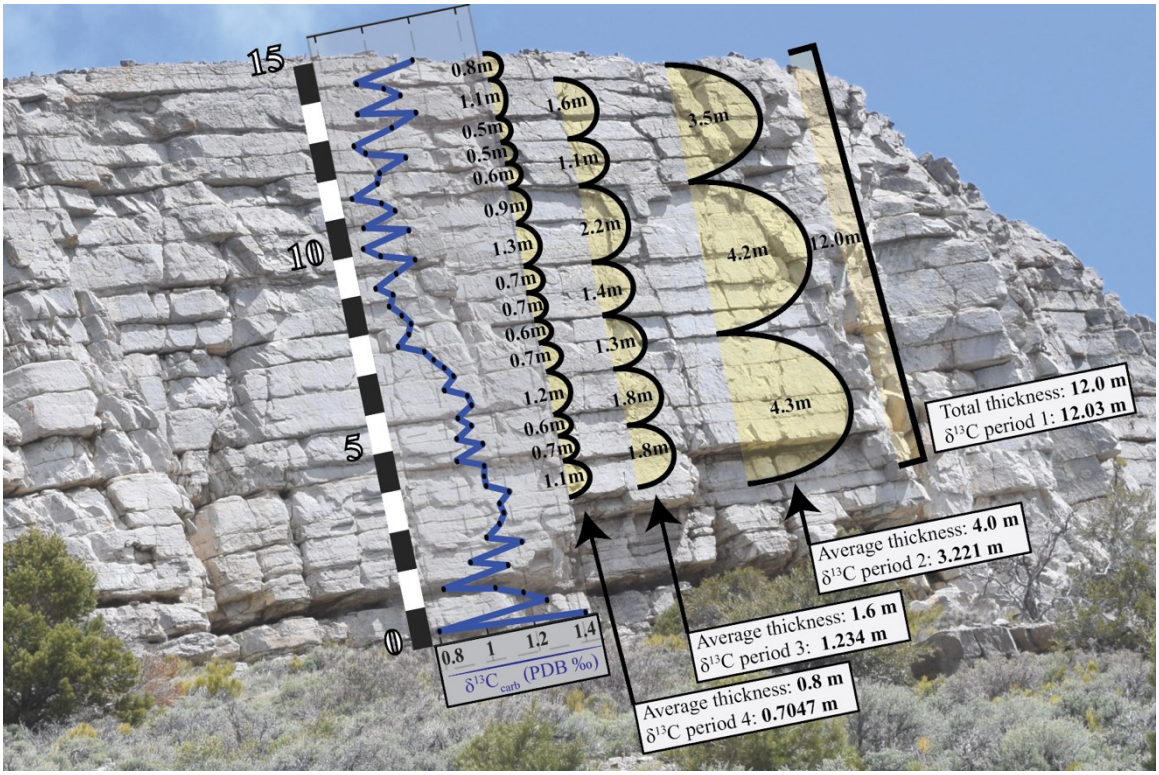

Figure 34 - Overlay of $\delta^{13}C$ profile and REDFIT periods on the Barton Canyon at Spring Gulch. Cycle thickness and periods determined in the $\delta^{13}C$ profiles correlate favorably. Other periods calculated correlate to bundling of the cycles.

Spectral peaks at Spring Gulch compare remarkably well with expected Milankovitch cycle periods determined from estimated sedimentation rates. Based on estimated sedimentation rates, a precessional period would be expected between 0.6 m to 0.7 m. The highest frequency period in the $\delta^{13}C$ profile at Spring Gulch is 0.7047 m. An obliquity period is expected at 1.4 m. This is close to the third period at Spring Gulch, which is calculated at 1.234 m. Finally, an eccentricity period that correlates to the 99-123 kyr cycle would be expected between 3.4 m to 4.3 m. The second spectral peak at Spring Gulch occurs just below these values, at 3.221 m.

The match between the predicted periods corresponding to Milankovitch cycles and the actual periodicity recorded in the rock is remarkable. However, the estimated sedimentation rate used in this study is an average rate that does not consider the variability of sediment influx, nor does this value correct for compaction or bioturbation. Further, modern timing of Milankovitch cycles was used for the calculation of precession and obliquity bands. During the Cambrian precession and obliquity would have almost certainly been shorter periods. Precession during the Cambrian could have been as short as approximately 17 kyr and obliquity could have been 28 kyr (Walker & Zahnle, 1986). Eccentricity is a result of interplanetary gravitational interactions between the Sun, the Earth, and Jupiter so the periods of approximately 100 kyr and 400 kyr would have likely remained stable for the at least the Phanerozoic (Algeo & Wilkinson, 1988). Taking this into consideration only slightly alters the expected periods. For example, a 17 kyr precessional cycle would yield a predicted period of 0.58m in Utah. This is just less than the expected period determined from a 19 to 23 kyr period, which is between 0.6 m to

0.7m. If obliquity was only a 28 kyr cycle in the Cambrian, the period would 0.96 m, which is just under the 1.234 m period two that was detected at Spring Gulch.

Period four matching the cycle thickness, period three approximating a 2:1 bundling of cycles, and period two approximating a 5:1 bundling is probably the most convincing argument for astronomical forcing controlling sedimentation. Regardless of the actual timing of the succession, if these cycles were a result of Milankovitch forcing, a 1:1, 2:1, and 5:1 bundling of periods would be expected. For example, obliquity is approximately twice the period of precession, thus a 2:1 relationship. Eccentricity is approximately five times the period of precession, thus a 5:1 relationship. This ratio provides convincing evidence of putative Milankovitch style cyclicity recorded at Spring Gulch.

Three of the four spectral peaks detected at Spring Gulch are above a 90% confidence interval, meaning that there is a one-in-ten chance that the peak is a result of noise. This is fairly high confidence, and these peaks are most likely real. Period three which occurs at 1.234 m is lowest confidence peak, only falling above the 80% confidence interval. There is a 20% chance that this peak is a result of noise. However, if this peak does correspond to an obliquity cycle, the lower relative amplitude of this band could be explained by the paleogeographic location of Laurentia. During the Cambrian, Utah and Nevada were located at equatorial latitudes. Because changes in insolation due to variations in tilt of the Earth are less at equatorial latitudes, the obliquity band may be suppressed in tropical successions.

Values of $\delta^{13}C$ appear to closely track lithologies at Spring Gulch. This is quantitatively supported by power-spectral analysis and sinusoidal regression. Comparing

peaks and troughs of $\delta^{13}C$ values to measured cycle thickness qualitatively demonstrates that secular variations in isotopic values exist between cycles. These carbonate cycles fit the definition of parasequences, which are believed to be the result of 5thorder sea-level cycles. Referring to the sea-level cycles of Sloss (1963), 5th order parasequences are high-frequency cycles that form as the result of minor sea-level fluctuations, on the amplitude of 1 – 150 m. Parasequence cycle duration is believed to occur on the time-scale of 0.01 to 0.1 Myr (Sloss, 1963). These minor sea-level fluctuations are superimposed on higher order sea-level cycles. As a result, during a large-scale transgression, minor shallowing events may be recorded with the overall sea-level rise as parasequences. The tops of the cycles present at Spring Gulch are homogeneous mudstone capped by a more argillaceous, nodular lime mudstone. Upward-shallowing of cycles is indicated by increased siliciclastic content in the tops of the cycles. This represents a pulse of argillaceous material from the craton during a minor shallowing event. The rest of the cycle is clean carbonate, free of any siliciclastic content, indicating a period of somewhat deeper water conditions.

Clean carbonate produces lower $\delta^{13}C$ values relative to the recessive and nodular lime mudstone between the cycles. This is especially true higher in the Spring Gulch section. Conversely, recessive nodular lime mudstones between the cycles produce higher $\delta^{13}C$ values relative to the clean carbonate. If these cycles are a result of upward-shallowing during a minor regressive pulse of relative sea-level, trends in $\delta^{13}C$ values appear to roughly track changes in water depth. The Barton Canyon was deposited during a relative rise in sea-level, indicated by the overall fining-upward succession of grainstone to mudstone. Excluding the basal grainstone, the lower portion of the Barton

Canyon produces $\delta^{13}C$ values greater than 1.0 ‰. This lower section was deposited during early to mid-transgression, in presumably shallower water conditions. As transgression persisted, $\delta^{13}C$ values drop below 1.0 ‰, apart from several of the recessive beds between cycles and the upper most portion of the section. Lower in the section, where $\delta^{13}C$ values are on average higher, there is less variation in $\delta^{13}C$ values between the cycles. Up section however, there is more variation in $\delta^{13}C$ values between cycles, with higher $\delta^{13}C$ values almost perfectly lining-up with the recessive nodular lime mudstone between cycles.

If these cycles are shallowing-upward, the argillaceous material derived from the craton is potentially enriched in organic carbon. Because organic carbon is enriched in ^{12}C, it would lead to a relative increase in $\delta^{13}C$ values. Conversely, as sea-level rises and organic rich argillaceous material is cut-off from the basin, relative values of $\delta^{13}C$ would decrease. The overall trend of $\delta^{13}C$ values at Spring Gulch decrease from the base of the section towards the top as transgression progressed and water depths presumably increased. This hypothesis follows the explanation of the SPICE event by Saltzman et al. (2004), whom attributed the positive $\delta^{13}C$ excursion to enhanced weathering and burial of ^{12}C during the Sauk II-III regression. If the SPICE is possibly a result of regression related to a 1st order sea-level cycle, the secular variations of $\delta^{13}C$ between carbonate cycles of the Barton Canyon may be related to 5th order sea-level cycles.

Additional testing of this hypothesis is required and could involve either determining clastic content from insoluble residue percentages or determining total organic carbon (TOC). Insoluble resin percentages would quantitatively determine the clastic input between cycles in the recessive, argillaceous beds. Originally developed for

conodont biostratigraphy, this technique involves dissolving limestone and weighing the residual material This would provide further support for a pulse of siliciclastics during upward-shallowing of cycles. Determining TOC content would support the hypothesis that increased weathering and enhanced burial of organic rich sediment during regression is leading to the positive increase in $\delta^{13}C$ values, both between cycles and across the entire section.

Stratigraphic Trends of $\delta^{13}C$ Values at Candland Canyon

At Candland Canyon, an equally spaced sample interval was not maintained and therefore a significant portion of the section was omitted from the time series analysis. However, the Pterocephaliid-Ptychaspid biomere was chemostratigraphically identified by a + 2.6 ‰ excursion of $\delta^{13}C$ values in the upper portion of the section. This positive excursion was described in the House Range by Saltzman et al. (1998), and is attributed to the rise of anoxic water onto the shelf, enhancing the preservation of organic carbon. Anoxic conditions also provide a potential kill mechanism for mass mortality at the biomere boundary (Taylor, 2006). Although time series analysis was not possible with this upper section, the identification of the biomere boundary was worth the sampling and analysis of the entire succession.

The bottom 12 m at Candland Canyon is well exposed grainstone to packstone that fines-upward to mudstone by 6 m. Only this bottom 12 m of section were analyzed with the REDFIT method and sinusoidal regression. Five spectral peaks were identified; however, the fifth peak exceeds the Nyquist frequency and is therefore discarded. The other four spectral peak correlate well with Spring Gulch. For example, the fourth peak at

Candland Canyon correlates to a period of 0.5881 m. Compare this to the fourth peak at Spring Gulch, which corresponds to a period of 0.7047 m. This is a difference of only 11.66 cm, a rather favorable match. The Third peak at Candland Canyon correlates to a period of 1.22 m. This is virtually the same as Spring Gulch, which is at 1.234 m, a difference of 1.4 cm. The second peak at Candland Canyon occurs at 2.535 m. This differs from Spring Gulch by 0.686 m. However, the second peak at Candland Canyon is lower confidence and falls between the 80% and 90% confidence interval. Due to limitations of sampling resolution, the exact period recorded may not have been calculated perfectly. The first and largest peak at Candland Canyon correlates to a period of 12.29 m. This is very close to the period calculated at Spring Gulch which occurs at 12.03m, a difference of 26 cm.

These periods calculated at Candland Canyon were confirmed with sinusoidal regression and produce a good fit. However, the fit is not as ideal as Spring Gulch. This may be a result of the lithology sampled at Candland Canyon. Due to cover higher in the section, samples were only collected from the basal 12 m, which is mostly composed of grainstone and packstone. Because this rock contains little micrite, there is a higher likelihood of alteration. Although the values produced from this section appear robust, in that they fall within the generally accepted range for $\delta^{13}C$ values in lower Paleozoic carbonates. Caution is still taken when making any paleoclimatological interpretations from this data set.

Although the $\delta^{13}C$ periods calculated at Candland Canyon match the $\delta^{13}C$ periods calculated at Spring Gulch reasonably well, the isotopic values at Candland Canyon do not track lithology as close as at Spring Gulch. When $\delta^{13}C$ profiles are overlain on a

properly scaled photograph of the outcrop (Fig. 35), the more positive $\delta^{13}C$ values tend to fall between cycles in the argillaceous nodular lime mudstone. The actual cycles are much more difficult to distinguish in the isotope profile alone at Candland Canyon. For example, the fourth period at 0.5881 m does not correlate to cycle thickness at Candland Canyon. However, the next period at 1.22 m does in fact match the average cycle thickness. There were 10 cycles identified in this 12-m-thick section, so the average cycle thickness is 1.2 m, which matches very well with the period calculated at 1.22 m. Period two appears to correlate with a 2:1 bundling of average cycle thickness. The average thickness of two cycles in this 12 m section is 2.4 m, compared to the calculated period of 2.535 m. This is a close fit, with a difference of only 13.5 cm. Finally, the first peak of 12.29 m correlates with the entire section thickness of 12 m.

There are few explanations for $\delta^{13}C$ values not tracking lithology with the same degree of fit as Spring Gulch: first average cycle thickness varies more at Candland Canyon. At Candland Canyon, the cycles vary between 0.8 m to 1.7 m and continue to thicken upward. This is a difference of 0.9 m, which potentially explains the poorer fit that was determined with sinusoidal regression. Second this section was collected from a grainstone dominated succession. The lack of fine-grained micritic components in the matrix of these carbonates may have produced additional scatter in the data. Finally, there may be an optimal belt for recording robust climatic signals that is in relatively deep water distal from the influence of paleographic features.

The periods calculated from the REDFIT method at Candland Canyon do not match the estimated accumulation rates as well as in Nevada. The first calculated period of 0.5881 m is almost half of the expected cycle thickness predicted from sedimentation

rates. The second peak however, lines well with the expected period for precession as predicted from sedimentation rates. In Utah, a precessional period would be expected to fall between 1.4 m and 1.6 m based on sedimentation rates. The second period was calculated at 1.22 m, just below the expected range. The third period at 2.4 m also falls short of the predicted period of 3.1 m.

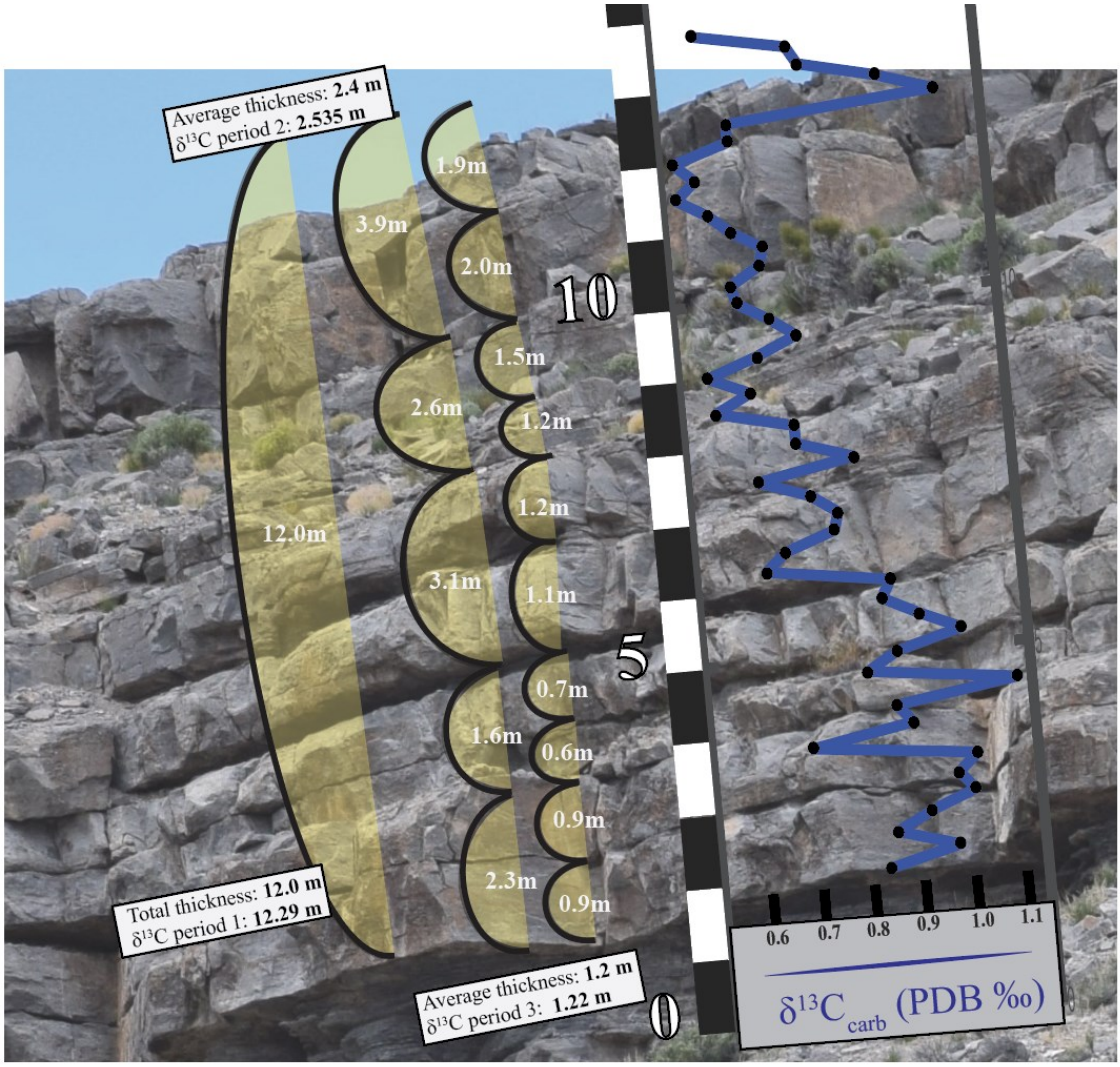

Figure 35 - Overlay of the $\delta^{13}C$ profile and REDFIT periods on the Sneakover Limestone at Candland Canyon. Higher values typically fall between cycles. The Cycle "10" can be just barely made out at the very top of the section. A positive excursion of $\delta^{13}C$ of 1.1 ‰ is observed below this cycle.

The estimated accumulation rates do not consider compaction or bioturbation; therefore, these estimated sedimentation rates could be greater than the actual measured value. These sedimentation rates also do not consider changes in sedimentation rates or the potential of a hiatus in deposition. It is very possible that sedimentation rates were higher in the overlying Hellnmaria Member, when accommodation was being filled by highstand normal regression.

Nevertheless, the 1:1 and 2:1 bundling of peaks two and three is strong evidence suggesting Milankovitch style cyclicity at Candland Canyon. Furthermore, period one at 0.5881 m is approximately half of period two at 1.22 m. As described in the results section, many of the sections in Utah contain cycles that have a dark bottom and a light top. The first spectral peak could be referring to the splitting of individual cycles. A possible environmental control on this could be simply explained by axial precession. Due to axial precessions gyroscopic motion, seasons in each hemisphere do not remain constant over entire precessional period. Winter and summer seasons in the northern and southern hemisphere alternate once over one precessional cycle. Although phenomena this would have a limited affect at equilateral latitudes, it is one possible explanation for the first spectral peak. Precession of the seasons may be responsible for the different coloration of beds that is observed in Utah, although there is limited supporting evidence for this concept.

Implications for Astronomical Forcing and Climate Change

Power-spectral analysis of $\delta^{13}C$ values from Candland Canyon and Spring Gulch reveal Milankovitch style cyclicity recorded in upper Cambrian carbonates. Similar

periodicities were calculated with power-spectral analysis from both sections. At Spring Gulch, periods predicted to be related to Milankovitch cycles match the actual periodicity favorably. Moreover, periods at Spring Gulch show a 1:1, 2:1, and 5:1 bundling of cycles. If cycles were a result of Milankovitch cycles, this same bundling would be expected with precession, obliquity, and eccentricity cycles. At Candland Canyon, the second and third spectral peaks appear to correlate cycle thickness. These values also are close to the periods predicted from sedimentation rates and exhibit a 1:1 and 2:1 bundling. This bundling of the cycles matches the bundling that would be expected for precession and obliquity cycles.

Carbon isotope values appear to roughly track lithology, with more positive $\delta^{13}C$ values occurring in argillaceous and presumably an organic-rich lithology at both sections. Pulses of argillaceous material in a carbonate succession indicate a shallowing of relative sea-level. As sea-level falls, argillaceous and potentially organic rich material is introduced and deposited in the basin. Because organic material is enriched in ^{12}C, the $\delta^{13}C$ values in sea-water will increase relatively. At both sections, $\delta^{13}C$ appears to track relative sea-level between 5^{th} or 6^{th} order parasequences.

Large-scale glaciation has the potential to produce cyclic sediments on the time scale of 5^{th} or 6^{th} order parasequences. However, evidence of glaciation in the Cambrian is limited, and this period is generally regarded as a greenhouse environment. Nevertheless, sequence stratigraphic patterns suggesting global eustatic events, interpretations of cold water faunas replacing warm-water adopted faunas at biomere boundaries (Stitt, 1975; Taylor, 2006) and putative Milankovitch cycles inferred in this study all suggest the possibility of Cambrian glaciation. High resolution

chronostratigraphic studies of the Cambrian system provide further support of the possibility of glaciation in the Cambrian (Babcock et al., 2015). From this notion, a possible story emerges. Recession of glaciers would lead to marine transgression. Fluctuations in ice volume could affect sea level and thereby produce cyclic sedimentation. As sea-level drops, a pulse of organic-rich argillaceous material would be deposited to the tops of the shallowing-upward cycles leading to positive $\delta^{13}C$ values. Near the zone of maximum flooding, before highstand, cool offshore, and potentially anoxic waters could have risen onto the shelf killing the trilobites of the Pterocephaliid biomere as cited by Stitt (1975). Anoxic conditions would promote the preservation of organic carbon and lead to the + 2.6 ‰ in $\delta^{13}C$ that is observed at the biomere boundary (Saltzman et al., 1998).

Limitations

Despite the evidence provided suggesting Milankovitch style cyclicity recorded in upper Cambrian sediments, a number of limitations must be addressed. First, this study determined expected Milankovitch periods based on estimated sedimentation rates. The sedimentation rates here assume a constant rate of accumulation. This assumption is deeply flawed in that cycles thicken-upward at Candland Canyon, indicating increasing sedimentation rates up-section in Utah. Second, this study assumes no hiatus in sedimentation throughout the interval examined. The only unconformable surface identified here was at the proposed sequence boundary observed at Candland Canyon, Lawson Cove, and Steamboat Mountain. The other potentially unconformable surface is the drowning unconformity identified above the Barton Canyon Member in Nevada. No

other obvious unconformities were identified, however the possibility for hiatus exists in all stratigraphic sections. Third, this study assumes the carbon isotope record is robust. Although micrite has been shown to be rock buffered over a wide range of diagenetic environments and values fell within the accepted range for lower Paleozoic carbonates, the possibility of alteration always exists. Finally, orbital parameters related to Milankovitch cycles may not have remained constant over time. The predicted periods based on sedimentation rates used modern Milankovitch cycle periods to determine approximate timing. Precession and obliquity cycles were almost certainly less at the beginning of the Paleozoic. However, the difference between the modern precession and obliquity periods was checked using estimated periods of Milankovitch cycles from the beginning of the Phanerozoic (Walker & Zahnle, 1986) and was found to not have a profound effect on the resulting predicted periods.

CONCLUSION

Cycle periods within the Barton Canyon Limestone Member and Sneakover Limestone compare favorably with periods that would be predicted if the succession was influenced by Milankovitch forcing. In addition, the 1:1, 2:1, and 5:1 bundling that was discovered at Spring Gulch further supports the possibility of Milankovitch style cyclicity in upper Cambrian carbonates. Nevertheless, several potentially disqualifying limitations exist, such as assumptions about constant sedimentation rates or no hiatus in deposition. Despite these limitations, this study presents a number of findings. First, this is the first centimeter-scale resolution study of $\delta^{13}C$ values in upper Cambrian carbonates of the Great Basin. Although these upper Cambrian rocks are among the most studied in the world, no other investigations have sampled for $\delta^{13}C$ values at a 25 cm interval. This study also demonstrates that isotopic values closely track lithologies and that small-amplitude variations in $\delta^{13}C$ values exist between 5^{th} and 6^{th} order carbonate cycles. The variations between cycles appears to be related to sea-level fluctuations, with positive $\delta^{13}C$ values resulting from pulses of argillaceous and organic-rich material being introduced into the basin during relative sea-level fall. However, note that this is not the only way to generate positive $\delta^{13}C$ excursions. For example, positive $\delta^{13}C$ excursions can be a result of increased primary productive during sea-level rise. Lastly, this study presents evidence of putative Milankovitch style cyclicity recorded in upper Cambrian carbonates. Power-spectral analysis and sinusoidal regression of $\delta^{13}C$ values quantitatively confirms the presence of Milankovitch style cyclicity and bundling of cycles in the Great Basin of Utah and Nevada.

REFERENCES

Adrain, J.M., Westrop, S.R. 2004, A Late Cambrian (Sunwaptan) silicified trilobite fauna from Nevada: Bulletins of American Paleontology, v. 365, p. 1-51.

Algeo, T.J., Wilkinson, B.H., 1988, Periodicity of mesoscale Phanerozoic sedimentary cycles and the role of Milankovitch orbital modulation: Journal of Geology, v. 96, p. 313-322.

Babcock, L.E., Peng, S., 2007, Cambrian Chronostratigraphy: current state and future plans: Paleogeography, Paleoclimatology, Paleoecology, v. 254, p. 62-66.

Babcock, L.E., Peng, S.C., Brett, C.E., Zhu, M.Y., Ahlberg, P., Robison, R. 2015, Global climate, sea level cycles, and biotic events in the Cambrian Period: Palaeoworld, v. 24, p. 5-15.

Berger, A., 1978, Long-term variations of caloric insolation resulting from the earth's orbital elements: Quaternary Research, v. 9, p. 139-167.

Blakey, R.C., 2013, Using paleogeographic maps to portray Phanerozoic geologic and paleotectonic history of western North America: AAPG Search and Discovery Article v. 30267, p. 1-61.

Brasier, M.D., 1993, Towards a carbon isotope stratigraphy of the Cambrian System: potential of the Great Basin succession: Geological Society, London Special Publication v. 70, p. 341-350.

Bristow, T.F., Kennedy, M.J., 2008, Carbon isotope excursions and the oxidant budget of the Ediacaran atmosphere and ocean: Geology, v. 36, p. 863-866.

Burns, F.E., Burley, S.D., Gawthorpe, R.L., Pollard, J.E., 2005, Diagenetic signatures of stratal surfaces in the Upper Jurassic Fulmar Formation, Central North Sea, UKCS: Sedimentology, v. 52, p. 1155-1185.

Catuneanu, O., 2006, Principles of Sequence Stratigraphy: Elsevier, p. 279-291.

Evans, K.R., 1997, Stratigraphic expression of middle and late Cambrian sea-level changes: examples from Antarctica and the Great Basin, USA.: Unpublished doctoral dissertation, The University of Kansas, p. 31-171.

Evans, K.R., Miller, J.F., Dattilo, B.F., 2003, Sequence stratigraphy of the Sauk Sequence: 40th anniversary field trip in western Utah: Geological Society of America Field Guide, v. 4, p. 17–35.

Evans, K.R., 2012, Gamma-ray cross sections – correlation of Steptoean strata in the eastern Great Basin using outcrop gamma-ray profiles: AAPG Memoir 98, p.365a-373a.

Fisher, A. G., de Boer, P. L., Premoli Silva, I, 1990, Cyclostratigraphy. In: Cretaceous, Resources, Events and Rhythms, Eds: R.N. Ginsburg, Beaudoin. Kluwer, Dordrecht, p.139-172.

Hammer, Ř., Harper, D.A.T., Ryan, P.D. 2001, PAST: Paleontological statistics software package for education and data analysis: Palaeontologia Electronica, v. 4(1), p. 9.

Hays, J. D., Imbrie, J., Shackleton, N. J., 1976, Variations in the Earth's orbit: pacemaker of the ice ages: Science, v. 194 no 4270, p.1121-1132.

Hilgen, F.J., Krijgsman, W., Langereis, C.G., Lourens, L.J., Santarelli, A., Zachariasse, W.J., 1995, Etending the astronomical (polarity) time scale into the Miocene: Earth Planet. Sci. Lett. v. 136, p. 495-510.

Hintze, L.F., Palmer. A.R., 1976, Upper Cambrian Orr Formation: Its Subdivisions and Correlatives in Western Utah: United States Geological Survey Bulletin 1405G. 3373 pc.

Hintze, L.F., 1988, Geologic history of Utah: Brigham Young University Geology Studies Special Publication, v. 7, p. 202.

Jaffres, J.B.D., Sheilds, G.A. Wallmann, K., 2007, The oxygen isotope evolution of seawater: a critical review of a long-standing controversy and an improved geological water cycle model for the past 3.4 billion years: Earth Science Reviews, v. 83, p. 83-122.

Kendall, C.G., Schlager, W., l98l, Carbonates and relative changes in sea level: Marine Geology v. 44, p. l8l-2l2.

Kump, L.R., Arthur, M.A., 1999, Interpreting carbon-isotope excursions: carbonates and organic matter: Chemical Geology, v. 161(1-3), p. 181–198.

Kurtz, V.E., 1971, Upper Cambrian Acrotretidae from Missouri: Journal of Paleontology, v. 45, p. 470 – 476.

Laskar, J., Gienga, A., Gastineau, M., Manche, H., 2011, La2010: a new orbital solution for the long-term motion of the Earth: Astronomy & Astrophysics, v. 532, A(89), p. 1-15.

Levy, M., Christie-Blick, N., 1989, Pre-Mesozoic palinspastic reconstruction of the eastern Great Basin (western United States): Science, v. 245, p. 1454-1462.

Lewis, K.W., Keller, T.L., Maloof, A.C. 2011, New software for plotting and analyzing stratigraphic data: EOS, v. 92, p 37-38.

Ludvigsen, R., Westrop, S.R. 1985, Three new upper Cambrian stages for North America: Geology. v. 13, p. 139-143.

Milankovitch, M., 1941, Canon of insolation in the Ice-Age problem: [English translation by Israel Program for scientific translation, Jerusalem 1969.] R. Serbian Acad. Spec. Publ. 132.

Miller, M.G., Kominz, M.A., Browing, J.V., Wright, J.D., Mountain, G.S., Katz, M.E., Sugarman, P.J., Cramer, B.S., Christie-Blick, N., Pekar, S.F. 2005, The Phanerozoic record of global sea-level change: Science, v. 310, p. 1293-1298.

Miller, J.F., Evans, K.R., Dattilo, B.F., 2012, The Great American Carbonate Bank in the Miogeocline of Western Central Utah: Tectonic Influences on Sedimentation: AAPG Memoir 98, p. 357a-363a.

O'Neil, J. R. 1987. Preservation of H, C and O isotopic ratios in the low temperature environment. *Stable Isotope Geochemistry of Low Temperature Fluids,* v. 13 (ed. T. K. Kyser), pp. 85-128. Saskatoon, SK, Canada: Mineralogical Association of Canada.

Osleger, D.A., 1991, Subtidal carbonate cycles: implications for allocyclic versus autocyclic controls: Geology, v. 19, p. 917-920.

Osleger, D.A., Read, J. F., 1993, Comparative analysis of methods used to define eustatic variations in outcrop: Late Cambrian interbasinal sequence development. American Journal of science, v. 293, p. 157-216.

Palmer, A.R., 1965a, Biomere—a new kind of biostratigraphic unit: Journal of Paleontology, v. 39, p. 149-153.

Palmer, A.R., 1965b, Trilobites of the Late Cambrian Pterocephaliid Biomere in the Great Basin, United States: U.S. Geological Survey, Professional Paper 493, p. 105.

Palmer, A.R., 1971, The Cambrian of the Great Basin: Cambrian of the new world, John Wiley & Sons Ltd. p.3.

Palmer, A.R., 1979. Biomere boundaries re-examined: Alcheringa *3*, 33-41.

Palmer, A.R., 1981, Subdivision of the Sauk sequence, in Taylor, M.E., ed., Short Papers for the Second International Symposium on the Cambrian System: U.S. Geological Survey, Open-File Report 81-743, p. 160–162.

Palmer, A.R., 1984, The biomere problem: evolution of an idea: Journal of Paleontology v. 58, p. 599-611.

Palmer, A.R., Taylor, M.E., 1984, Biomeres and biomere boundaries: field trip 2, *in* Lintz, J., Jr., Western Geological Excursions, Volume 1: Reno, Nevada, MacKay School of the Mines and Geological Society of American 1984 Annual Meeting Field Trip Guidebook, p. 87-100.

Peng, S., Babcock, L., Robison, R., Lin, H., Rees, M., Saltzman, M., 2004, Global Standard Stratotype-section and Point (GSSP) of the Furongian Series and Paibian Stage (China): Lethaia, v. 37 no. 4, p. 365–379.

Peng, S., Zhu, X., Zuo, J., Lin, H., Chen, Y., Wang, L., 2011, Recently Ratified and Proposed Cambrian Global Standard Stratotype-section and Points: *Acta Geologica Sinica (English Edition)*. v. 85, no. 2, p. 296–308.

Saltzman, M., Davidson, J., Holden, P., Runnegar, B., Lohmann, K. C., 1995, Sea-level-driven changes in ocean chemistry at an Upper Cambrian extinction horizon: Geology, p. 893-893.

Saltzman, M.R., Ripperdan, R.L., Brasier, M.D., Lohmann, K.C., Robison, R., Chang, W.T., Peng, S., Ergaliev, E.K., Runnegar, B., 2000, A global carbon isotope excursion (SPICE) during the Late Cambrian: Relation to trilobite extinctions, organic-matter burial and sea level: Palaeogeography, Palaeoclimatology, Palaeoecology, v. 162 no. 3-4, p. 211–223.

Saltzman, M.R., Cowan, C.A., Runkel, A.C., Runnegar, B., Stewart, M.C., Palmer, A.R., 2004, The Late Cambrian Spice (^{13}C) Event and the Sauk II-SAUK III Regression: New Evidence from Laurentian Basins in Utah, Iowa, and Newfoundland: Journal of Sedimentary Research, v. 74, no. 3, p. 366–377.

Schulz, M. & M. Mudelsee. 2002. REDFIT: estimating red-noise spectra directly from unevenly spaced paleoclimatic time series: Computers & Geosciences v. 28, p. 421-426.

Schwarzacher, W., 1975, Sedimentation models and quantitative stratigraphy, Elsevier, Amsterdam, p. 1-382.

Shackleton, N. J., Crowhurst, S. J., Weedon, G. P., Laskar, J., 1999, Astronomical calibration of Oligocene-Miocene time, Philos, Trans, R, Soc, Lond, v.357, p.1907-1929.

Sharp, Z., 2007, Principles of stable isotope geochemistry: Pearson Education Inc. p. 149-174.

Sierro, F.J., Santiago, L., Flores, J.-A., Torrescusa, S., and Martínez del Olmo, W., 2000, Sonic and gamma-ray astrochronology: Cycle to cycle calibration of Atlantic climatic records to Mediterranean sapropels and astronomical oscillations: Geology, 28, p. 695-698.

Sloss, L. L., 1963, Sequences in the cratonic interior of North America: Geological Society of America, Bulletin, v. 74, p. 93–114.

Stitt, J.H., 1975, Adaptive radiation, trilobite paleoecology, and extinction, Ptychaspid biomere, late Cambrian of Oklahoma: Fossils and Strata, v. 4 p. 381-390.

Taylor, J.F., 2006, History and Status of the Biomere Concept: Memoirs of the Association of Australasian Paleontologists v. 32, p. 247–65.

Walcott, C.D., 1908, Nomenclature of some Cambrian Cordilleran formations: Smithsonian Miscellaneous Collections, v. 53 no. 1, p. 1-12.

Walker, J.C., Zahnle, K.J., 1986, Lunar nodal tide and distance to the Moon during the Precambrian: Nature, v. 320, p. 600-602.

Weedon, G.P., 2003, Time-series Analysis and Cyclostratigraphy: first ed. Cambridge Univ. Press, Cambridge.

Westrop, S.R., 1988. Trilobite diversity patterns in an upper Cambrian stage: Paleobiology v. 14, p. 401-409.

Westrop, S.R., Adrain, J.M., 2004, A late Cambrian (Sunwaptan) silicified trilobite fauna from Nevada: Bulletins of American Paleontology, v. 365, p. 1-51.

Westrop, S.R., Adrain, J.M., 2016, Revision of *Irvingella tropica* Opik, 1963 from Australia and related species from North America: implications for correlation of the base of Jiangshanian Stage (Cambrian, Furongian): Memoirs of the Association of Australasian Paleontologists, v. 49, p.395-432.

Wu, Huaichun, Shihong Zhang, Linda a Hinnov, Ganqing Jiang, Qinglai Feng, Haiyan Li, and Tianshui Yang. 2013, Time-Calibrated Milankovitch Cycles for the Late Permian. Nature Communications 4. Nature Publishing Group: 2452.

Vail, P. R., Mitchum, R. M., Todd, R. G., Widmer, J. W., Thompson, S., Sangree, J. B., Bubb, J. N., Hatlelid, W. G., 1977, Seismic stratigraphy and global changes of sea level. In: Seismic Stratigraphy – Application to Hydrocarbon exploration. Ed: C. E. Payton. Am. Assoc. Petrol. Geol. Mem. v.26. p. 46-212.

Van Wagoner, J.C., Posamentier, H.W., Mitchum, R.M., Vail, P.R., Sarg, J.F., Loutit, T.S., Hardenbol, J., 1988, An overview of sequence stratigraphy and key definitions. In: Wilgus, C.K., Hastings, B.S., Kendall, C.G.St.C., Posamentier, H.W., Ross, C.A., Van Wagoner, J.C. (Eds.), Sea Level Changes—An Integrated Approach, vol. 42. SEPM Special Publication, pp. 39–45.

Van Wagoner, J.C. 1995, Overview of sequence stratigraphy of foreland basin deposits: terminology, summary of papers, and glossary of sequence stratigraphy: In Sequence Stratigraphy of foreland basin deposits (J. C. Van Wagoner and G. T. Bertram, Eds.), p. ix-xxi. American Association of Petroleum Geologists Memoir 64.

Zhu, Mao-yan, Loren E Babcock, and Shan-chi Peng, 2006, Advances in Cambrian Stratigraphy and Paleontology: Integrating Correlation Techniques, Paleobiology, Taphonomy and Paleoenvironmental Reconstruction: Palaeoworld, v. 15, p.217-222.

APPENDICES

Appendix A. Stratigraphic sections

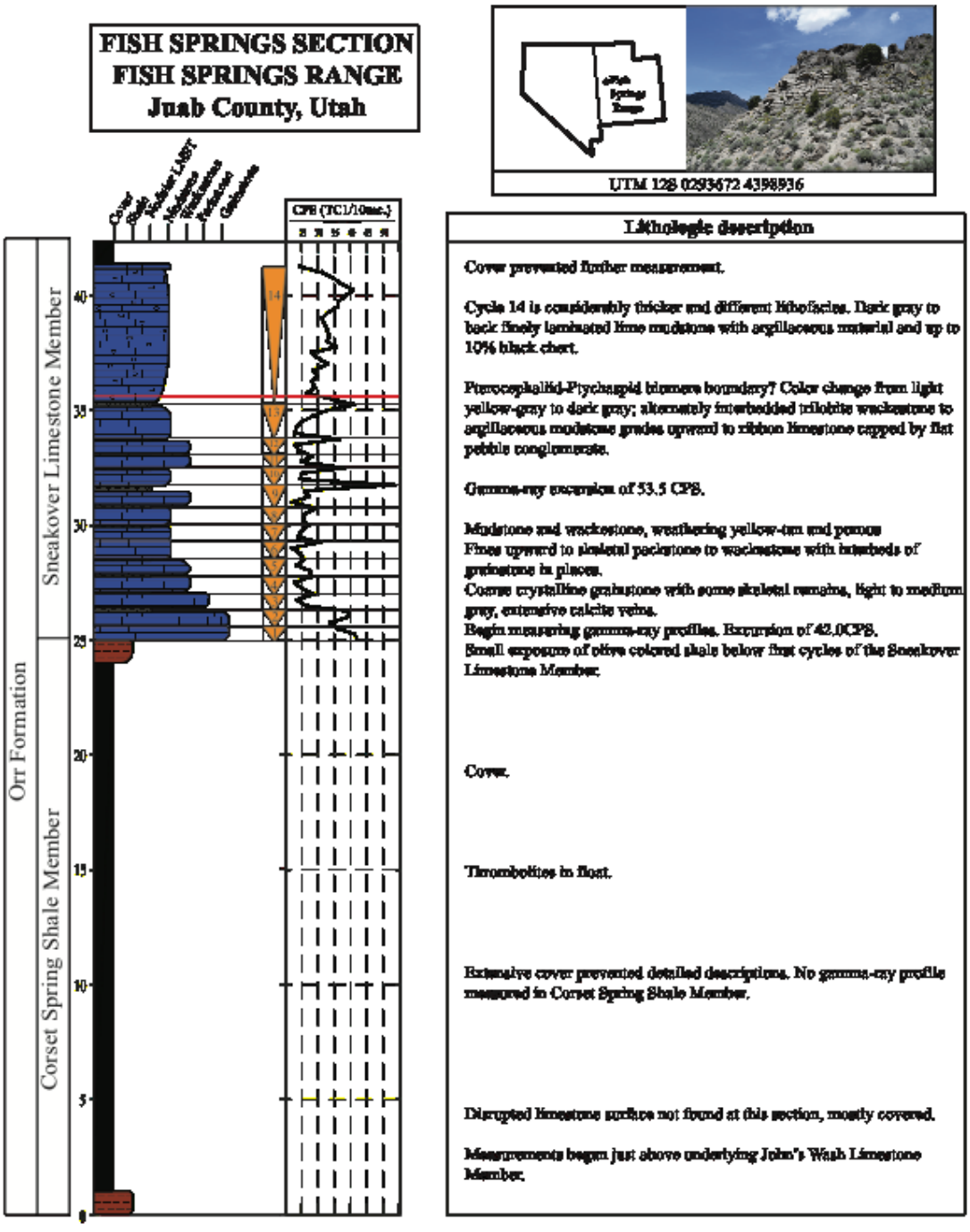

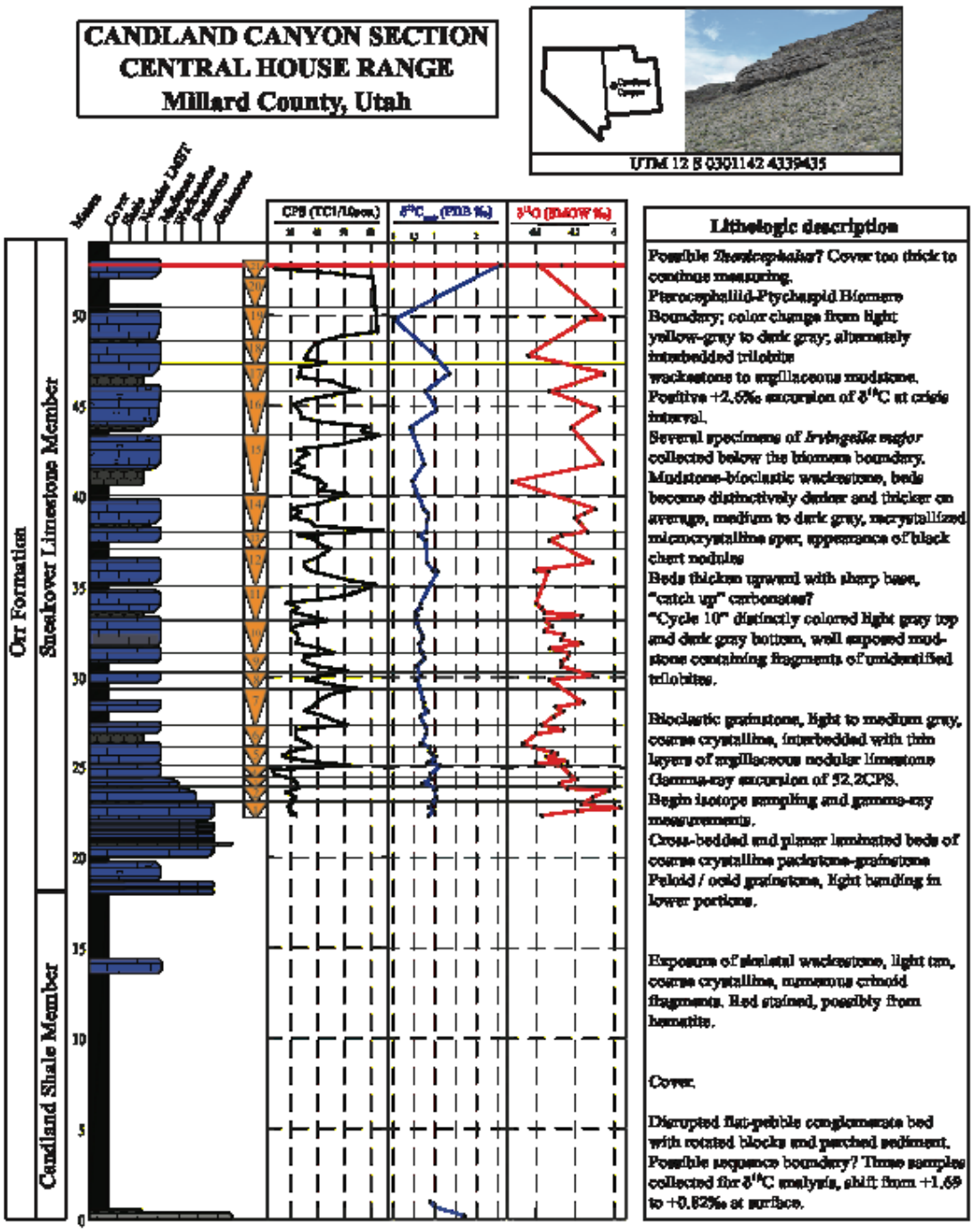
CANDLAND CANYON SECTION
CENTRAL HOUSE RANGE
Millard County, Utah
UTM 12 S 0301142 4339435
Orr Formation
Sneakover Limestone Member
Candland Shale Member
CPS (TC1/10sec)
δ13C carb (PDB ‰)
δ18O (SMOW ‰)
Lithologic description
Possible Ibexicephalus? Cover too thick to continue measuring.
Pterocephalid-Ptychaspid Biomere Boundary; color change from light yellow-gray to dark gray; alternately interbedded trilobite wackestone to argillaceous mudstone.
Positive +2.6‰ excursion of δ13C at crisis interval.
Several specimens of Irvingella major collected below the biomere boundary.
Mudstone-bioclastic wackestone, beds become distinctively darker and thicker on average, medium to dark gray, recrystallized microcrystalline spar, appearance of black chert nodules
Beds thicken upward with sharp base, "catch up" carbonates?
"Cycle 10" distinctly colored light gray top and dark gray bottom, well exposed mudstone containing fragments of unidentified trilobites.
Bioclastic grainstone, light to medium gray, coarse crystalline, interbedded with thin layers of argillaceous nodular limestone
Gamma-ray excursion of 52.2CPS.
Begin isotope sampling and gamma-ray measurements.
Cross-bedded and planar laminated beds of coarse crystalline packstone-grainstone
Peloid / ooid grainstone, light banding in lower portions.
Exposure of pisolatal wackestone, light tan, coarse crystalline, numerous crinoid fragments. Red stained, possibly from hematite.
Cover.
Disrupted flat-pebble conglomerate bed with rotated blocks and parched sediment. Possible sequence boundary? Three samples collected for δ13C analysis, shift from +1.69 to +0.82‰ at surface.

STEAMBOAT MOUNTAIN SECTION
SOUTHERN HOUSE RANGE
Millard County, Utah

UTM 12 S 0301314 4339010

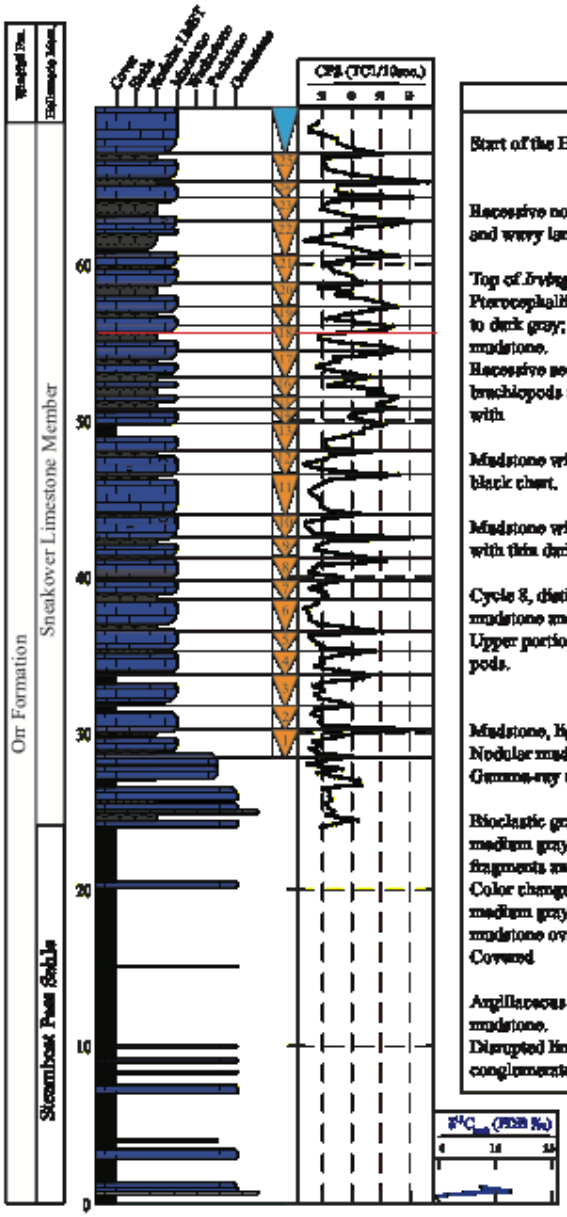

Lithologic description

Start of the Hellnorgia Member of the Weeksville Formation.

Recessive nodular limestone transitions into ledges of mudstone with chert and wavy laminations.

Top of *Irvingella major* subzone
Pterocephaliid-Ptychaspid Biomere boundary; color change light yellow gray to dark gray; alternately interbedded trilobite wackestone to argillaceous mudstone.
Recessive section of nodular lime mudstone with silt interbeds and abundant brachiopods and some unidentified trilobite fragments, black to tan in color with

Mudstone with pockets of skeletal material, homogeneous, appearance of black chert.

Mudstone with discontinuous beds of packstone to wackestone, light gray with thin dark band towards bottom of cycle.

Cycle 8, distinctive bed with dark gray bottom and light gray top, lower bed is mudstone and burrowed, darker band of skeletal packstone to grainstone. Upper portion of the cycle is mudstone to wackestone containing brachiopods.

Mudstone, light to medium gray, burrowed, fine crystalline, stylolites.
Nodular mudstone forming recesses between cycles.
Gamma-ray excursion of 62.1 CPS.

Bioclastic grainstone fines upward to wackestone / packstone, light to medium gray, weathering orange in places, coarse crystalline, trilobite fragments and shelly material.
Color change from medium gray-brown to
medium gray, decrease in grainsize upward, burrowed wackestone to mudstone overlies rippled grainstone to burrowed packstone
Covered

Argillaceous grainstone, brown to medium gray, interbeds of nodular lime mudstone.
Disrupted limestone surface; chaotic flat-pebble conglomerate in narrow channels between fenestellites. Overlain by grain-

Four samples collected for $\delta^{13}C$ analysis, values range from -0.05 and 0.16‰ below the surface, and 1.28 and 0.74‰ above the surface.

LAWSON COVE SECTION
WAH WAH MOUNTAINS
Millard County, Utah

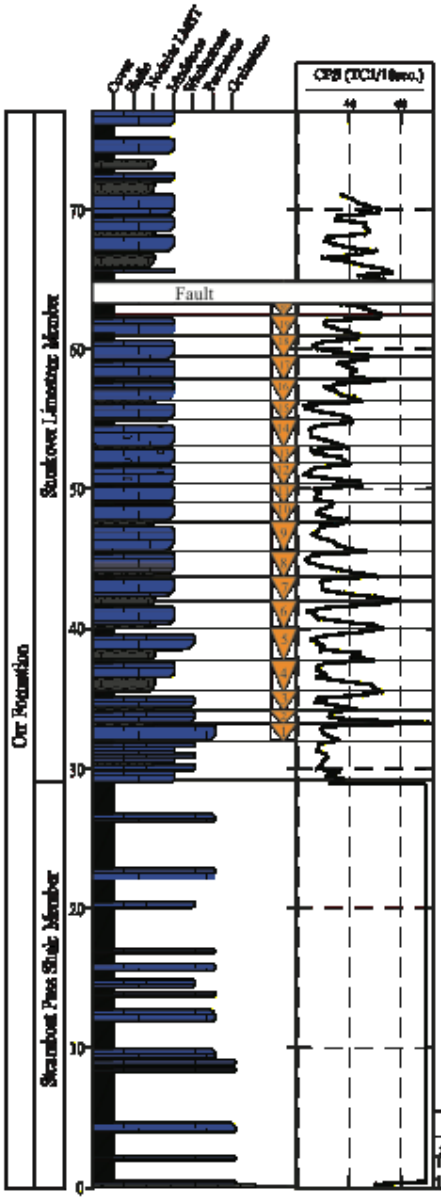

Lithologic description

Measurements ended at cliff forming Hellmanseia Formation.

Fault; repeated section

Pterocephaliid-Ptychagnid biomere boundary? Color change from light yellow-gray to dark gray; alternately interbedded trilobite wackestone to argillaceous mudstone.
Mudstone, medium gray, homogeneous color, burrowed, packstone interbeds. *Irvingella taylor* collected?
Recesses between cycles composed of argillaceous nodular lime mudstone.
Mudstone with skeletal wackestone to packstone interbeds, medium gray, black chert present.
Mudstone beds with light gray top and dark gray bottom.

Cycle 8, half light gray, half dark gray with darker band of skeletal grainstone in middle.

Thicker cycles forming step ledges with recessive nodular lime mudstone between.
Grain size fines upward from skeletal grainstone and packstone to burrowed mudstone, light to medium gray.
Gamma-ray excursion of 70.3CPS.
Thin bedded mudstone with interbeds of skeletal wackestone, light gray to dark gray banded. Some recessive nodular lime mudstone.
Start of Skunkover Limestone, continue with gamma-ray logs.

Wackestone to packstone, light gray, wavy bedding, spar filled burrows.

Skeletal packstone, medium gray, grainstone interbeds, mostly covered.

Skeletal packstone to grainstone, dark gray to brown, burrowed and wavy laminated, minor black chert.

Gamma-ray log discontinued due to extensive cover between limestone outcrops.
Disrupted limestone; paleokarst / solution pits?
Autoclastic breccia and perched sediment; lower bed 30-40cm thrombolite bioherms with inter-thrombolite breccia.

Three samples collected for $\delta^{13}C$ analysis, shift from +2.17 to +1.89‰ at surface. Also a shift from 50.6 to 68.9 CPS in the gamma-ray log is observed over the surface.

SPRING GLUCH SECTION
NORTHERN SCHELL CREEK RANGE
White Pine County, Nevada

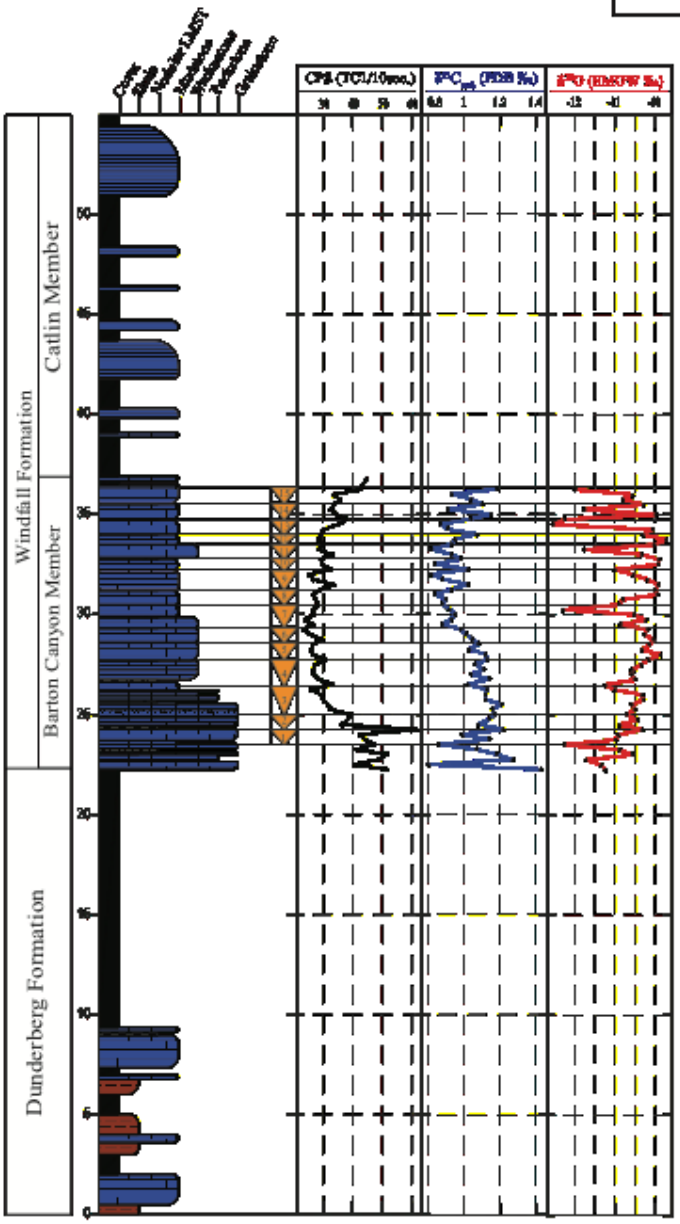

Lithologic description

Catlin Member continues above, cover prevented measurement.
Thinly bedded lime mudstone with calcisiltite and argillaceous material.

Wavy laminations, calcite veins
Abundant trilobites including *Parabolinoides*, *Ptarmagnis*, *Nevadia* and numerous other unidentified Agnostid and Polymerid trilobites.

Medium to dark gray thin bedded mudstone, homogeneous with planar laminations, some beds fine upward.

Catlin member, cycles end.
Covered, end of gamma-ray log and isotope sampling.
Color change from light gray to dark, porous with calcite geodes and veins, fractured.
Rubbly and nodular lime mudstone between cycles.
Mudstone with skeletal wackestone, calcite veins, medium crystalline, some wavy laminations.
Mudstone, light to medium gray.
Grainstone fines upward to burrowed lime mudstone to trilobite wackestone.
Eckinoderm grainstone with small cryptomicrobial and thrombolitic bioherms.
Thin beds of skeletal grainstone and packstone.
Start of the Barton Canyon Member, begin gamma-ray logging and isotope sampling.

Cover.

Mudstone, light to medium gray-brown, recessive parts nodular lime mudstone.
Shale, olive green to brown, friable mostly covered.

No sequence boundary located, correlative conformity?

NORTH EGAN RANGE SECTION
NORTH EGAN RANGE
White Pine County, Nevada

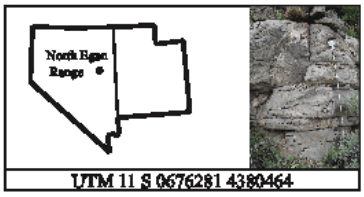

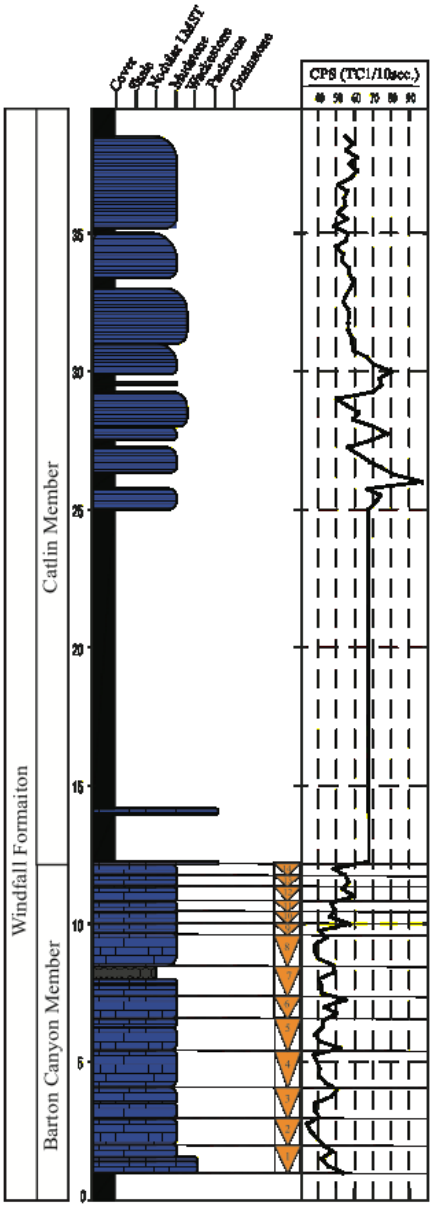

Lithologic description

Cover, end of measurements.

Thin bedded mudstone, medium to dark gray, wavy bedding and planar laminations, silty, some thicker beds present.

Mudstone with argillaceous layers of calcisiltite between beds, bed thickness between 5-50cm, very homogenous, trace chert.
Mudstone, possible ripple laminations, some surfaces are truncated, variable bed thickness, no fossils or accessories.
Gamma-ray cleaning upward.
1-10cm thick lenses of lime mudstone, pinch out laterally within 50-100cm.
Mudstone, medium to dark gray-brown, very silty, gamma-rays clean upward, minor black chert.

Outcrop of Catlin Member.

Covered.

10cm exposure of grainstone overlain by mostly covered darker limestone, cycles shut-off.
Pterocephaliid biomere boundary no located.
Cover prevented gamma-ray logging.
Cycles thin upward.
Homogeneous mudstone, light to medium gray, abundant calcite veins, no other accessories.
Recessive bed of nodular lime mudstone with interbedded silt.

Homogeneous mudstone, light to medium gray, medium crystalline, stylolites, occasional trilobite fragments, numerous calcite veins.
Wackestone fines upward into homogeneous mudstone, light to medium gray, darker than other Nevada sections.
No sequence boundary, covered or correlative conformity.

MCGILL SECTION
DUCK CREEK RANGE
White Pine County, Nevada

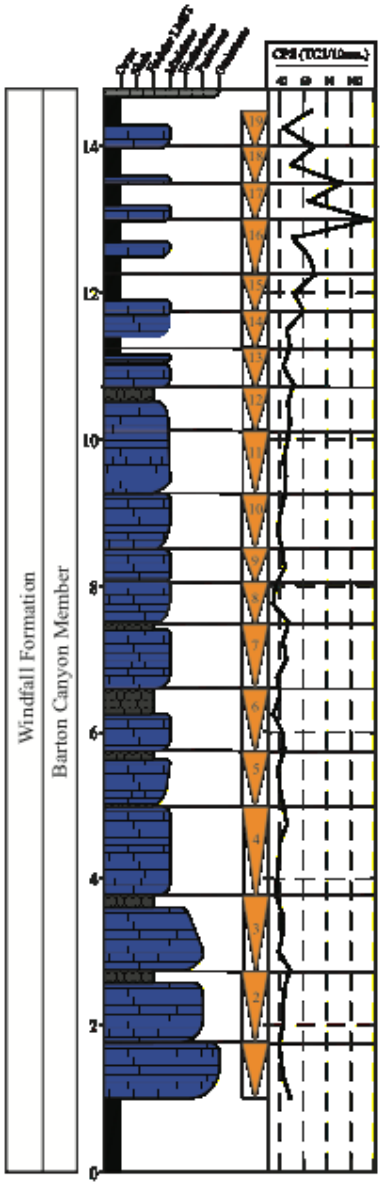

Lithologic description

Catlin Member poorly exposed.
Pterocephaliid-Ptychaspid Biomere boundary projected from Palmer (1965b) coincides with color change from light to darker gray.

Gamma-ray excursion of 116.8 CPS.

Recessed with increasing cover, mudstone becomes darker up section.

Spar filled burrows, thinner bedding within cycles.

White to light gray peloid packstone to lime mudstone; spar-filled burrows.

Homogeneous lime mudstone, light tan to light gray, some calcite veins.

Mudstone with interbedded lenses of peloid grainstone, some minor pyrite and wavy laminations.

Nodular lime mudstone between cycles, darker gray and silty

Mudstone with interbeds of grainstone, light to medium gray, coarse crystalline, calcite veins and trace pyrite.

Fining upward packstone to wackestone with some thin interbeds of grainstone. Light gray to buff, homogeneous color throughout bed.

Peloid grainstone, light tan to buff white-gray.

Dunderberg Shale poorly exposed and mostly covered.
No Sequence boundary, covered or correlative conformity.

SHINGLE PASS SECTION
SOUTH EGAN RANGE
Lincoln County, Nevada

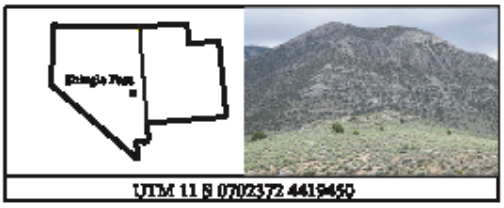

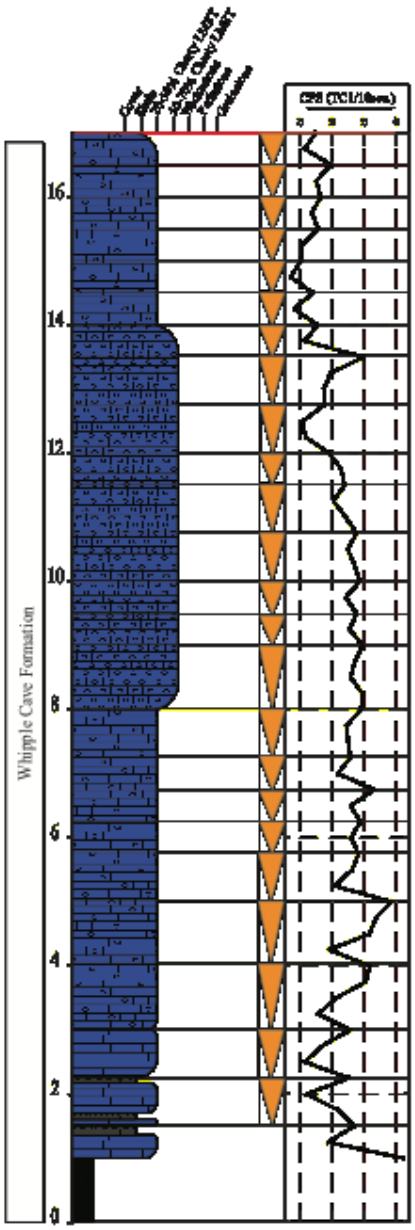

Lithologic description

Top of Pterocephaliid Biomere not reached, section continues as cherty homogeneous lime mudstone above.

Massive mudstone, medium gray, decreasing black chert up section, bedding impossible to distinguish.

Cherty mudstone, no distinct bedding, chert possibly filling bedding planes?

Cherty mudstone to wackestone, medium to dark gray, nearly 60% black chert, nodular weathering.

Mudstone to wackestone, medium to dark gray, coarse crystalline neomorphic spar, some peloids, brachiopod and trilobite fragments, discontinuous wavy like laminations filled with chert.

Mudstone to wackestone, medium gray, coarse crystalline, massive, burrowed, trilobite fragments, abundant black chert.

Mudstone to wackestone, medium to dark gray, coarse crystalline neomorphic spar, brachiopod and trilobite fragments, discontinuous wavy like laminations filled with chert.

Thick to massive bedded lime mudstone to wackestone with black to orange weathering chert layers.

Mudstone, medium gray, coarse crystalline, massive, no apparent bedding.

Mudstone ledges at bottom of section, light to medium gray, nodular lime mudstone between ledges, no chert.

Appendix B. Geochemical data

Sample ID	$d^{13}C$	$d^{18}O$	[V]sa	% Difference	Pmv1	Exp	Exp. 2	Exp. 3	Strat Height
NBS-19 avg.	1.89	-2.22							
NBS-19 st.dev.	0.02	0.07							
NBS-19/7 grains/	1.85	-2.18	3.23	13.45	766	0	0	0	
NBS-19/6 grains/	1.88	-2.21	2.45	6.41	695	0	0	0	
NBS-19/7 grains/	1.9	-2.19	3.05	9.02	743	0	0	0	
NBS-19/10 grains/	1.9	-2.32	1.96	5.33	855	605	0	0	
NBS-19/5 grains/	1.9	-2.26	2.09	4.79	626	0	0	0	
NBS-19/7 grains/	1.88	-2.15	2.32	5.92	684	0	0	0	
NBS-19/7 grains/	1.92	-2.08	2.36	5.66	689	0	0	0	
NBS-19/7 grains/	1.91	-2.15	2.93	8.08	717	0	0	0	
NBS-19/5 grains/	1.89	-2.29	2.05	5.81	621	0	0	0	
NBS-19/10 grains/	1.88	-2.31	2.08	10.78	935	633	0	0	
NBS-19/6 grains/	1.9	-2.2	3.17	12.1	737	0	0	0	
NBS-19/7 grains/	1.86	-2.21	3	7.68	729	0	0	0	
NBS-19/9 grains/	1.89	-2.19	3.69	11.9	780	0	0	0	
NBS-19/8 grains/	1.9	-2.16	3.54	10.73	767	0	0	0	
NBS-19/7 grains/	1.89	-2.17	2.62	7.26	697	0	0	0	
NBS-19/6 grains/	1.91	-2.14	2.48	5.95	684	0	0	0	
NBS-19/9 grains/	1.83	-2.26	3.49	10.54	762	0	0	0	
NBS-19/13 grains/	1.87	-2.29	2.34	6.4	1027	663	0	0	
NBS-19/6 grains/	1.92	-2.28	2.04	5.22	625	0	0	0	
NBS-19/4 grains/	1.86	-2.31	1.58	4.86	544	0	0	0	
NBS-19/7 grains/	1.88	-2.21	2.91	7.46	716	0	0	0	
Wes's Data									
CC/01/	**0.84**	**-9.37**	2	4.9	888	616	0	0	**0**
CC/02/	**0.98**	**-9.19**	1.75	3.75	576	0	0	0	**0.25**
CC/02 RR/	**0.93**	**-9.11**	2.38	7.19	665	0	0	0	**0.25**
CC/03/	**0.86**	**-8.96**	4.09	13.55	1406	849	0	0	**0.4**
CC/03 RR/	**0.89**	**-8.97**	1.03	4.57	406	0	0	0	**0.4**
CC/04/	**0.93**	**-9.17**	3.39	12.09	1748	1375	783	0	**0.6**
CC/05/	**1.02**	**-9.11**	3.07	8.47	1718	1310	756	0	**1**

Sample ID	$d^{13}C$	$d^{18}O$	[V]sa	% Difference	Pmv1	Exp	Exp. 2	Exp. 3	Strat Height
CC/06/	**0.99**	**-9.03**	2.97	7.26	1720	1295	746	0	**1.4**
CC/07/	**1.03**	**-9.24**	2.16	5.84	1531	1009	650	0	**1.5**
CC/08/	**0.71**	**-9.28**	3.47	14.34	1361	783	0	0	**1.8**
CC/09/	**0.91**	**-9.25**	2.01	4.84	1773	1478	953	631	**2**
CC/09 RR/	**0.91**	**-9.19**	2.89	9.01	1207	724	0	0	**2**
CC/10/	**0.88**	**-9.23**	2.65	6.44	706	0	0	0	**2.25**
CC/11/	**1.12**	**-9.27**	2.07	4.82	949	635	0	0	**2.75**
CC/12/	**0.83**	**-9.4**	2.39	7.72	1533	1054	672	0	**2.9**
CC/13/	**0.89**	**-9.24**	2.41	6.36	1080	679	0	0	**3**
CC/14/	**1.02**	**-9.35**	1.98	4.62	933	622	0	0	**3.25**
CC/15/	**0.94**	**-9.29**	3.32	8.41	760	0	0	0	**3.4**
CC/16/	**0.87**	**-9.32**	3.42	11.88	1697	1328	774	0	**3.5**
cc/17/	**0.89**	**-9.41**	2.34	6.62	1129	684	0	0	**3.75**
cc/18/	**0.65**	**-9.47**	1.74	5.21	1447	857	593	0	**4**
cc/19/	**0.69**	**-9.46**	1.85	4.15	898	606	0	0	**4**
CC/20/	**0.79**	**-9.4**	2.11	5.76	922	630	0	0	**4.5**
CC/21/	**0.8**	**-9.26**	3.25	12.83	1771	1386	781	0	**4.75**
CC/22/	**0.75**	**-9.37**	1.89	5.3	970	625	0	0	**5**
CC/23/	**0.66**	**-9.46**	1.7	3.85	1459	851	587	0	**5.5**
CC/23 RR/	**0.65**	**-9.31**	2.38	6.71	678	0	0	0	**5.5**
CC/24/	**0.84**	**-9.26**	2.57	7.49	1172	706	0	0	**5.75**
CC/25/	**0.73**	**-9.3**	2.07	5.23	927	629	0	0	**6**
CC/26/	**0.73**	**-9.16**	3.21	8.95	750	0	0	0	**6.25**
CC/27/	**0.58**	**-9.33**	3.68	11.74	1318	776	0	0	**7.5**
CC/28/	**0.65**	**-9.11**	4.21	11.34	822	0	0	0	**7.75**
CC/29/	**0.57**	**-9.27**	3.99	10.73	1359	797	0	0	**8.25**
CC/30/	**0.67**	**-9.27**	2.08	4.84	916	629	0	0	**8.5**
CC/31/	**0.75**	**-9.24**	3.86	14.85	1328	787	0	0	**8.75**
CC/31 RR/	**0.74**	**-9.23**	3.85	14.18	792	0	0	0	**8.75**
CC/32/	**0.7**	**-9.23**	2.29	6.98	986	653	0	0	**9**
CC/33/	**0.64**	**-9.33**	2.28	6.14	986	651	0	0	**9.25**
CC/34/	**0.63**	**-9.17**	3.64	13.27	1293	772	0	0	**9.5**
CC/35/	**0.69**	**-9.27**	2.9	7.63	1160	714	0	0	**9.75**
CC/36/	**0.7**	**-9.26**	3.25	10.66	780	0	0	0	**10**
cc/37/	**0.64**	**-9.36**	3.52	12.68	1381	788	0	0	**10.25**
cc/38/	**0.6**	**-9.32**	3.89	9.74	824	0	0	0	**10.5**

Sample ID	$d^{13}C$	$d^{18}O$	[V]sa	% Difference	Pmv1	Exp	Exp. 2	Exp. 3	Strat Height
cc/39/	**0.54**	**-9.36**	3.79	14.45	1412	810	0	0	**10.85**
cc/40/	**0.55**	**-9.42**	1.81	4.21	1443	865	599	0	**11.1**
CC/40 RR/	**0.58**	**-9.17**	2.15	5.26	638	0	0	0	**11.1**
cc/41/	**0.54**	**-9.36**	2.66	8.58	1160	706	0	0	**11.25**
cc/42/	**0.65**	**-9.37**	2.86	7.54	1230	728	0	0	**11.5**
cc/43/	**0.65**	**-9.4**	3.06	7.94	1230	738	0	0	**11.75**
cc/44/	**1.03**	**-9.34**	3.22	8.86	1246	748	0	0	**13.5**
CC/44 RR/	**1.06**	**-9.2**	1.63	5.7	559	0	0	0	**13.5**
cc/45/	**0.95**	**-9.41**	1.93	4.54	865	605	0	0	**13.6**
CC/46/	**0.8**	**-9.11**	4.05	15.38	1375	799	0	0	**14**
CC/47/	**0.78**	**-9.33**	2.06	5.67	912	622	0	0	**15.25**
CC/48/	**0.6**	**-9.27**	3.33	11.37	755	0	0	0	**15.5**
CC/49/	**0.8**	**-9.14**	3.21	8.27	1213	740	0	0	**15.75**
CC/50/	**0.8**	**-9.18**	2.8	7.04	1564	1134	710	0	**16.25**
CC/51/	**0.84**	**-9.2**	3.73	14.28	782	0	0	0	**16.5**
CC/51 RR/	**0.85**	**-9.13**	3.05	8.36	735	0	0	0	**16.5**
CC/52/	**0.83**	**-9.15**	3.45	13.84	763	0	0	0	**16.75**
CC/53/	**0.73**	**-9.1**	4.11	11.57	1351	795	0	0	**17**
CC/54/	**0.46**	**-9.52**	2.11	7.35	931	630	0	0	**18.5**
CC/55/	**0.74**	**-9.06**	3.73	13.94	784	0	0	0	**19.5**
CC/56/	**0.41**	**-9.22**	4.27	12.39	1357	804	0	0	**21.5**
CC/57/	**1.05**	**-9.08**	4.1	13.46	1371	812	0	0	**22.5**
CC/58/	**0.77**	**-9.33**	2.16	5.25	1461	941	638	0	**23.5**
CC/59/	**1.35**	**-9.05**	2.39	5.69	1027	671	0	0	**24.5**
CC/60/	**0.98**	**-9.44**	3.1	9.6	1590	1195	734	0	**25.5**
CC/61/	**0.02**	**-9.14**	3.95	10.85	1340	788	0	0	**27.5**
CC/61 RR/	**0.04**	**-9.05**	2.75	8.5	706	0	0	0	**27.5**
CC/62/	**2.56**	**-9.39**	4.05	15.2	1377	799	0	0	**30.5**
CC/62 RR/	**2.6**	**-9.27**	2.88	7.18	717	0	0	0	**30.5**
CC/SB-1/	**0.73**	**-10.98**	2.68	7.16	1125	697	0	0	
CC/SB-2/	**0.55**	**-11.07**	4.41	14.84	1369	849	0	0	
CC/SB-LDF/	**1.69**	**-11.05**	3.81	14.45	1310	778	0	0	
CC/SB-MDF/	**1**	**-10.12**	2.03	4.62	900	619	0	0	
CC/SB-UDF/	**0.82**	**-10.68**	3.41	10.7	761	0	0	0	

Sample ID	$d^{13}C$	$d^{18}O$	[V]sa	% Difference	Pmv1	Exp	Exp. 2	Exp. 3	Strat Height
NSC/01/	**1.42**	**-11.24**	2.82	12.22	1578	1168	718	0	**0.25**
NSC/01 RR/	**1.43**	**-11.33**	2.89	7.5	723	0	0	0	**0.25**
NSC/02/	**0.72**	**-11.17**	2.13	6.01	1463	947	635	0	**0.50**
NSC/02 RR/	**0.8**	**-11.35**	2.56	7.33	685	0	0	0	**0.50**
NSC/03/	**1.27**	**-11.73**	2.04	5.52	1425	884	614	0	**0.75**
NSC/04/	**1.18**	**-10.56**	3.08	10.38	738	0	0	0	**1.00**
NSC/05/	**1.07**	**-10.89**	3.18	8.43	1244	748	0	0	**1.25**
NSC/06/	**0.88**	**-12.27**	3.62	14.33	782	0	0	0	**1.50**
NSC/06 RR/	**0.86**	**-12.25**	3.52	13.75	778	0	0	0	**1.50**
NSC/07/	**1.14**	**-10.98**	2.33	5.92	984	658	0	0	**1.75**
NSC/08/	**0.99**	**-10.93**	2.83	7.18	706	0	0	0	**2.00**
NSC/09/	**1.22**	**-10.32**	2.13	5.48	927	632	0	0	**2.25**
NSC/10/	**1.08**	**-10.88**	3.33	11.29	750	0	0	0	**2.50**
NSC/11/	**1.14**	**-10.45**	3.6	14.14	771	0	0	0	**2.75**
NSC/12/	**1.16**	**-10.71**	3.35	11.87	1218	745	0	0	**3.00**
NSC/12 RR/	**1.17**	**-10.71**	1.78	4.33	582	0	0	0	**3.00**
NSC/13/	**1.16**	**-10.5**	4.15	14.34	796	0	0	0	**3.25**
NSC/14/	**1.21**	**-10.59**	2.27	6.33	982	650	0	0	**3.50**
NSC/15/	**1.12**	**-10.29**	2.11	6.69	908	625	0	0	**3.75**
NSC/16/	**1.12**	**-10.33**	2.89	7.98	1152	715	0	0	**4.00**
NSC/17/	**1.13**	**-11**	2.63	6.72	690	0	0	0	**4.25**
NSC/18/	**1.02**	**-11.24**	3.35	12.26	750	0	0	0	**4.50**
NSC/19/	**1.14**	**-10.5**	4.28	15.85	818	0	0	0	**4.75**
NSC/20/	**1.04**	**-10.59**	2.25	7.45	972	644	0	0	**5.00**
NSC/21/	**1.11**	**-10.58**	2.64	8.97	1084	690	0	0	**5.25**
NSC/22/	**1.06**	**-10.35**	3.17	7.74	741	0	0	0	**5.50**
NSC/23/	**1.13**	**-10.16**	2.96	7.78	1152	717	0	0	**5.75**
NSC/24/	**1.12**	**-9.85**	2.29	6.04	970	649	0	0	**6.00**
NSC/24 RR/	**1.15**	**-9.73**	3.14	7.99	737	0	0	0	**6.00**
NSC/25/	**1.03**	**-10.32**	2.98	11.69	732	0	0	0	**6.25**
NSC/26/	**1.08**	**-10.14**	1.29	1.56	473	0	0	0	**6.50**
NSC/26 RR/	**1**	**-10.18**	3.33	7.98	753	0	0	0	**6.50**
NSC/27/	**1.05**	**-10.03**	2.91	7.21	1146	714	0	0	**6.75**
NSC/28/	**1.01**	**-10.26**	3.29	8.32	1240	747	0	0	**7.00**
NSC/29/	**0.98**	**-10.19**	2.63	9.75	1113	696	0	0	**7.25**

Sample ID	$d^{13}C$	$d^{18}O$	[V]sa	% Difference	Pmv1	Exp	Exp. 2	Exp. 3	Strat Height
NSC/30/	**0.88**	**-10.87**	2.05	5.6	900	619	0	0	**7.50**
NSC/31/	**0.93**	**-10.23**	2.13	7.23	927	630	0	0	**7.75**
NSC/32/	**0.95**	**-10.53**	3.3	11.3	752	0	0	0	**8.00**
NSC/33/	**0.92**	**-12.5**	2.63	10.22	1072	692	0	0	**8.25**
NSC/33 RR/	**0.92**	**-12.29**	2.12	6.29	632	0	0	0	**8.25**
NSC/34/	**0.88**	**-10.91**	4.25	16.71	826	0	0	0	**8.50**
NSC/35/	**0.9**	**-10.8**	2.34	7.54	1000	657	0	0	**8.75**
NSC/35 RR/	**0.88**	**-10.64**	3.27	12.38	750	0	0	0	**8.75**
NSC/36/	**0.84**	**-9.94**	2.9	9.01	1148	713	0	0	**9.00**
NSC/38/ should be 37	**0.93**	**-10**	3.91	12.99	793	0	0	0	**9.25**
NSC/39/ should be 38	**1.02**	**-9.91**	2.36	7.35	1019	660	0	0	**9.50**
NSC/39/	**0.88**	**-10.2**	1.96	10.63	1429	890	619	0	**9.75**
NSC/40/	**0.82**	**-10.54**	3.91	14.99	791	0	0	0	**10.00**
NSC/41/	**1.02**	**-11.01**	2.87	8	1160	714	0	0	**10.25**
NSC/42/	**0.84**	**-9.92**	3.65	10.14	776	0	0	0	**10.50**
NSC/43/	**0.98**	**-9.89**	2.71	7.41	1144	705	0	0	**10.75**
NSC/44/	**0.93**	**-10.32**	2.69	7.09	1107	697	0	0	**11.00**
NSC/45/	**0.82**	**-11.77**	2.84	8.5	1123	712	0	0	**11.25**
NSC/46/	**0.93**	**-10.01**	2.7	7.14	1101	697	0	0	**11.50**
NSC/47/	**0.95**	**-9.71**	4.23	15.79	1379	822	0	0	**11.75**
NSC/48/	**1.07**	**-10.3**	2.12	6.49	927	629	0	0	**12.00**
NSC/49/	**0.91**	**-10.05**	1.95	4.67	1406	863	608	0	**12.25**
NSC/50/	**0.87**	**-12.56**	3.49	12.95	1261	769	0	0	**12.50**
NSC/50 RR/	**0.89**	**-12.41**	2.31	5.83	1006	656	0	0	**12.50**
NSC/51/	**1.04**	**-12.25**	3.15	8.31	1203	736	0	0	**12.75**
NSC/52/	**1.15**	**-9.98**	3.16	8.12	1222	742	0	0	**13.00**
NSC/53/	**0.91**	**-11.77**	2.05	6.04	890	618	0	0	**13.25**
NSC/54/	**1.1**	**-10.29**	2.37	7.43	1019	662	0	0	**13.50**
NSC/55/	**1.04**	**-10.8**	3.97	13.89	1345	789	0	0	**13.75**
NSC/56/	**0.93**	**-10.57**	2.52	6.94	1496	1072	684	0	**14.00**
NSC/57/	**1.18**	**-11.98**	2.09	4.86	1414	900	629	0	**14.25**
NSC /57 RR/	**1.17**	**-11.92**	2.83	6.98	1191	716	0	0	**14.25**
LC-SB/1/	**1.89**	**-11.22**	2.38	8.2	1011	662	0	0	

Sample ID	$d^{13}C$	$d^{18}O$	[V]sa	% Difference	Pmv1	Exp	Exp. 2	Exp. 3	Strat Height
LC-SB/2/	**2.17**	**-10.69**	2.13	5.42	1445	927	633	0	
LC-SB/3/	**1.91**	**-11.01**	3.4	11.08	1256	754	0	0	
SBM/A/	**0.86**	**-9.07**	2.02	5.05	1431	884	616	0	
SBM/B/	**1**	**-9.16**	3.7	11.61	1297	774	0	0	
SBM/C/	**1.51**	**-8.8**	4.22	14.94	1400	847	0	0	
SBM/1/	**-0.05**	**-10.57**	2.28	5.9	1013	657	0	0	
SBM/2/	**0.16**	**-10.63**	3.17	12.43	1250	744	0	0	
SBM/3/	**1.28**	**-9.45**	4.25	15.97	1404	838	0	0	
SBM/4/	**0.74**	**-9.95**	2.04	5.68	1465	920	625	0	

Appendix C. Gamma-ray data

FSR Depth	FSR CPS	CC Depth	CC CPS	LC Depth	LC CPS	SG Depth	SG CPS	NER Depth	NER CPS	MG Depth	MG CPS	SP Depth	SP CPS
16.25	24.2	30.5	24.2	42	37	14.75	56.4	11.25	67.8	13.5	67.5	16	27.5
16	31.1	30.25	44.6	41.75	40.9	14.5	44.6	11	48.4	13.25	43.3	15.75	25.8
15.75	34.7	30	60.7	41.5	42.9	14.25	43.4	10.75	54.9	13	69.3	15.5	29.9
15.5	37.1	29.75		41.25	46.7	14	42.8	10.5	56.8	12.75	49.9	15.25	27.6
15.25	40.8	29.5		41	51.8	13.75	33.4	10.25	53.6	12.5	92.7	15	28.3
15	38.7	29.25		40.75	51.5	13.5	35.8	10	59.9	12.25	64.9	14.75	26.9
14.75	36.4	29		40.5	35.6	13.25	33.6	9.75	47	12	116.8	14.5	27.9
14.5	35.9	28.75		40.25	35	13	32.6	9.5	49.1	11.75	51.1	14.25	25.3
14.25	32.9	28.5		40	45.9	12.75	34.6	9.25	46.3	11.5	65	14	25.2
14	31.2	28.25		39.75	46.2	12.5	38.1	9	57.3	11.25	69.9	13.75	23.6
13.75	32	28		39.5	47.6	12.25	35.2	8.75	40.5	11	52.2	13.5	27.1
13.5	32.7	27.75		39.25	46.3	12	30.2	8.5	44.8	10.75	60.4	13.25	24.1
13.25	33.5	27.5		39	31.3	11.75	29.2	8.25	38.3	10.5	46.3	13	27.8
13	32.8	27.25	49.4	38.75	30.8	11.5	28.3	8	38.3	10.25	49	12.75	25.8
12.75	35.5	27	62.4	38.5	34.1	11.25	30.1	7.75	39.9	10	43.1	12.5	35
12.5	27.8	26.75		38.25	40.1	11	28.3	7.5	48.3	9.75	51.7	12.25	29.8
12.25	30.3	26.5		38	50.5	10.75	32.9	7.25	49	9.5	47	12	28.8
12	33	26.25		37.75	42.9	10.5	29.3	7	40.1	9.25	49	11.75	28.8
11.75	28.6	26		37.5	29.7	10.25	29.5	6.75	42	9	46.8	11.5	25.5
11.5	29.2	25.75		37.25	39.2	10	32.8	6.5	41.6	8.75	43.9	11.25	25.9
11.25	28.2	25.5	35.4	37	44.6	9.75	25.2	6.25	55.2	8.5	45.1	11	29.6
11	28.2	25.25	40	36.75	53.1	9.5	26.8	6	43.3	8.25	44.8	10.75	31.5
10.75	26.6	25	43	36.5	56.5	9.25	33.6	5.75	50.1	8	40.9	10.5	32
10.5	33.7	24.75	33.6	36.25	43.6	9	28.9	5.5	43	7.75	38.3	10.25	30.3
10.25	41.1	24.5	32.6	36	53.6	8.75	26.8	5.25	42.2	7.5	42.1	10	32.2
10	32.6	24.25	45.4	35.75	54	8.5	27.4	5	38.5	7.25	44.5	9.75	33.9
9.75	28.6	24	49.3	35.5	34.1	8.25	28.4	4.75	40.6	7	36.5	9.5	32.5
9.5	24.8	23.75	55.3	35.25	45	8	26.5	4.5	52.5	6.75	34.6	9.25	33.6
9.25	23.4	23.5		35	45.4	7.75	27	4.25	37.7	6.5	47.7	9	34.4
9	22.8	23.25	36	34.75	39.3	7.5	23.8	4	39.5	6.25	43.2	8.75	32.2
8.75	36.5	23	31.2	34.5	35.4	7.25	26.6	3.75	40.8	6	45.8	8.5	33.9
8.5	23	22.75	32.4	34.25	36.9	7	23.1	3.5	40.4	5.75	38	8.25	32.8
8.25	23.9	22.5	33.8	34	45.2	6.75	25.5	3.25	44.1	5.5	40.2	8	34.9
8	28.4	22.25	34.1	33.75	47.9	6.5	29.7	3	50.6	5.25	34.8	7.75	33.6
7.75	24.7	22	41.6	33.5	52.2	6.25	26.7	2.75	47.2	5	42.4	7.5	33

FSR Depth	FSR CPS	CC Depth	CC CPS	LC Depth	LC CPS	SG Depth	SG CPS	NER Depth	NER CPS	MG Depth	MG CPS	SP Depth	SP CPS
7.5	37.9	21.75	58.4	33.25	51.7	6	26.5	2.5	38.4	4.75	44.1	7.25	34.8
7.25	25	21.5	56.6	33	31.2	5.75	26.5	2.25	38.4	4.5	38.9	7	34.6
7	24.4	21.25	62.7	32.75	30.1	5.5	30.9	2	40.6	4.25	40.1	6.75	32.3
6.75	53.5	21		32.5	33.9	5.25	27.4	1.75	33.9	4	43	6.5	32.6
6.5	25.8	20.75		32.25	38.75	5	26.8	1.5	36	3.75	46.4	6.25	32.9
6.25	27.3	20.5	32.5	32	43.6	4.75	28.6	1.25	39.2	3.5	40.4	6	31
6	21.8	20.25	36.5	31.75	42.9	4.5	28.6	1	43.1	3.25	39.3	5.75	36.7
5.75	29.4	20	33.6	31.5	29.5	4.25	33.4	0.75	47.7	3	37.9	5.5	32.9
5.5	26.2	19.75	31.8	31.25	25.8	4	26.1	0.5	42	2.75	37.7	5.25	34.5
5.25	25.2	19.5	35	31	27.5	3.75	29.2	0.25	45.3	2.5	42.5	5	33
5	27.3	19.25	30.8	30.75	36.4	3.5	30.1	0	53.2	2.25	42.3	4.75	34.2
4.75	30.8	19	36.3	30.5	47.5	3.25	31.5			2	39.7	4.5	33.2
4.5	23.7	18.75	40.9	30.25	46.6	3	32.5			1.75	48.9	4.25	30.4
4.25	30.8	18.5	43	30	35.7	2.75	39.5			1.5	44	4	39.4
4	22	18.25	41.5	29.75	38.8	2.5	38.4			1.25	43.6	3.75	36.9
3.75	24.5	18	50.9	29.5	42.3	2.25	36.4			1	42.9	3.5	35.9
3.5	25.7	17.75		29.25	40.6	2	61.6			0.75	40.1	3.25	29.6
3.25	23.3	17.5		29	41.8	1.75	42.4			0.5	41.3	3	36
3	27.6	17.25	30.5	28.75	53.6	1.5	44.1			0.25	44	2.75	35.3
2.75	27.8	17	33.8	28.5	35.8	1.25	47.2			0	49.3	2.5	30.7
2.5	22.6	16.75	30.4	28.25	30.7	1	41.2					2.25	27.9
2.25	24.9	16.5	37.5	28	34.3	0.75	51.7					2	32.9
2	28.8	16.25	38.8	27.75	36.3	0.5	48.5					1.75	28.5
1.75	23.4	16	64.5	27.5	41.8	0.25	40.7					1.5	25.8
1.5	26.3	15.75	32.8	27.25	44.5	0	51.5					1.25	32.7
1.25	29.3	15.5	39.1	27	21.8							1	26.1
1	29	15.25	40.6	26.75	23.3							0.75	31
0.75	33.7	15	44.8	26.5	29							0.5	33.5
0.5	36.2	14.75		26.25	37.2							0.25	29.4
0.25	41.4	14.5		26	40.4							0	41.1
0	42	14.25	35.2	25.75	40.5								
		14	35.1	25.5	26.6								
		13.75	37.3	25.25	24.6								
		13.5	45	25	25.2								
		13.25	51.8	24.75	25.1								
		13	61.6	24.5	30.6								
		12.75		24.25	35.1								

FSR Depth	FSR CPS	CC Depth	CC CPS	LC Depth	LC CPS	SG Depth	SG CPS	NER Depth	NER CPS	MG Depth	MG CPS	SP Depth	SP CPS
		12.5		24	39								
		12.25		23.75	25.2								
		12	28.5	23.5	26.9								
		11.75	32.6	23.25	36.3								
		11.5	30.6	23	38.1								
		11.25	37.1	22.75	40.2								
		11	43.6	22.5	26.6								
		10.75	32.2	22.25	24.4								
		10.5	30.1	22	21.8								
		10.25	32.5	21.75	31.2								
		10	32.6	21.5	44.1								
		9.75	32	21.25	44.3								
		9.5	40.5	21	26.8								
		9.25	46.1	20.75	28.3								
		9	35	20.5	27								
		8.75	34.7	20.25	26.5								
		8.5	39.2	20	33.6								
		8.25	50.9	19.75	32.6								
		8		19.5	28.3								
		7.75	35.7	19.25	27.5								
		7.5	44.1	19	30.5								
		7.25	54.3	18.75	38.8								
		7		18.5	37.6								
		6.75		18.25	28.7								
		6.5		18	27.8								
		6.25	38.1	17.75	25.5								
		6	35.4	17.5	28.3								
		5.75	42.2	17.25	33.5								
		5.5	45.9	17	35.1								
		5.25	50.8	16.75	38.7								
		5	31.9	16.5	46.4								
		4.75	32	16.25	25.6								
		4.5	32	16	23.4								
		4.25	35.9	15.75	24.2								
		4	37.6	15.5	28.4								
		3.75	29.4	15.25	35								
		3.5	26.9	15	42.2								

FSR Depth	FSR CPS	CC Depth	CC CPS	LC Depth	LC CPS	SG Depth	SG CPS	NER Depth	NER CPS	MG Depth	MG CPS	SP Depth	SP CPS
		3.25	35.5	14.75	51								
		3	52.2	14.5	29.4								
		2.75	23.1	14.25	29.1								
		2.5	23.9	14	29.5								
		2.25	30.9	13.75	29.8								
		2	32.2	13.5	38								
		1.75	32.6	13.25	50.3								
		1.5	28.5	13	58.8								
		1.25	31.7	12.75	50.8								
		1	31	12.5	31.4								
		0.75	29.1	12.25	23.8								
		0.5	29.4	12	26.2								
		0.25	31.9	11.75	27.9								
		0	38.5	11.5	36.6								
				11.25	49.7								
				11	52.9								
				10.75	44.9								
				10.5	30.4								
				10.25	25								
				10	27.4								
				9.75	29.8								
				9.5	28.7								
				9.25	44								
				9	41.3								
				8.75	49.1								
				8.5	30.2								
				8.25	27.7								
				8	27.6								
				7.75	30.5								
				7.5	27								
				7.25	36.7								
				7	48.4								
				6.75	49.6								
				6.5	52.8								
				6.25	45.2								
				6	27.8								
				5.75	26.8								

FSR Depth	FSR CPS	CC Depth	CC CPS	LC Depth	LC CPS	SG Depth	SG CPS	NER Depth	NER CPS	MG Depth	MG CPS	SP Depth	SP CPS
				5.5	35								
				5.25	42.3								
				5	32.9								
				4.75	32.1								
				4.5	37.3								
				4.25	70.3								
				4	29.9								
				3.75	29.1								
				3.5	29.6								
				3.25	32.5								
				3	35.4								
				2.75	28.2								
				2.5	27.9								
				2.25	27.3								
				2	31								
				1.75	31.1								
				1.5	29.7								
				1.25	29.3								
				1	27.1								
				0.75	35.8								
				0.5	31.1								
				0.25	27.9								
				0	32.6								